

**INVESTIGATIONS ON STRUCTURAL RESPONSE OF
WATER BACKED PERFORATED PLATES**

A THESIS

submitted by

O.R.NANDAGOPAN

for the award of the degree

of

DOCTOR OF PHILOSOPHY



**DEPARTMENT OF SHIP TECHNOLOGY
COCHIN UNIVERSITY OF SCIENCE AND TECHNOLOGY
KOCHI – 682 022, KERALA**

NOVEMBER 2010

THESIS CERTIFICATE

This is to certify that the thesis entitled **INVESTIGATIONS ON STRUCTURAL RESPONSE OF WATER BACKED PERFORATED PLATES** submitted by **O.R.NANDAGOPAN**, to the Cochin University of Science and Technology, Kochi for the award of the degree of **Doctor of Philosophy** is a bonafide record of research work carried out by him under my supervision. The contents of this thesis, in full or in parts, have not been submitted to any other Institute or University for the award of any degree or diploma. The research work has been carried out at Cochin University of Science and Technology, Naval Physical and Oceanographic Laboratory, DRDO, Kochi and Naval Science and Technology Laboratory, DRDO, Visakhapatnam.

Place: Kochi
Date:

Dr.C.G.Nandakumar
Research Guide,
Dept. of Ship Technology,
Cochin University of Science and
Technology, Kochi.

DECLARATION

This is to certify that the thesis entitled **INVESTIGATIONS ON STRUCTURAL RESPONSE OF WATER BACKED PERFORATED PLATES** submitted to the Cochin University of Science and Technology, in partial fulfillment of the requirements for the award of the degree of **Doctor of Philosophy** is a bonafide record of research work carried out by me. The contents of this thesis have not been submitted and will not be submitted to any other Institute or University for the award of any degree.

Place: Kochi
Date:

O.R.Nandagopan,
Scientist (Reg. No. 3161),
Naval Physical & Oceanographic
Laboratory, DRDO,
Thrikkakara, Kochi.

ACKNOWLEDGEMENTS

I would like to express my immense gratitude and sincere thanks to my research guide, Dr.C.G.Nandakumar, Reader, Dept. of Ship Technology for his inspiring guidance, constant encouragement, and supervision throughout the course of my research work. This work could not have been accomplished, but for his constructive reviews and profound advice.

I express my sincere thanks to Head of the Department of Ship Technology, Dr.K.P.Narayanan for his positive criticism and useful suggestions.

I convey my appreciation and thanks to Dr.K.Sudarsan, Scientist 'F', Group Head (Engineering), Naval Physical and Oceanographic Laboratory, (NPOL) Kochi, for his exciting direction in carrying forward my research work.

I express my sincere gratitude to Shri. S. Anantha Narayanan, Director, Dr. A. Unnikrishnan, Associate Director, Smt. Lasitha Ranjit, Scientist E, Co-chairman, HRD, Shri.Nandadulaldas, CAO, NPOL for facilitating this research work.

I am most indebted to Shri.V.Chander, former Director, NPOL who has motivated me to take up this doctoral program and given constant encouragement and moral support with his most valuable and fruitful suggestions.

I also express my profound thanks to Shri.S.Ranjith kumar, SRF, NPOL, Kochi and Shri.AVS.Chari, Scientist G, NSTL, Visakhapatnam for facilitating the numerical analysis and experimental facilities to accomplish the research work.

I thank Shri.Unnikrishnan and Smt.Sagitha, Department of Ship Technology, for their support.

I express my appreciation to Sameer Abdul Azeez, K.Ajithkumar, Lijo Vijayan, V.M.Dhiwakar, P.Rajan, K.Manoharan, R.Rajesh, T.C.Vidhun, S.Usha, V.Neelan, K.T.John of NPOL for their technical support during the research work and K.V.S.Subramaniveswar Rao and Janardhana Rao of NSTL for their practical support in carrying out the experiments.

I am grateful to my parents Shri.O.K.Ramanandam and Smt.O.R.Lalitha for their love and inspiration.

With deep sense of gratitude, I would like to acknowledge the understanding and patience shown by my wife O.N.Lalithamai and my daughters O.N.Niwhashini and O.N.Nikkilamai who missed most of their valuable time with me during this period. This work would never have been completed without their appeal to almighty, encouragement and shouldering most of the responsibilities at home. I thank all my relatives and friends, who had helped me to accomplish this work.

All this would not have been possible without the grace of the GOD. I thank Him for the blessings.

O.R.NANDAGOPAN

INVESTIGATIONS ON STRUCTURAL RESPONSE OF WATER BACKED PERFORATED PLATES

ABSTRACT

KEYWORDS: Perforated plate, perforated plate with lining, Finite element analysis, fluid structure interaction, shock tank tests, water backed plate, noncontact underwater explosion.

The study envisaged herein contains the numerical investigations on Perforated Plate (PP) as well as numerical and experimental investigations on Perforated Plate with Lining (PPL) which has a variety of applications in underwater engineering especially related to defence applications. Finite element method has been adopted as the tool for analysis of PP and PPL. The commercial software ANSYS has been used for static and free vibration response evaluation, whereas ANSYS LS-DYNA has been used for shock analysis. SHELL63, SHELL93, SOLID45, SOLSH190, BEAM188 and FLUID30 finite elements available in the ANSYS library as well as SHELL193 and SOLID194 available in the ANSYS LS-DYNA library have been made use of. Unit cell of the PP and PPL which is a miniature of the original plate with 16 perforations have been used. Based upon the convergence characteristics, the utility of SHELL63 element for the analysis of PP and PPL, and the required mesh density are brought out. The effect of perforation, geometry and orientation of perforation, boundary conditions and lining plate are investigated for various configurations. Stress concentration and deflection factor are also studied. Based on these investigations, stadium geometry perforation with horizontal orientation is recommended for further analysis.

Linear and nonlinear static analysis of PP and PPL subjected to unit normal pressure has been carried out besides the free vibration analysis. Shock analysis has also been carried out on these structural components. The analytical model measures 0.9m x 0.9m with stiffener of 0.3m interval. The influence of finite element, boundary conditions, and

lining plate on linear static response has been estimated and presented. Comparison of behavior of PP and PPL in the nonlinear strain regime has been made using geometric nonlinear analysis. Free vibration analysis of the PP and PPL has been carried out ‘in vacuum’ condition and in water backed condition, and the influence of water backed condition and effect of perforation on natural frequency have been investigated.

Based upon the studies on the vibration characteristics of NPP, PP and PPL in water backed condition and ‘in vacuum’ condition, the reduction in the natural frequency of the plate in immersed condition has been rightly brought out. The necessity to introduce the effect of water medium in the analysis of water backed underwater structure has been highlighted.

Shock analysis of PP and PPL for three explosives viz., PEK, TNT and C4 has been carried out and deflection and stresses on plate as well as free field pressure have been estimated using ANSYS LS-DYNA. The effect of perforations and the effect of lining plate have been predicted. Experimental investigations of the measurement of free field pressure using PPL have been conducted in a shock tank. Free field pressure has been measured and has been validated with finite element analysis results. Besides, an experiment has been carried out on PPL, for the comparison of the static deflection predicted by finite element analysis.

The distribution of the free field pressure and the estimation of differential pressure from experimentation and the provision for treating the differential pressure as the resistance, as a part of the design load for PPL, has been brought out.

TABLE OF CONTENTS

Title	Page No.
ACKNOWLEDGEMENTS	i
ABSTRACT	iii
TABLE OF CONTENTS.....	v
LIST OF TABLES	xi
LIST OF FIGURES	xv
ABBREVIATIONS	xxiv
NOTATIONS	xxvi

CHAPTER 1 INTRODUCTION

1.1 Introduction	01
1.2 Structural Analysis of PP and PPL	02
1.3 Fluid Structure Interaction	03
1.4 Underwater Explosion	05
1.5 Scope and Objectives	07
1.6 Organisation of thesis	08

CHAPTER 2 LITERATURE REVIEW

2.1 Introduction	09
2.2 Perforated Plate	10
2.3 Vibration of Plate	12
2.4 Underwater Explosion	13
2.5 Comments	18

**CHAPTER 3 STRUCTURAL ANALYSIS AND NUMERICAL MODELS
OF UNIT CELL, PERFORATED PLATE AND
PERFORATED PLATE WITH LINING**

3.1	Introduction	19
3.2	Geometry of Perforation.....	19
3.3	Type of Analysis	20
3.4	Unit Cell	22
3.5	Plate Model	22
3.6	Solid Model	23
3.7	Grillage Model	24
3.8	Boundary Conditions	24
3.9	Material	25
3.10	Description of Finite Element Software	26
3.11	Description of Finite Elements	27
3.11.1	SHELL63 element	27
3.11.2	SHELL93 element	27
3.11.3	SOLID45 element	28
3.11.4	SOLSH190 element	28
3.11.5	BEAM188 element	29
3.11.6	FLUID30 element	30
3.11.7	SHELL163 element	30
3.11.8	SOLID164 element	30
3.12	System Configuration	31

CHAPTER 4 LINEAR STATIC ANALYSIS OF UNIT CELL

4.1	Introduction.....	32
4.2	Description	32
4.3	Finite Element Analysis	32
4.3.1	Non Perforated Plate	33

4.3.2	Stadium Horizontal Perforation	35
4.3.3	Stadium Vertical Perforation	38
4.3.4	Elliptical Horizontal Perforation	40
4.3.5	Discussion on Convergence	43
4.3.6	Elliptical Vertical Perforation	48
4.3.7	Stadium Horizontal Perforation of PPL.....	49
4.3.8	Stadium Vertical Perforation of PPL	51
4.3.9	Elliptical Horizontal Perforation of PPL	53
4.3.10	Elliptical Vertical Perforation of PPL	55
4.4	Results and Discussion	57
4.4.1	Effect of lining plate	57
4.4.2	Effect of perforation orientation	60
4.4.3	Effect of release of rotation restraint at the boundary nodes	61
4.4.4	Effect of perforation geometry	63
4.4.5	Effect of nodal rotational degrees of freedom of the elements	65
4.4.6	Effect of higher order element	67
4.4.7	Evaluation of Stress Concentration and Deflection factor	68
4.4.8	Recommendations	73

CHAPTER 5 NUMERICAL INVESTIGATIONS ON PERFORATED PLATE

5.1	Introduction	75
5.2	Description of Perforated Plate	75
5.3	Linear Static Analysis	76
5.3.1	Plate model	76
5.3.2	Solid model	78
5.4	Results and Discussion	80
5.5	Geometric Nonlinear Analysis	82
5.5.1	Description of finite element analysis	82

5.5.2	Results and Discussion	83
5.6	Free Vibration Analysis	84
5.6.1	Description of finite element analysis	84
5.6.2	Validation	85
5.6.3	Finite element model of Non Perforated Plate	86
5.6.4	Finite element model of Perforated Plate	87
5.7	Results and Discussion	88
5.7.1	Effect of water backed condition on natural frequency	90
5.7.2	Effect of perforation on natural frequency	91
5.8	Shock Analysis	92
5.8.1	Calculation of pressure and explosive load	92
5.9	Finite Element Analysis	93
5.9.1	Description of finite element analysis	94
5.9.2	Equation Of State for explosive: JWL (Jones – Wilkens – Lee)	94
5.9.3	Material model for explosive: Explosive Burn	95
5.9.4	Equation of state for water: Gruneisen	95
5.9.5	Material model for water: Null Material	96
5.9.6	Description of finite element model	97
5.9.7	Units	97
5.10	Results and Discussion	97

CHAPTER 6 NUMERICAL INVESTIGATIONS ON PERFORATED PLATE WITH LINING

6.1	Introduction	105
6.2	Description of Perforated Plate with Lining	105
6.3	Linear Static Analysis	105
6.3.1	Plate model	106
6.3.2	Solid model	108
6.3.3	Grillage model	110

6.3.4	Results and Discussion	114
6.4	Geometric Nonlinear Analysis	116
6.5	Free Vibration Analysis	116
6.5.1	Effect of water medium on natural frequency	121
6.5.2	Effect of lining plate on natural frequency	121
6.6	Shock Analysis	123
6.6.1	Description of finite element analysis	123
6.6.2	Results and Discussion	124

**CHAPTER 7 EXPERIMENTAL INVESTIGATIONS ON PERFORATED
PLATE WITH LINING**

7.1	Introduction	129
7.2	Experimental Investigations for static deflection.....	129
7.2.1	Experimental setup	130
7.2.2	Experimental procedure	131
7.3	Validation using Finite Element Analysis	133
7.3.1	Description of the Finite Element Model	133
7.3.2	Results and Discussion	135
7.4	Experimental Investigations on Underwater Explosion	137
7.4.1	Experimental set up	137
7.4.2	Instrumentation	137
7.4.3	Experimental procedure	138
7.4.4	Results and Discussion	139
7.5	Numerical Investigations	143
7.5.1	Finite element analysis	143
7.5.2	Results and Discussion	143

CHAPTER 8 SUMMARY AND CONCLUSIONS

8.1 Summary 148
8.2 Conclusions and Recommendations 149
8.3 Significant contributions 152
8.4 Recommendations for the future work 152

REFERENCES 153

PUBLICATIONS BASED ON THIS THESIS 158

LIST OF TABLES

Table No.	Title	Page No.
1.1	Methods and features for structural analysis of underwater structures	04
3.1	Details of boundary conditions applied for PP and PPL of dimension 0.9 m x 0.9 m	25
3.2	Material properties of Titanium alloy	26
3.3	Element features	31
4.1	Details of boundary conditions applied for unit cell	33
4.2	Details of finite element model and static structural responses of non perforated plate of unit cell for pressure of 1 Pa.....	35
4.3	Details of finite element model and static structural responses of stadium horizontal perforation of unit cell for pressure of 1 Pa	37
4.4	Details of finite element model and static structural responses of stadium vertical perforation of unit cell for pressure of 1 Pa	40
4.5	Details of finite element model and static structural responses of elliptical horizontal perforation of unit cell for pressure of 1 Pa	42
4.6	Details of convergence of deflection, von Mises stress and maximum principal stress for various configurations.	47
4.7	Details of finite element model and static structural responses of elliptical vertical perforation of unit cell for pressure of 1 Pa	49
4.8	Details of finite element model and static structural responses of various configurations of unit cell of perforated plate with lining for pressure of 1 Pa.	58
4.9	Effect of lining plate on static structural responses for various configurations of unit cell in terms of percentage	59
4.10	Effect of orientation of perforation on static structural responses for various configurations of unit cell in terms of percentage	61

4.11	Effect of BC3 and BC4 boundary conditions on static structural responses for various configurations of unit cell in terms of percentage	62
4.12	Effect of stadium and elliptical geometry of perforation on static structural responses for various configurations of unit cell in terms of percentage	64
4.13	Effect of nodal rotational degrees of freedom of SHELL63 and SHELL93 for various configurations of unit cell on static structural responses in terms of percentage	66
4.14	Effect of number of nodes in elements of SHELL63 and SHELL93 for various configurations of unit cell on static structural responses in terms of percentage	68
4.15	(a) Stress concentration factor for SHP for BC3 and BC4.....	69
	(b) Deflection factor for SHP for BC3 and BC4.	69
	(c) Stress concentration factor for SVP for BC3 and BC4.	69
	(d) Deflection factor for SVP for BC3 and BC4.	69
	(e) Stress concentration factor for EHP for BC3 and BC4.	70
	(f) Deflection factor for EHP for BC3 and BC4.	70
	(g) Stress concentration factor for EVP for BC3 and BC4.	70
	(h) Deflection factor for EVP for BC3 and BC4.	70
	(i) Stress concentration factor of PPL for SHP for BC3 and BC4.	71
	(j) Deflection factor of PPL for SHP for BC3 and BC4	71
	(k) Stress concentration factor of PPL for SVP for BC3 and BC4.	71
	(l) Deflection factor of PPL for SVP for BC3 and BC4	71
	(m) Stress concentration factor of PPL for EHP for BC3 and BC4.	72
	(n) Deflection factor of PPL for EHP for BC3 and BC4	72
	(o) Stress concentration factor of PPL for EVP for BC3 and BC4.	72
	(p) Deflection factor of PPL for EVP for BC3 and BC4	72
4.16	SCF and DF of unit cell for various configurations using SHELL63 element .	73
5.1	Effect of perforation on NPP and PP of static structural responses of different models for BC1and BC2	81
5.2	Static structural responses of NPP and PP due to geometric nonlinearity of the plate for BC1	84
5.3	Comparison of natural frequency for various finite elements of NPP with BC3	85
5.4	Natural frequencies of NPP and PP ‘in vacuum’ and in water backed condition for SHELL63 element for BC1.	89

5.5	Free field pressure estimation for given explosive, weight of explosive and stand off distance as per Cole’s empirical formula.....	93
5.6	Details of EOS parameters and Material properties of PEK, TNT and C4 explosives	95
5.7	Details of EOS parameters and Material properties of water	96
5.8	Material properties of Titanium alloy for shock analysis	97
5.9	Free field pressure and structural responses of NPP and PP due to 30gm weight and 1m stand off distance for explosions of PEK, TNT and C4 for BC1....	103
5.10	Variation of deflection and principal stress in percentage due to the perforation for PEK, TNT and C4 explosives	104
6.1	Static structural responses of PPL for different finite element models and for BC1 and BC2 at centroid for 1 Pa	115
6.2	Effect of lining plate on PP and PPL of static structural responses of different models for BC1and BC2 for an equivalent load (PPL * COA)	117
6.3	Static structural responses of PPL from the geometric nonlinear analysis for BC1	118
6.4	Natural frequencies of PPL ‘in vacuum’ and in water backed condition for SHELL63 element for BC1	120
6.5	Free field pressure and structural responses of PPL due to 30gm weight and 1m stand off distance for explosions of PEK, TNT and C4 for BC1	128
6.6	Variation of Deflection and Principal Stress in percentage due to the lining plate for PEK, TNT and C4 explosives	128
7.1	Experimental measurement of load - deflection of PPL for BC3	134
7.2	Comparison of deflection measured from experiment and estimated deflection through finite element method	136
7.3	Free field pressure measured by pressure blast gauges from noncontact underwater shock explosion experiments for 30gm of PEK explosive placed at a stand off distance of 1m from PPL	142
7.4	Estimation of free field pressure and structural responses of PPL due to shock analysis	144

7.5	Comparison of free field pressure obtained from experiment and finite element method due to noncontact underwater explosion using PEK on PPL for BC3	144
7.6	Comparison of free field pressure obtained from Cole's method and finite element method due to noncontact underwater explosion using TNT on PPL .	144

LIST OF FIGURES

Figure	Title	Page No.
1.1	Submarine with PPL dome configuration	02
1.2	PPL under investigation	02
3.1	(a) Geometry of Stadium Perforation	20
	(b) Geometry of Elliptical Perforation	20
3.2	(a) Geometry of unit cell of SHP plate	23
	(b) Geometry of unit cell of SVP plate	23
	(c) Geometry of unit cell of EHP plate	23
	(d) Geometry of unit cell of EVP plate	23
	(e) Geometry of unit cell of Non Perforated Plate	23
3.3	Configuration of T beam of the PPL with Grillage Model	25
3.4	Schematic sketch of continuous plate considered for investigation to describe boundary conditions	26
3.5	Geometry & kinematics of SHELL63 element.....	28
3.6	Geometry & kinematics of SHELL93 element.....	28
3.7	Geometry & kinematics of SOLID45 element.....	29
3.8	Geometry & kinematics of SOLSH190 element.....	29
3.9	Geometry & kinematics of BEAM188 element.....	29
3.10	Geometry & kinematics of FLUID30 element.....	29
3.11	Geometry & kinematics of SHELL163 element.....	31
3.12	Geometry & kinematics of SOLID164 element.....	31
4.1	(a) Finite Element Model of NPP with SHELL63 element for BC3	33
	(b) Deflection Contour of NPP for 1Pa for BC3	33
	(c) von Mises Stress Contour of NPP for 1Pa for BC3	33
	(d) Maximum Principal Stress Contour of NPP for 1Pa for BC3	33
	(e) Deflection Contour of NPP with SHELL63 element for BC4 for 1 Pa	34

	(f) von Mises Stress Contour of NPP for 1Pa for BC4	34
	(g) Maximum Principal Stress Contour of NPP for 1Pa for BC4	34
4.2	(a) Finite Element Model of SHP with SHELL63 element for BC3	36
	(b) Deflection Contour of SHP for 1Pa for BC3	36
	(c) von Mises Stress Contour of SHP for 1Pa for BC3	36
	(d) Maximum Principal Stress Contour of SHP for 1Pa for BC3	36
	(e) Deflection Contour of SHP with SHELL63 element for BC4 for 1 Pa	36
	(f) von Mises Stress Contour of SHP for 1Pa for BC4	36
	(g) Maximum Principal Stress Contour of SHP for 1Pa for BC4	37
4.3	(a) Finite Element Model of SVP with SHELL63 element for BC3	38
	(b) Deflection Contour of SVP for 1Pa for BC3	38
	(c) von Mises Stress Contour of SVP for 1Pa for BC3	39
	(d) Maximum Principal Stress Contour of SVP for 1Pa for BC3	39
	(e) Deflection Contour of SVP with SHELL63 element for BC4 for 1 Pa	39
	(f) von Mises Stress Contour of SVP for 1Pa for BC4	39
	(g) Maximum Principal Stress Contour of SVP for 1Pa for BC4	39
4.4	(a) Finite Element Model of EHP with SHELL63 element for BC3	41
	(b) Deflection Contour of EHP for 1Pa for BC3	41
	(c) von Mises Stress Contour of EHP for 1Pa for BC3	41
	(d) Maximum Principal Stress Contour of EHP for 1Pa for BC3	41
	(e) Deflection Contour of EHP with SHELL63 element for BC4 for 1 Pa	41
	(f) von Mises Stress Contour of EHP for 1Pa for BC4	41
	(g) Maximum Principal Stress Contour of EHP for 1Pa for BC4	42
4.5	(a) Convergence of deflection for NPP of different elements for BC3	44
	(b) Convergence of maximum principal stress for NPP of SHELL63 and SHELL93 elements for BC3	45
	(c) Convergence study of maximum principal stress for NPP of SOLID45 and SOLSH190 elements for BC3	45
4.6	Convergence of deflection for SHELL63 & SHELL93 elements for BC3	45
4.7	Convergence of deflection for SHELL63 & SHELL93 elements for BC4	45
4.8	Convergence of deflection for SOLID45 & SOLSH190 elements for BC3	45
4.9	Convergence of VMS for SHELL63 & SHELL93 elements for BC3	45
4.10	Convergence of VMS for SHELL63 & SHELL93 elements for BC4	46
4.11	Convergence of VMS for SOLID45 & SOLSH190 elements for BC3	46
4.12	Convergence of MPS for SHELL63 & SHELL93 elements for BC3	46

4.13	Convergence of MPS for SHELL63 & SHELL93 elements for BC4.....	46
4.14	Convergence of MPS for SOLID45 and SOLSH190 elements for BC3	46
4.15	(a) Finite Element Model of EVP with SHELL63 element for BC3	48
	(b) Deflection Contour of EVP for 1Pa for BC3	48
	(c) von Mises Stress Contour of EVP for 1Pa for BC3	49
	(d) Maximum Principal Stress Contour of EVP for 1Pa for BC3	49
4.16	(a) Finite Element Model of SHP of PPL with SHELL63 element for BC3	50
	(b) Deflection Contour of SHP of PPL for 1Pa for BC3	50
	(c) von Mises Stress Contour of SHP of PPL for 1Pa for BC3	50
	(d) Maximum Principal Stress Contour of SHP of PPL for 1Pa for BC3	50
	(e) Deflection Contour of SHP of PPL with SHELL63 element for BC4 for 1 Pa	50
	(f) von Mises Stress Contour of SHP of PPL for 1Pa for BC4	50
	(g) Maximum Principal Stress Contour of SHP of PPL for 1Pa for BC4	51
4.17	(a) Finite Element Model of SVP of PPL with SHELL63 element for BC3 ...	52
	(b) Deflection Contour of SVP of PPL for 1Pa for BC3	52
	(c) von Mises Stress Contour of SVP of PPL for 1Pa for BC3	52
	(d) Maximum Principal Stress Contour of SVP of PPL for 1Pa for BC3	52
	(e) Deflection Contour of SVP of PPL with SHELL63 element for BC4 for 1 Pa	52
	(f) von Mises Stress Contour of SVP of PPL for 1Pa for BC4	52
	(g) Maximum Principal Stress Contour of SVP of PPL for 1Pa for BC4	53
4.18	(a) Finite Element Model of EHP of PPL with SHELL63 element for BC3	54
	(b) Deflection Contour of EHP of PPL for 1Pa for BC3	54
	(c) von Mises Stress Contour of EHP of PPL for 1Pa for BC3	54
	(d) Maximum Principal Stress Contour of EHP of PPL for 1Pa for BC3	54
	(e) Deflection Contour of EHP of PPL with SHELL63 element for BC4 for 1 Pa	54
	(f) von Mises Stress Contour of EHP of PPL for 1Pa for BC4.....	54
	(g) Maximum Principal Stress Contour of EHP of PPL for 1Pa for BC4	55
4.19	(a) Finite Element Model of EVP of PPL with SHELL63 element for BC3	56
	(b) Deflection Contour of EVP of PPL for 1Pa for BC3	56
	(c) von Mises Stress Contour of EVP of PPL for 1Pa for BC3	56
	(d) Maximum Principal Stress Contour of EVP of PPL for 1Pa for BC3	56
	(e) Deflection Contour of EVP of PPL with SHELL63 element for BC4 for 1 Pa	56
	(f) von Mises Stress Contour of EVP of PPL for 1Pa for BC4	56
	(g) Maximum Principal Stress Contour of EVP of PPL for 1Pa for BC4	57

4.20	Effect of perforation from horizontal to vertical orientation of unit cell for various elements on deflection represented in terms of percentage	62
4.21	Effect of boundary conditions BC3 and BC4 of unit cell for SHELL63 and SHELL93 elements on deflection represented in terms of percentage	62
4.22	Effect of Geometry from stadium to elliptical perforation of unit cell for various elements and boundary conditions on deflection represented in terms of percentage	63
4.23	Effect of nodal DOF of SHELL and SOLID45 elements of unit cell on deflection represented in terms of percentage	67
4.24	Effect of number of nodes of SHELL63 and SHELL93 elements of unit cell on deflection represented in terms of percentage	67
5.1	Geometry of Perforated Plate considered for the investigation	76
5.2	(a) Finite Element Model of PP with SHELL63 element for BC1	77
	(b) Deflection Contour of PP for 1Pa for BC1	77
	(c) von Mises Stress Contour of PP for 1Pa for BC1	77
	(d) Maximum Principal Stress Contour of PP for 1Pa for BC1	77
	(e) Deflection Contour of PP with SHELL63 element for BC2 for 1 Pa	77
	(f) von Mises Stress Contour of PP for 1Pa for BC2	77
	(g) Maximum Principal Stress Contour of PP for 1Pa for BC2	78
5.3	(a) Finite Element Model of PP with SOLID45 element for BC1	79
	(b) Deflection Contour of PP with SOLID45 element for 1Pa for BC1.....	79
	(c) von Mises Stress Contour of PP with SOLID45 element for 1Pa for BC1.	79
	(d) Maximum Principal Stress Contour of PP for 1Pa for BC1	79
	(e) Deflection Contour of PP with SOLSH190 element for BC1 for 1 Pa	79
	(f) von Mises Stress Contour of PP with SOLSH190 element for 1Pa for BC1	79
	(g) Maximum Principal Stress Contour of PP with SOLSH190 element for 1Pa for BC1	80
5.4	Finite element model of NPP with SHELL63 element and BC1	83
5.5	Finite element model of PP with SHELL63 element and BC1	83
5.6	Load – deflection plot for each load step for the configuration of NPP and PP	83
5.7	(a) FE model of NPP with SHELL63 element for BC3	85
	(b) Mode shape for m=1 and n=1 of NPP for BC3	85
5.8	(a) FE model of NPP with SHELL63 element for BC1.....	86

	(b) Mode shape for m=1 and n=1 of NPP for BC1	86
5.9	(a) FE model of water backed NPP with SHELL63 element for BC1	86
	(b) Mode shape for m=1 and n=1 of water backed NPP for BC1	86
5.10	(a) FE model of PP with SHELL63 element for BC1	87
	(b) Mode shape for m=1 and n=1 of PP for BC1	87
5.11	(a) FE model of water backed PP with SHELL63 element for BC1	87
	(b) Mode shape for m=3 and n=1 of PP for BC1	87
	(c) Mode shape for m=1 and n=1 of PP for BC1	88
5.12	Natural frequency of NPP and PP ‘in vacuum’ for modal index m=1 to m=3..	88
5.13	Natural frequency of NPP and PP in water backed condition for modal index m=1 to m=3	89
5.14	Effect of water backed condition on natural frequency of NPP for modal index m=1 to m=3	91
5.15	Effect of water backed condition on natural frequency of PP for modal index m=1 to m=3	91
5.16	Effect of perforation for ‘in vacuum’ on natural frequency for modal index m=1 to m=3	91
5.17	Effect of perforation for water backed condition on natural frequency for modal index m=1 to m=3	91
5.18	(a) Finite Element model of NPP with SHELL163 element for geometry and SOLID164 element for PEK explosive and fluid for BC1	98
	(b) Free field pressure history plot in front of Lining Plate for NPP due to explosion of PEK	98
	(c) Deflection history plot for NPP due to explosion of PEK	99
	(d) Principal stress history plot for NPP due to explosion of PEK	99
5.19	(a) Free field pressure history plot in front of Lining Plate for NPP due to explosion of TNT for BC1	99
	(b) Deflection history plot for NPP due to explosion of TNT	99
	(c) Principal stress history plot for NPP due to explosion of TNT	99
5.20	(a) Free field pressure history plot in front of Lining Plate for NPP due to explosion of C4 for BC1	100
	(b) Deflection history plot for NPP due to explosion of C4	100
	(c) Principal stress history plot for NPP due to explosion of C4	100

5.21	(a) Finite Element model of PP with SHELL163 element for geometry and SOLID164 element for PEK explosive and fluid for BC1	100
	(b) Free field pressure history plot in front of Lining Plate for PP due to explosion of PEK	100
	(c) Deflection history plot for PP due to explosion of PEK	101
	(d) Principal stress history plot for PP due to explosion of PEK	101
5.22	(a) Free field pressure history plot in front of Lining Plate for PP due to explosion of TNT for BC1	101
	(b) Deflection history plot for PP due to explosion of TNT	101
	(c) Principal stress history plot for PP due to explosion of TNT	102
5.23	(a) Free field pressure history plot in front of Lining Plate for PP due to explosion of C4 for BC1	102
	(b) Deflection history plot for PP due to C4 explosion of C4.....	103
	(c) Principal stress history plot for PP due to explosion of C4	103
6.1	Geometry of Perforated Plate with Lining	106
6.2	(a) Finite Element Model of PPL with SHELL63 element for BC1	107
	(b) Deflection Contour of PPL for 1Pa for BC1	107
	(c) von Mises Stress Contour of PPL for 1Pa for BC1	107
	(d) Principal Stress Contour of PPL for 1Pa for BC1	107
	(e) Deflection Contour of PPL with SHELL63 element for BC2 for 1 Pa	107
	(f) von Mises Stress Contour of PPL for 1Pa for BC2	107
	(g) Maximum Principal Stress Contour of PPL for 1Pa for BC2	108
6.3	(a) Finite Element Model of PPL with SOLID45 element for BC1	109
	(b) Deflection Contour of PPL with SOLID45 element for 1Pa for BC1	109
	(c) von Mises Stress Contour of PPL with SOLID45 element for 1Pa for BC1	109
	(d) Maximum Principal Stress Contour of PPL with SOLID45 element for 1Pa for BC1	109
	(e) Deflection Contour of PPL with SOLSH190 element for BC1 for 1 Pa	109
	(f) von Mises Stress Contour of PPL with SOLSH190 element for 1Pa for BC1	109
	(g) Maximum Principal Stress Contour of PPL with SOLSH190 element for 1Pa for BC1	110
6.4	(a) Approximated geometry of the perforation to rectangular configuration – type1	111
	(b) Approximated geometry of the perforation to rectangular configuration – type2	111
6.5	(a) Finite Element Model of PPL with type1 perforation configuration, BEAM188 element for BC1	111

	(b) Deflection Contour of PPL for 1Pa for BC1	111
	(c) von Mises Stress Contour of PPL for 1Pa for BC1	112
	(d) Maximum Principal Stress Contour of PPL for 1Pa for BC1	112
	(e) Deflection Contour of PPL with type1 perforation configuration, BEAM188 element for BC2 for 1 Pa	112
	(f) von Mises Stress Contour of PPL for 1Pa for BC2	112
	(g) Maximum Principal Stress Contour of PPL for 1Pa for BC2	113
6.6	(a) Deflection Contour of PPL with type2 perforation configuration, BEAM188 element for BC1 for 1 Pa	113
	(b) von Mises Stress Contour of PPL for 1Pa for BC1	113
	(c) Maximum Principal Stress Contour of PPL for 1Pa for BC1	114
	(d) Deflection Contour of PPL for 1Pa for BC2	114
	(e) von Mises Stress Contour of PPL for 1Pa for BC2	114
	(f) Maximum Principal Stress Contour of PPL for 1Pa for BC2	114
6.7	(a) Load – Deflection plot for each load step for the configuration of PPL	118
	(b) Load – Deflection plot for each load step for the configuration of NPP, PP and PPL	118
6.8	(a) FE model of PPL ‘in vacuum’ with SHELL63 element for BC1	118
	(b) Mode shape for m=3 and n=1 of PPL for BC1.....	118
	(c) Mode shape for m=1 and n=1 of PPL for BC1	119
6.9	(a) FE model of water backed PPL with SHELL63 element for BC1	119
	(b) Mode shape for m=1 and n=1 of PPL for BC1	119
6.10	(a) Natural frequency of PPL ‘in vacuum’ for modal index m=1 to m=3	121
	(b) Natural frequency of PPL in water backed condition for modal index m=1 to m=3	121
6.11	Effect of water medium on natural frequency of PPL for modal index m=1 to m=3	122
6.12	Effect of lining plate ‘in vacuum’ on natural frequency for modal index m=1 to m=3	122
6.13	Effect of lining plate for water backed condition on natural frequency for modal index m=1 to m=3	123
6.14	(a) Finite Element model of PPL with SHELL163 element for geometry and SOLID164 element for PEK explosive and fluid for BC1	124
	(b) Free field pressure history plot in front of Lining Plate for PPL due to explosion of PEK	124
	(c) Deflection history plot for PPL due to explosion of PEK	125
	(d) Principal Stress history plot for PPL due to explosion of PEK	125

6.15	(a) Free field pressure history plot in front of Lining Plate of PPL due to explosion of TNT for BC1	125
	(b) Deflection history plot for PPL due to explosion of TNT	125
	(c) Principal Stress history plot for PPL due to explosion of TNT	126
6.16	(a) Free field pressure history plot in front of Lining Plate of PPL due to explosion of C4 for BC1	126
	(b) Deflection history plot for PPL due to explosion of C4	127
	(c) Principal Stress history plot for PPL due to explosion of C4	127
7.1	Geometry of PPL as specimen for experimental investigations	129
7.2	Dimensioned sketch of Pressure Testing Chamber designed to provide pressure loading on PPL	131
7.3	(a) Experimental setup for load – deflection investigation of the perforated plate with lining	132
	(b) Side view of the experimental setup indicating the pressure testing chamber and PPL	132
	(c) View of digital based micro pressure gauge to measure the applied pressure on the lining side of the PPL	133
	(d) View of the vernier caliper to measure the deflection of the plate at the perforated plate side of PPL	133
7.4	Finite element model of PPL with SHELL63 element for BC3	135
7.5	Load – Deflection plots of PPL obtained from experiment and from finite element method	136
7.6	Schematic sketch of plan view of experimental set up indicating PPL with acoustic barrier, explosion location, 8 numbers of pressure blast gauge positions and data acquisition system	138
7.7	(a) View of lining plate along with the acoustic barrier made of plywood assembled with the PPL	140
	(b) View of perforated plate along with the acoustic barrier made of plywood assembled with the PPL	140
	(c) Two numbers of blast gauge placed in front of the lining plate	140
	(d) Six numbers of blast gauge placed at the rear side of lining plate and at the perforated plate side	140
	(e) Plume emanating from water surface after explosion of 30 gm of PEK explosive placed at a stand off distance of 1m	140
	(f) Time history plot of free field pressure recorded by 8 numbers of pressure blast gauges using data acquisition system	140
	(g) Time history plot of free field pressure recorded by pressure blast gauge	

	positioned in front of lining plate through channel 2	141
	(h) Time history plot of free field pressure recorded through channel 2 for 400 microsecs	141
	(i) Time history plot of free field pressure recorded by pressure blast gauge positioned at the rear side of lining plate through channel 3	141
7.8	Maximum pressure at various distances as measured using pressure blast gauges superimposed with the PPL	142
7.9	(a) Finite Element model of PPL with SHELL163 element for geometry and SOLID164 element for PEK explosive and fluid for BC3	145
	(b) Free field pressure history plot in front of Lining Plate for PPL due to explosion of PEK	145
	(c) Free field pressure history plot in front of Lining Plate for PPL due to explosion of PEK for 2000 microsecs	145
	(d) Deflection history plot at centroid of lining plate of PPL due to explosion of PEK	146
	(e) Principal Stress history plot at centroid of lining plate of PPL due to explosion of PEK	146

ABBREVIATIONS

ALE	Arbitrary Lagrangian - Eulerian
AUV	Autonomous Underwater Vehicle
BC	Boundary Condition
BC1	Boundary Condition 1 - Nodes at top and bottom horizontal edges: all degree of freedom arrested, Other 2 continuous side vertical edges: symmetry boundary condition (U_x , θ_y and θ_z arrested) and Along stiffener positions: transverse translation U_z arrested.
BC2	Boundary Condition 2 - Nodes at top and bottom horizontal edges: U_x , U_y and U_z are arrested, Other 2 continuous side vertical edges: symmetry boundary condition (U_x , θ_y and θ_z arrested) and Along stiffener positions: transverse translation U_z arrested.
BC3	Boundary Condition 3 - all nodes along four edges fixed.
BC4	Boundary Condition 4 - all nodes along the four edges : U_x , U_y and U_z are arrested.
C4	Composition 4 explosive
CEL	Coupled Eulerian - Lagrangian
COA	Coefficient of Area
COP	Coefficient of Perforation
DAA	Doubly Asymptotic Approximation
Def	Deflection
DF	Deflection Factor
EBC	Effect of Boundary Condition
EBT	Explosive Bulge Test
EHP	Elliptical Horizontal Perforation
EOS	Equation Of State
EP	Elliptical Perforation
EQS	EQuivalent Solid

EVP	Elliptical Vertical Perforation
FSI	Fluid Structure Interaction
ft	feet
HP	Horizontal Perforation
Hz	Hertz
JWL	Jones – Wilkens – Lee
k	keyword file
kPa	kilo Pascal
KSF	Keel Shock Factor
lb	pound
m	meter
mm	millimeter
Mbar	Mega bar
MIL	Military
MPa	Mega Pascal
MPS	Maximum Principal Stress
NPP	Non Perforated Plate
psi	pound per square inch
Pa	Pascal
PEK	Plastic Explosive Kirkee
PP	Perforated Plate
PPL	Perforated Plate with Lining
SCF	Stress Concentration Factor
SHP	Stadium Horizontal Perforation
SP	Stadium Perforation
SPSS	Statistical Package for the Social Sciences
SVP	Stadium Vertical Perforation
TNT	Tri Nitro Toluene
VMS	von Mises Stress
VP	Vertical Perforation

NOTATIONS

Alphabets

2-D	2 Dimensional
3-D	3 Dimensional
a	First order volume correction to γ_0
A, B	User defined input parameters and constant for each type of explosives.
C	Intercept of the v_s - v_p curve,
D	Detonation velocity
E	internal energy density per initial volume
F	Burn fractions
K	linear elastic stiffness
K_G	geometric stiffness matrix
m, n	Modal indices
p	Input pressure
P_0	Initial peak pressure
$p(t)$	Pressure at time (t)
R	Stand off distance
R_1, R_2	User defined input parameters and constant for each type of explosives.
S_1, S_2, S_3	Coefficients of the slope of the $v_s - v_p$ curve,
t	Thickness of the lining plate.
t_0	Time for pressure to reduce to (P_0/e) , referred as time constant.
t_1	Thickness of the perforated plate
U_x, U_y, U_z	Translation along x, y and z coordinates
v_p	Particle velocity
v_s	Shock velocity
V	pressure as a function of relative volume
w	Charge weight

x, y, and z	Axis of the coordinate system
γ_0	Gruneisen gamma
$\theta_x, \theta_y, \theta_z$	Rotation about x, y and z coordinates
μ	$\mu = \frac{\rho}{\rho_0} - 1$
ρ	Current density of seawater (or) material
ρ_0	Initial density
ω	User defined input parameters and constant for each type of explosives.

Miscellaneous

%	Percentage symbol used to express comparison
ANSYS	Finite element analysis software
ANSYS LS-DYNA	Finite element explicit analysis software
BEAM188	Structural element used from ANSYS
FLUID30	Fluid element used from ANSYS
SHELL63	Structural element used from ANSYS
SHELL93	Structural element used from ANSYS
SHELL163	Structural element used from ANSYS LS-DYNA
SOLID45	Structural element used from ANSYS
SOLID164	Structural element used from ANSYS LS-DYNA
SOLSH190	Structural element used from ANSYS

CHAPTER 1

INTRODUCTION

1.1 INTRODUCTION

Plate is two dimensional structural continuums which have small thickness compared to lateral dimensions. These structural members resist transverse loads by bending. Plates constitute a variety of structural components like flanges of a beam or floor, side shell and deck of a ship. These members are generally stiffened to control the deflections and stress levels.

Perforations are geometric discontinuities made in the plate by removing the material in a particular geometry as warranted by the situation. These perforations may be provided for the passage of some attachments like pipelines or for positioning transducers. Plates with perforations are generally referred as Perforated Plate (PP). There are situations where the perforated plate is provided with a lining on one side making it Perforated Plate with Lining (PPL). The acoustically transparent domes to protect the underwater sonar arrays are the best example for PPL.

The geometric discontinuities impart stress concentration and PP and PPL are no way immune to this. The problems of rectangular plate with circular or elliptical cutouts subjected to in-plane loads are dealt by Timoshenko (1959). A few more configurations are solved and equations for stress and deflection are given by Young (1989). The analysis of multi holed plate has attracted the attention of many engineers and designers due to its widespread use in underwater platforms, in the heat exchangers and in other similar equipments. The problem addressed in the present study pertains to the estimation of structural response of PP and PPL with large number of geometric discontinuities used in the underwater applications by finite element method and their validation by experiments.

Domes are widely used in subsea environment as structural members associated with acoustic systems like sonar. These domes are positioned in the free flooded area and hence referred as ‘water backed structures’ (Rajendran and Lee, 2008) where the structure is immersed in water medium. Such domes form part of the outer hull of a submarine, acting as an acoustically transparent screen and protecting the sonar arrays. Perforated plate with lining, thin and thick plate and double wall structure are different type of domes required in such applications. These domes may be exposed to the underwater explosions and the domes have to remain functional after exposure to shock loads. These domes are usually made of Titanium grade alloy metals. Fig.1.1 is the view of a submarine with acoustic domes. Fig. 1.2 is a view of PPL dome used in bow, top of the submarine. This dome has a streamlined shape considering hydrodynamics and acoustic aspects. The protective cover in the form of a lining plate is an essential structural requirement in order to minimize the drag and hydrodynamic noise.



Fig. 1.1: Submarine with PPL dome configuration

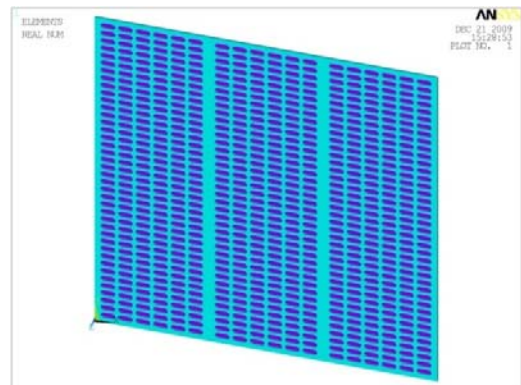


Fig. 1.2: PPL under investigation

1.2 STRUCTURAL ANALYSIS OF PP AND PPL

Analysis of PP and PPL cannot be kept in the purview of conventional plate analysis. The most adopted and preferred procedure is the one using finite element method. Thin and thick plate theories exist for the analysis of plate which eventually differ based on the accountability of shear effects and based on these theories, various finite elements are

made available in commercial software packages. Many of them are made immune to inherent deficiencies like shear locking etc., The structural behavior of the plate is normally influenced to a great extent by the presence of geometric imperfections in the form of cutouts. This is beyond the level of consideration for stress concentrations. The geometry of the PP resembles a grillage and there may be much of the plate action that may be lost. When PPL is considered, the lining plates make the plate a structural composition of continuous strips of different but uniform thicknesses. In this context, it is relevant to investigate the structural behavior of PP and PPL with plate, solid and beam finite elements.

Since the sonar domes are positioned in the free flooded area, hydrostatic pressure head is not active on the PP or PPL. The sonar domes are used in the moving platforms and drag generated during the specified speed of the platform is the dominant load acting on PPL. This load varies and depends on the shape of the bow end of the outer hull and the type of the platform. As per the convention, the underwater sonar domes are to be designed for the hydrodynamic drag and analysed for noncontact underwater explosion. Here the noncontact is defined when the stand off distance between the explosive charge and target, is more than 10 times the radius of the explosive charge (Rajendran and Lee, 2008).

1.3 FLUID STRUCTURE INTERACTION

Many interaction problems involving various continuous media arise in engineering fields and one of them is 'Fluid Structure Interaction' (FSI). The term FSI describes those problems in which the structural and fluid responses are strongly coupled. In other words, the structural dynamic response is significantly affected by the presence of the fluid. Dynamics of an elastic body interacting with a fluid medium is substantially different in the absence of that medium. The fluid structure interaction arises when fluid and structure undergo motion and in the process exert forces upon each other. FSI problems are encountered in the analysis of floating structures and underwater bodies and vehicle like towed objects, submarines and Autonomous Underwater Vehicle (AUV).

The fluid structure interaction problem requires the simultaneous solution of the structural equations of motion and the acoustic wave equation, while enforcing an interface boundary condition at the “wetted” surface of the structure. This interface boundary condition, in effect, couples the two systems of structural and acoustic equations. The structural response depends upon the pressure loads applied by the fluid and the fluid pressures are themselves affected by the structural motions. In general, considering the complexity of fluid structure interface, the analytical solution is difficult. Hence finite element analysis is essential for such problems.

Vibration of structure in contact with surrounding fluid exerts a reaction force on the structure which is represented as added mass to the dynamic response of the component without affecting its structural stiffness (Sinha et. al, 2003). The kinetic energy of the fluid couples to that of the structure, thus producing an added mass effect with respect to the structural responses (ANSYS, 1992). For moderate to high frequencies of vibration, the compressibility of the medium comes into play and it becomes an acoustic FSI problem.

When the pressure pulse generated due to an underwater explosion comes in contact with any structure present in the fluid medium, the structure undergoes rigid body motion and elastic or plastic deformation occurs. The surrounding fluid medium is disturbed because of the scattering of shock waves due to the presence of the structure. The methods used for solving the structural problems and their features are given in Table 1.1. Studies using software based on finite element method are adopted in the present investigations.

Table 1.1: Methods and features for structural analysis of underwater structures

Sl.No.	Method	Feature
1	Exact solution by series expansion	Results available only for simple models
2	Finite element method	Larger computer memory, Fluid mesh shows the wave propagation, Memory can be limited by usage of infinite number of elements.
3	Doubly asymptotic approximation	Accurate for both late & early time but the fluid is not modeled.
4	Boundary element method	Small densely populated matrices

1.4 UNDERWATER EXPLOSION

When an explosion occurs in water, a pressure wave with high magnitude arrives at the boundary between the reacting explosive and water, and begins to be relieved along with an outward motion of water. The resulting pressure wave has practically a discontinuous rise in pressure followed by an exponential decay, with duration of microseconds. This disturbance in water, which is a steep fronted wave referred as the shock wave, is propagated radially outward as a wave of compression in water.

After the emission of the shock wave, the initial high pressure in the gas bubble decreases considerably. However, it is still much higher than the equilibrium hydrostatic pressure. The water in the vicinity of the bubble has a large outward velocity and the diameter of the bubble increases rapidly. The expansion continues for a relatively long time and the internal gas pressure decreases gradually, but the motion persists because of the inertia of the outward flowing water. Later, the gas pressure falls below the equilibrium value determined by the sum of the atmospheric and hydrostatic pressures. Then the outward flow stops and the boundary of the bubble begin to contract at an increasing rate. The inward motion continues until the compressibility of the gas acts as a powerful check to reverse the motion abruptly. Thus an oscillating system is constituted by the inertia of water together with the elastic properties of the gas and water, and the bubble undergoes repeated cycles of expansion and contraction. At each of the reversal of contraction to expansion, energy is emitted in the form of pressure wave advancing radially outward from the bubble. The peak pressure in the first bubble pulse is less than 10 to 20% of that of the primary shock wave, but its duration is much larger, and the areas under the two pressure-time curves are comparable. Because of buoyancy when in equilibrium with the surrounding pressure, the gas bubble eventually rises to the surface. On the arrival of the incident shock wave at the free surface, a spray dome can be observed. Then, due to the bubble pulses, white plumes burst into the air, followed by a black plume caused by the gaseous products of explosion.

As a result of underwater explosion, primary and secondary shock waves are formed. The primary shock waves are generated because of localized compression of surrounding water media. Secondary shock waves are generated by the oscillating bubble of detonation products (gas bubble) of low intensity but of longer durations. A detailed propagation of bubble oscillation due to the underwater explosion has been described by Cole (1948).

In a complex engineering study, utilization of numerical methods as an adjunct to experiment is of proven value. Analysis based upon valid techniques not only permits enlightened interpretation of experimental data, but provides a rational basis for interpolation and extrapolation of the data. Analytical extension of data is often essential since the complexity of today's problems, frequently does not permit exhaustive experimental work without prohibitive cost and effort. But the validity of a predictive method must be assessed before it can be applied with confidence. The way in which an analyst attempts to solve any shock problem depends on the scope and complexity of the structural configuration, the degree of accuracy expected on the response prediction and the available level of computational resources. Analysis methods and procedures which exist may be placed into two broad categories viz., the numerical and the experimental.

Early studies of the shock problem for which closed form solutions are obtained have been limited to the simple geometries and even in those cases the evaluation of solutions has been difficult during the initial phase of shock wave transmission. Widely accepted methods to predict dynamic response of underwater shock, are finite element method and boundary element technique.

Assisted by the growth of digital computing and the availability of a number of software codes, the finite element method is increasingly applied to solve complex structural configurations for underwater shock. Lagrangian finite element methods are commonly used to model the structure, while Eulerian method is used to model the water medium.

1.5 SCOPE AND OBJECTIVES

By keeping in view of the specific structural features of PP and PPL, and effects of explosion load, the following are set as the objectives of the present study.

- a. To propose unit cell configuration for PP and PPL and to establish its utility in the linear static analysis.
- b. To conduct finite element analysis of PP and to study the linear elastic behavior, geometrically nonlinear behavior, free vibration characteristics. The structural response due to underwater explosion has also been estimated using finite element method incorporating fluid structure interaction effects.
- c. To conduct finite element analysis of PPL and to study the linear elastic behavior, geometrically nonlinear behavior, free vibration characteristics. The structural response due to underwater explosion has also been estimated using finite element method incorporating fluid structure interaction effects. It is also envisaged to conduct a pressure testing chamber experiment to obtain load deflection curve for PPL.
- d. To conduct finite element analysis of PPL, to estimate the free field pressure and structural responses of the plate due to underwater explosion.
- e. To perform experimental investigations on the PPL to measure the free field pressure due to underwater explosion using shock tank facility.

Finite element method has been adopted for the linear static, geometrically nonlinear and free vibration analysis and commercial software ANSYS (1992) has been used for this purpose. The explicit method based software ANSYS LS-DYNA (2003) has been used for the shock analysis with fluid structure interaction. A few of the finite elements available in the software library are experimented to identify the suitable one, for the above purpose. The influence of rotation restraints along the boundary is also investigated upon. The scope of this numerical investigation has been extended to elliptical geometry perforation with horizontal and vertical orientations apart from stadium geometry perforation.

1.6 ORGANISATION OF THESIS

Chapter 1 deals with the introduction to PP, PPL and the related analysis with their applications along with the scope and objectives. Chapter 2 gives the review of the literature and the research reported in similar area have been presented. Chapter 3 lists out the details on modeling of the perforated plate and various techniques used in the analysis. This chapter also gives brief description on finite element software and other parameters like loading, boundary conditions etc., considered in the analysis. In chapter 4 the concept of unit cell, convergence features, parametric study and the stress concentration and deflection factor at the perforations have been calculated and presented. In chapter 5, the investigations are focused on linear static, geometric nonlinear, free vibration and shock analysis of perforated plate. Chapter 6 introduces a lining plate on perforated plate and its effect has been estimated on structural and vibration responses. Chapter 7 deals with experimental studies on PPL, to plot the load deflection curve and to measure the free field pressure for the given explosive load. Chapter 8 gives the summary and conclusions of the investigations and recommendations for future work.

CHAPTER 2

LITERATURE REVIEW

2.1 INTRODUCTION

This chapter presents a comprehensive review of the literature dealing with various studies carried out on perforated plate for static, nonlinear, vibration and shock analysis. Many classical books are available on the theory of plate and shell. Compilation of structural responses like displacements and stresses for various configuration of plate and shell for various loading and boundary conditions and which can be used as ready reckon to arrive at the responses are available and the one authored by Young (1989) has been frequently used. Similarly Blevins (1978) contains the compilation on natural frequencies and mode shapes of plate and shell.

The transient interaction between a flexible structure and the surrounding infinite medium using Doubly Asymptotic Approximation (DAA) approach has been investigated by Geers (1978); Geers and Felippa (1983); Geers and Zhang (1994a; 1994b). These publications give qualitative and quantitative estimations of Fluid Structure Interaction (FSI) of components of spherical geometry immersed in water. The superiority of second order DAA over the first-order DAA technique has been explored as well. Namkoong et al. (2005) have applied P2P1 Galerkin finite element method to Navier-Stokes equation in conjunction with the Arbitrary Lagrangian-Eulerian (ALE) technique for solving FSI problems. The effect of Reynolds' number, geometry, damping, fluid density and fluid viscosity have been studied. It has been concluded in this paper that the added mass is linearly proportional to the fluid density but independent of fluid viscosity. While using finite element solution for dynamic problems involving elastic structure and fluid, pressure and displacement are taken as unknown parameters and the disadvantages in each case have been discussed in an article appeared in the "letter to the editor" by Everstine (1981). A velocity based finite element formulation is recommended in lieu of pressure based finite element formulation in this study by author.

In case of shell with stiffener, Prusty and Satsangi (2001) carried out static analysis by applying improvement over the degenerated shell concept. The new method to calculate stiffness matrix of arbitrary oriented stiffeners in the plate element on the basis of equal displacements at the junction of plate and stiffener is adopted for static analysis. The authors have used eight noded shell and three noded curved element for stiffener.

The detailed review of literature related to the present study has been given under subsequent subheadings viz., perforated plate, vibration of plate and underwater explosion.

2.2 PERFORATED PLATE

Usages of ‘unit cell’ concept and ‘equivalent solid method’ concept have been widely employed for estimating the structural response of perforated plate. The circular perforation geometry with regular penetration pattern for the in-plane loading has been investigated by many and has been reported. However, Imaizumi et al. (1993) have studied the irregular penetration pattern and the procedure for evaluating real stresses has been devised through stress multiplier factor and nominal stresses using equivalent elastic constant method. The deflection and stress estimated from numerical results are validated with the experimental methods. Jones et al. (1999) have developed an algorithm to extend the concept of Equivalent Solid (EQS) method of perforated plate for elastic-perfectly plastic material and demonstrated this aspect with a number of example problems. Hauptmann et al. (2001) have brought out advantages of “solid-shell” element over the conventional shell element, for the application of metal forming and impact analysis involving large stretching and bending with small radii. Harnau and Schweizerhof (2002) also have discussed the characteristics of “solid-shell” elements including locking phenomenon and in order to avoid the effects of transverse shear and membrane locking, assumed strain method has been proposed. Cantemir et al. (2004) have used equivalent solid method for analyzing perforated plates in the finite element modeling and simulation. The equivalent solid method has been employed for the estimation of equivalent material property for the triangular penetration pattern. In order to compute stresses in the perforated plate with this method, the weakening effect of

holes has been described in terms of the ratios of the elastic properties of perforated and solid plates.

Most of the reported numerical analysis have been carried out using the finite element software ANSYS (2004). The influence of various finite elements on the analysis of perforated plate has been discussed for specific boundary conditions and loadings. Kaap et al. (1997) have discussed the finite element modeling of perforated plates using ANSYS and dynamic effective stiffness has been estimated. SHELL63 element gave better performance in the prediction of static deflection and mode frequencies for solid plate, whereas SHELL93 element has been found suitable for perforated plate. In case of vibration problems, dynamic effective stiffness has been reported to be more appropriate than equivalent static stiffness. Webb et al. (1995) have used unit cell concept for regular perforated plate and have used solid brick shaped module of an equivalent anisotropic plate in lieu of isotropic perforated plate. Stress multiplier factor has been used to predict the behavior of plate on the periphery of perforations for square and triangular patterns. Cantemir et al. (2007) also used the concept of unit cell and also applied equivalent solid method. The ratio of elastic properties, Young's modulus and Poisson's ratio for a perforated plate and a solid one have been used in stress estimation. Perforated plate modeling and analysis using finite element method is illustrated in this paper. However Prabu et al. (2004) have applied the concept of unit cell in the metal matrix composites to analyse the effects of volume, fraction, fiber shape, fiber distribution and matrix on stress and strain status as well as potential damage to fiber cracking or interface debonding. A thick plate with large number of holes has been analysed by David and Hoshi (1983) using an equivalent homogeneous material with numerically modified effective elastic constants and yield stress. Maiorana et al. (2009) have dealt with the perforated plates subjected to in-plane compressive loads. Four noded plate element has been used for the numerical analysis. Elastic instability has been studied for square and rectangular plate with centralized or eccentric circular holes.

The nonlinear analysis of perforated plate has been dealt by Paik (2007) with parametric study on perforation dimension using ANSYS and he has come up with the predominant status of ultimate strength over buckling strength. The author has derived an empirical

formula for first-cut strength estimates in reliability analysis. Suneel et al. (2007) have discussed the ultimate strength analysis using nonlinear static method with ANSYS. With proper validation and convergence studies, authors have extended the study to stiffened plate with opening. Using Statistical Package for the Social Sciences (SPSS), regression analysis has been carried out and design equations are developed and reported. The dynamic behavior of perforated plate submerged in water has been studied by Jo and Jo (2006a). The authors have brought out the difficulty to model perforated plate submerged in fluid and an attempt has been made to make an equivalent solid model with effective elastic constants. In order to study the impact analysis on perforated plate, Guo et al. (2003) used LSDYNA (2007) tool. Investigation has been focused on the usage of shell elements compared to conventional modeling with solid element for thin target plates. The behavior of the perforated plate at elevated temperature has been analysed by Nakamura et al. (2003) with equivalent solid material and validated with experimental results.

2.3 VIBRATION OF PLATE

Literature available on dynamic analysis of perforated plate is only a few. Peter (2001) has given an elaborate experimental procedure for the determination of the vibration characteristics of a plate. Chen et al. (1994) have developed a spline compound strip theory for the free vibration analysis of one directional stiffened and cross stiffened plates. The outcome of this method is in good agreement with that of experiment and analysis using finite difference method.

The easiness in usage of finite element method and computational effectiveness of the finite element formulations for free vibration analysis is brought out by Singh and Smith (1994). Four general finite element formulations viz., h – formulations, p – formulations, exact and mixed formulations and the dynamic element formulation have been discussed for simple cases like undamped, linear beam, frame and truss systems. From the studies based on these formulations, the relevance of free vibration analysis of slender structures like ship and submarine has been emphasized. George (1970) has studied slender structure like ship on flexural vibrations due to underwater explosion. The effect of

parameters like charge composition, weight, stand off distance, and volume of explosion bubble have been considered in this study. The principal mode patterns are verified by independent experiments. While carrying out dynamic analysis of this type of water backed structures, the added mass becomes a very important factor. Hagedorn (1994) brought out the difference in natural frequency for a plate ‘in vacuum’ and for water backed condition. An exact solution method is formulated to include “added virtual mass factor” in this study. Hence thrust has been given to estimate the added mass. Equations are formulated for different configuration of the plates and are tabulated by Blevins (1978). However such details are not available for perforated plates. Sinha et al. (2003) have brought out an approximate method to arrive at the effect of added mass and damping for plate and for perforated plate. The effect of perforation on these two factors has been brought out. The validation is done with experimental approach. The effect of damping becomes negligible while water medium is considered as incompressible. Considering the difficulties with perforated plate and surrounding fluid medium, Jo and Jo (2006b) have restored to finite element method and solution is arrived at using ANSYS. The free vibration analysis of perforated plate submerged in fluid is modeled using elements SHELL63 and FLUID80 of ANSYS. Authors have attempted to place an equivalent solid, considering weakening effect of perforations.

While considering acoustic transmission and reflection characteristics of submerged plates, Nedwell et al. (1989) used plane wave theory to determine transmission and reflection coefficient. The authors have considered elastic properties of material and have verified these experimentally. The scattering of waves at the edge of the panel and boundaries of the tank are also considered. An experimental method of transmission coefficient is presented.

2.4 UNDERWATER EXPLOSION

The literature available on the study of air blast and the subsequent loading sequence and after effect on the structures has been reviewed. Nagesh (2005) has brought out with brief introduction on the propagation of pressure wave due to air blast at near field and far field. A typical solid plate with unstiffened and stiffened condition has been

considered for the finite element analysis and the responses are compared with those available from experimental method. However less number of literature are available on the study of underwater explosion and corresponding damage potential for the structures surrounded with water. Cole (1948) has brought out the theory of explosion with sequence of events in underwater explosion, its initial conditions and the dynamical properties of water in his text book. The author has used propagation theories to establish hydrodynamic relations for shock waves. He has performed detailed evaluation of shock wave propagation, and described the features of shock waves and stated a comparison of various shock wave theories. The author has given details on measurement of underwater explosion pressure using various equipments and provides photographs of various explosion cases. Details regarding motion of gas sphere, secondary pressure waves and surface effects of underwater explosion are also given. Similar studies are carried out by Singh (1982) for the propagation and attenuation of spherical shock waves in water using Whitham's method and Energy Hypothesis method. This theoretical study is validated experimentally and concluded that energy hypothesis method is more realistic towards experimental one.

Mair (1999a) has discussed four hydrocode methodologies based Lagrangian, Eulerian, Coupled Eulerian – Lagrangian (CEL) and Arbitrary Lagrangian – Eulerian formulations to deal with Fluid Structure Interaction. It has been concluded that ALE is best suited to study structural response to underwater explosions from among the four. Similar results are reported by Kim and Shin (2008) on the application of ALE technique for an underwater structural design problem and they have concluded with the suitability of ALE based code to evaluate structural damage due to underwater explosion. Their investigations extended to the numerical experimentations with various mesh densities for finite element models at sea water and the explosives. The reported research are on the air backed structures like ship and submarine pressure hull structures rather than water backed structures like sonar dome. For example, Liang and Tai (2006) have developed a procedure to examine the transient responses of a ship hull subjected to noncontact underwater explosions. They have coupled the nonlinear finite element method with DAA method. The transient dynamic effect, geometric nonlinearities,

elastoplastic material behavior and fluid-structure interaction have been considered in the formulation. The authors have concluded the importance of Keel Shock Factor (KSF) to describe shock severity considering various charge weights, distance and incident angle. They obtained acceleration, velocity and displacement time histories due to underwater shock at different locations. Ramajeyathilagam (2000) has described various FSI techniques that can be applied to shock related problem and explained structural analysis methodologies under shock loads. The author proposed mathematical formulation of the problem for nonlinear dynamic analysis and proposed elastoplastic model for dealing with material nonlinearity. He has also explained the failure criterion in detail. The importance of FSI interaction on submerged structure was also brought out by Lai (2007). Transient dynamic analysis of a spherical shell with an opening and exposed to underwater explosion is carried out. The effect of stand off distance and shock waves in sea and in air are compared. In order to carry out experimental study for the failure of air backed structure, Explosive Bulge Test (EBT) is a standard procedure to be followed and Keith (2007) has studied on air backed ship like structures for a given underwater explosion and EBT experiment has been carried out on sample plates using Tri Nitro Toluene. The author has also discussed various numerical solvers available on FSI problems and recommendations are given for usage. Rajendran (2009a) has provided a method to carryout numerical study of the air backed plate for explosion bulge test. The outcomes of the numerical investigations are experimentally validated.

A number of commercial software packages are available to deal with underwater explosion problems along with FSI. Mair (1999b) has attempted the comparison of DAA and various hydrocodes like DYNA, FSI ADINA, USA, DYNA3D, LSDYNA, MSC DYTRAN. Shin and Santiago (2002) have used USA code coupled with NASTRON CFA code for underwater shock problems. The fluid cavitation effect has been studied on the surface ship modeling and method of avoidance / implementation of cavitation has been suggested. They have recommended for the inclusion of cavitation effect within the DAA boundary.

Many of the studies are based on sample specimen of circular and rectangular plates for air backed conditions whereas those on water backed structure are only a few. Rajendran

and Narasimhan (2006) have developed mathematical models for circular and rectangular plates. It is observed that maximum von Mises stress for rectangular plate is 1.132 times more than that of the circular plates and this has been validated with experiments. Detailed phenomena of reloading effects on a circular and rectangular air backed plates are enumerated by Rajendran (2008). The author has also brought out that the cavitation and gas bubble loading are part of reloading. Damage due to reloading is maximum and equal to that of primary shock loading for a depth of explosion that is twice the stand off. The phenomena of air and underwater explosions and their effects on plates have been brought out by Rajendran and Lee (2009) in a detailed review. Various phases of the explosion have been discussed thoroughly. On study of potential damage due to air backed and water backed condition, Rajendran and Lee (2008) have brought out the damage potential due to noncontact underwater explosion for air and water backed plates. The analytical approach is adopted to find out maximum velocity and displacement of the plate for the two conditions. The authors have concluded that water backed plates attain a maximum kick off velocity of 65% to that of air backed plates and 50% displacement to that of air backed plates. Rajendran (2009b) has discussed on the effect of coupling factor and its influences on shock factor. The concept of shock factor is introduced for inelastic damage of target plate. This is applied for air backed and water backed plates for comparison. It is concluded that inelastic deformation undergone by the water backed plates is significant in comparison with that of the air backed plates. Comparison of air blast and underwater explosion has also been made by Lal and Rajesh Kumari (2004). The authors have brought out a method to correlate shock decay pattern of air blast and underwater explosion using bulk modulus of medium. This has been experimentally validated.

In order to study the effect of underwater explosion using numerical methods, many authors used different software existing in this field. MSC Dytron and UNDEX were among the few of such software used during initial days. Peiran and Arjaan (2006) have described the method to carry out simulation of underwater explosion for air backed structures using MSC Dytron. The procedure is compared with UNDEX and advantages of MSC Dytron are brought out. Now a days, software such as ABAQUS and LSDYNA

are used for the study of underwater explosion. D'Souza et al. (2006) have used ABAQUS to study the stresses in the water backed structure due to underwater explosion. An overall concept on the modeling and methodology on the design of sonar dome has been presented. The design and analysis have been based on with the finite element analysis software package ABAQUS. This model includes water flooded compartment and exterior fluid region where FSI is relevant and the stress field in the structure has been examined. Ma and Andrews (2001) brought out the pros and cons of cavitations in the underwater explosion scenario and also highlighted various methods of implementation while using LSDYNA software. The investigation using LSDYNA includes variety of explosives, its orientation, stand off distance and results are established with validation through experiments. Adamik et al., (2004) have discussed the effect of orientation of charges; and suitability of Jones – Wilkens – Lee (JWL) method as Equation Of State (EOS) for TNT, and ideal gas equation for air. The outcome of the analysis using LSDYNA has been validated with experimental results. The study is based on air blast waves. A brief summary on advantages and disadvantages on Eulerian and Lagrangian codes have been given. Vulitsky and Karni (2009) have used LSDYNA for the shock analysis of air backed ship structure. EOS of JWL has been used for high explosive TNT. They also brought out the limitations of carrying out shock analysis in two stages. A quarter of the physical problem was made in LSDYNA and physical quantities such as stresses, displacements etc have been computed. Urtiew et al. (2008) investigated pressure gauge data during shock initiation process with explosive Composition B and Composition 4 (C4). They used modeling and then experimentally validated pressure. Sourne et al. (2003) have studied the structural response of submarine for underwater explosion using LSDYNA and has been experimentally validated. The various effects of shock wave and bubble pulsation on ship structure have been studied. The response parameters viz., deflection and stresses are the output from the analysis. Hung et al. (2009) have analysed cylindrical shell structures for underwater explosion and experimentally validated. Three structures with varying stand off distance have been analysed. It is concluded that the response received by structure in shallow depth gives less energy and smaller strains.

Few authors have studied the effect of underwater explosion for the fiber reinforced composites and sandwich structures. Batra and Hassan (2007) have discussed the effect of underwater explosion load to fiber reinforced composites. The structural damage due to fiber breakage, matrix cracking, fiber or matrix debonding and delamination have been studied. The results give preliminary information on composite structure's design for maximizing the energy absorption and hence increasing structure's resistance to blast loads. Similarly, Qiu et al (2003) have analysed sandwich beam for pressure due to shock loading and compared with that available in literature. The effect of material elasticity and strain hardening of steel on the beam response have been studied and the influence of the core of sandwich beam on dynamic response has also been brought out.

2.5 COMMENTS

Knowledge and information base are available in the form of several text books and volumes of research publications in analysis of plate and shell structures. But the source is not exhaustive as far as perforated plates are concerned. A definite dearth of research especially regarding the assessment of behavior of structural components constituted with PP subjected to underwater explosion has been felt. From the review of literature the extensive application of finite element method for the structural analysis has been noted and relevance of experimental investigations for the validation has also been felt. Application of finite element software ANSYS for the structural analysis and ANSYS LS-DYNA for shock analysis have been recognized by the earlier authors. Based upon these observations, the objective of the present investigations have already been set as the numerical investigations on PP and PPL using ANSYS and ANSYS LS-DYNA and experimental investigations on PPL using shock tank facility.

CHAPTER 3

STRUCTURAL ANALYSIS AND NUMERICAL MODELS OF UNIT CELL, PERFORATED PLATE AND PERFORATED PLATE WITH LINING

3.1 INTRODUCTION

The present study involves the numerical investigations pertaining to the finite element analysis of PP. It is essential in this context to discuss the various aspects of geometry of PP, concept of unit cell and the basis of development of analytical models for them. The necessity for description of the relevance and details of static and dynamic analysis of underwater PP has also been felt. These aspects are dealt in this chapter.

3.2 GEOMETRY OF PERFORATION

PP has single or multiple cutouts of specific geometry and orientation. These perforations are geometric discontinuities in the plate and result in stress concentration which can cause local failure by yielding. The geometry of the perforation studied herein, is that with two semi circles at the shorter sides of a rectangle and is named “Stadium Perforation” (SP). A dimensioned sketch of the stadium perforation is shown in Fig. 3.1(a). In addition to the stadium geometry, elliptical geometry is also considered in the present study and referred as “Elliptical Perforation” (EP). A dimensioned sketch of the elliptical perforation is shown in Fig. 3.1(b). The stadium configuration has no sharp corners and is immune to the ill effects of stress concentration to some extent. A plate of same dimensions as that of PP, but without any cutout is considered for the analysis for the sake of comparison of deflection and stresses and is termed as Non Perforated Plate (NPP).

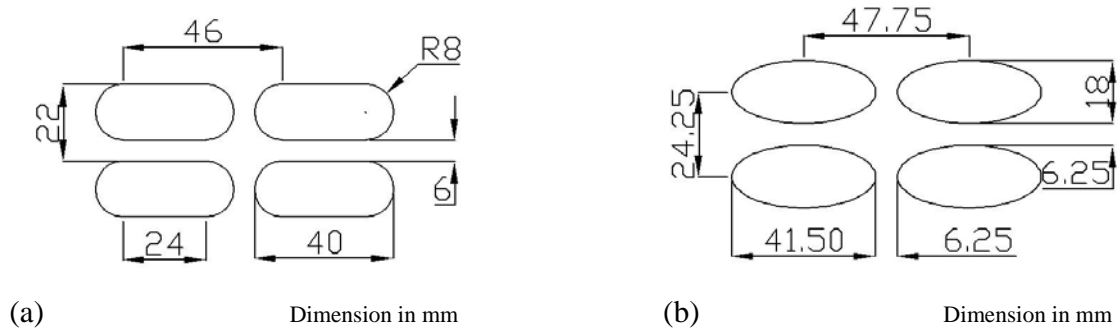


Fig. 3.1: (a) Geometry of Stadium Perforation and (b) Geometry of Elliptical Perforation

The perforations are arranged in rectangular array ‘i x j’ with ‘i’ number of rows along the X axis (longitudinal) and ‘j’ number of columns along the Y axis (transverse). The spacing between the two perforations in both the directions is maintained as equal and termed as ligament width.

3.3 TYPE OF ANALYSIS

It is proposed to conduct linear static analysis, geometric nonlinear analysis, free vibration analysis and shock analysis in the present investigation. Linear static analysis is concerned with the linear behavior of elastic continua under prescribed boundary conditions and statically applied loads, where the principle of superposition is valid. This analysis of plate is based on the small deflection theory where the stress strain relations and strain displacement relations are linearised. In this method of analysis the change in geometry of the structure is not taken into account while deriving the equilibrium equations or stiffness matrix. In general, applied loads include prescribed forces and pressures. Displacement and stresses are the desired quantities from this analysis. In finite element linear static analysis, the structure stiffness matrix is calculated and is treated with applied loads to evaluate the nodal displacements, which are subsequently operated on, to find out stresses. The components of the nodal stresses are further used to calculate von Mises Stress (VMS) and Maximum Principal Stress (MPS). The geometric nonlinear analysis deals with the nonlinear behavior of structure under static loading. This is carried out with an incremental and iterative procedure.

The free vibration analysis is a prerequisite for carrying out transient dynamic analysis in order to determine the natural frequency of the structure which is a vital parameter that decides the total time period for transient dynamic analysis. The natural frequencies and mode shapes of plates are functions of two integer indices (modal index) 'm' and 'n'. Each of these indices is associated with a flexural half wave number in one of the two plate dimensions. For each 'm' and 'n', a vibration mode exists, which gives rise to a natural frequency and an associated mode shape. Hence the natural frequency and corresponding mode shapes are studied for each configuration of plates. Fluid coupled vibration response of a plate is substantially different from its uncoupled motions. In the presence of fluid, hydrodynamic pressures are generated by the vibrating plate. These pressures modify the structural motion, which in turn modify the hydrodynamic pressure, resulting in a strong coupling between the fluid and the structure. Hence for a coupled structural fluid problem, the structure has to be modeled together with the fluid.

Underwater explosion creates impulse pressure which can severely damage subsea structures and systems. A prerequisite for analysis of dynamic response of such structures is the description of free field pressure waves. In order to estimate the influence of this on the structure, one needs to study the coupled problem of structure and fluid, in other words, the fluid structure interaction. The response of submerged structures to pressure pulses created by underwater explosions can in principle be predicted by shock analysis where the FSI problem is solved which involves the interaction of the vibrating structure with the surrounding water as well as with the pressure waves that are incident on the structure. The hydrodynamic pressure experienced by the structure is a result of radiation and diffraction effects associated with the FSI.

It is proposed to conduct static linear and nonlinear, free vibration and shock analysis using finite element method. It is proposed to use the commercial software ANSYS (1992) and ANSYS LS-DYNA (2003) to the above mentioned analysis. It is also projected to carry out the validation using experiments to measure deflection of PPL considering geometric nonlinear and free field pressure due to underwater explosion.

3.4 UNIT CELL

A 'Unit Cell' of PP is a geometric miniature and is carved out from a real PP where the dimensions of the perforation, ligament width and thickness are preserved but the number of perforation is restricted to 16. The perforations which are placed horizontally and oriented along the smaller side of the Unit Cell (X axis) are termed as "Horizontal Perforation" (HP) and geometry of Stadium Horizontal Perforation (SHP) plate is shown in Fig. 3.2(a). The perforations which are placed vertically and oriented along the longer side of the Unit Cell are termed as "Vertical Perforation" (VP) and geometry of Stadium Vertical Perforation (SVP) plate is shown in Fig. 3.2(b). The Fig. 3.2(c) gives the Elliptical Horizontal Perforation (EHP) plate and Fig. 3.2(d) shows the Elliptical Vertical Perforation (EVP) plate. Fig. 3.2(e) gives the dimension of Non Perforated Plate. The thickness of the plate is 6 mm.

The ratio of the area of the perforations to the area of the non perforated plate is termed as Coefficient of Perforation and this is kept same for both the horizontal and vertical perforated plates.

3.5 PLATE MODEL

The plate model of PP is composed by treating it as an assemblage of plate elements at interfacing nodes running orthogonally in longitudinal and transverse directions. The width of the plate element running in longitudinal direction is equal to portion of plate between the perforations in the transverse direction. The width of plate element running in transverse direction is equal to spacing between the perforations in longitudinal direction.

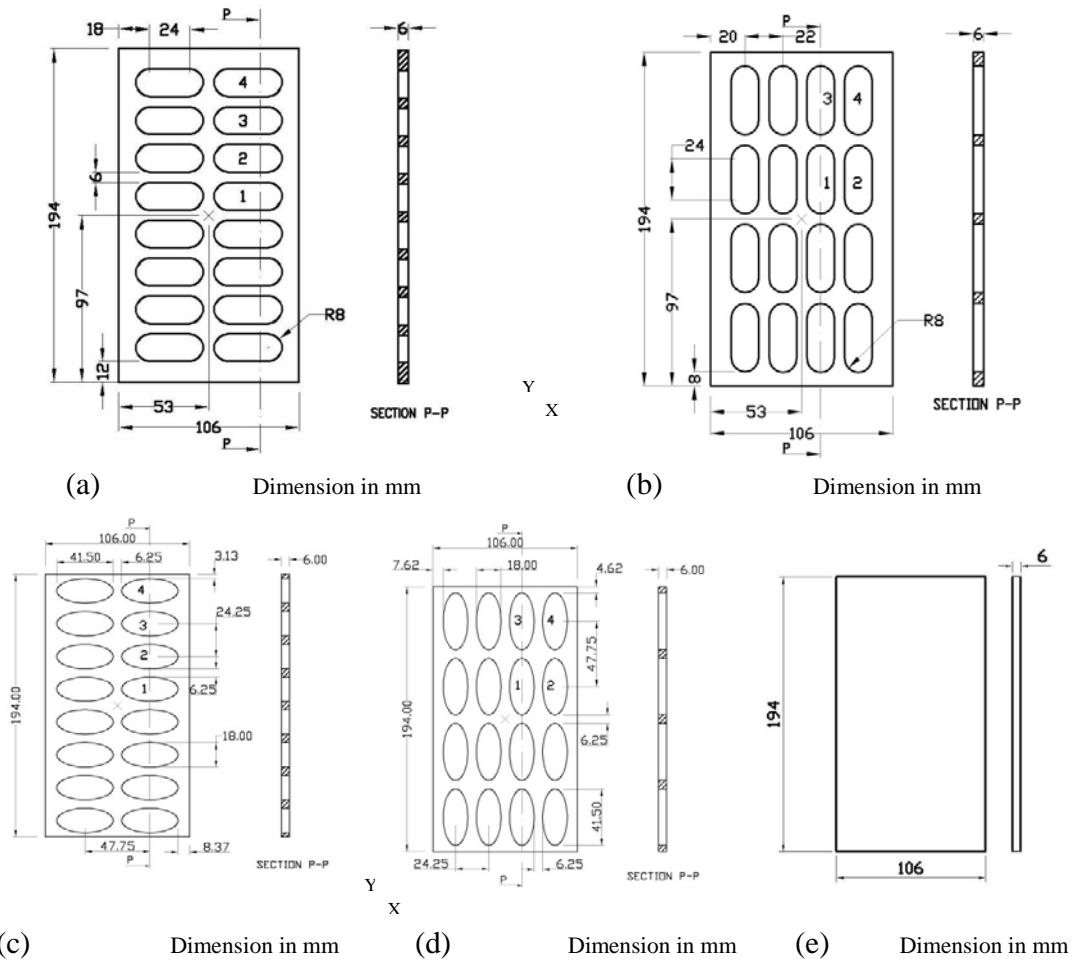


Fig. 3.2: (a) Geometry of unit cell of SHP plate, (b) Geometry of unit cell of SVP plate, (c) Geometry of unit cell of EHP plate, (d) Geometry of unit cell of EVP plate and (e) Geometry of unit cell of Non Perforated Plate.

In the plate model of perforated plate with lining, in order to get the effect of both perforated plate and the lining plate together, coupling of nodes with constraint equation method has been followed.

3.6 SOLID MODEL

The solid model of perforated plate is composed of solid or brick finite elements which do not possess bending characteristics. For PPL, the perforated plate and the lining plate are projected independently and nodes of each of the solid / brick elements of plate are coupled using constraint equations.

3.7 GRILLAGE MODEL

Grids or grillages are composed of beams intersecting orthogonally each other. The perforated plate with lining is replaced by a series of 'T' beams intersecting at right angles. The lining plate constitutes the flange of the 'T' beam and the perforated plate the web. The flange length of the 'T' beam running in longitudinal direction (X axis) is the center to center distance between two adjacent perforations in the transverse direction. The depth of the flange is equal to the thickness of the lining plate (t). The width of the web is the spacing between the two adjacent perforations in the transverse direction, and depth is equal to the thickness of the perforated plate (t_1). The flange width of the 'T' beam running in transverse direction (Y axis) is the center to center distance between two adjacent perforations (already closed with lining) in the longitudinal direction. The edge beams running in the transverse direction are modeled as 'L' beams. The flange width is equal to sum of edge clearance of perforations in the perforated plate and half the length of one perforation in that direction. The depth of flange is same as that of thickness of the lining plate. The configuration of the 'T' beam of the grillage model of PPL is shown in Fig. 3.3.

3.8 BOUNDARY CONDITIONS

The perforated plate with lining under investigation is a part of an acoustic dome of an underwater platform. The acoustic dome is a continuous plate along the X direction with 0.9 m as height (Y direction) and stiffened at an equal spacing of 0.3 m. The schematic sketch of a continuous plate is shown in Fig. 3.4. Considering the ship structural design method, 1-1-1 concept is adopted and thereby a plate of 0.9 m x 0.9 m is carved out for further analysis. The boundary conditions applied for this plate is tabulated in Table 3.1 and explained with reference to Fig.3.4.

Table 3.1: Details of boundary conditions applied for PP and PPL of dimension 0.9 m x 0.9 m

Sl.No.	Boundary condition	Constraints (reference to Fig.3.4)
1	BC1	Along edges 1 and 2 (AB and CD): all degree of freedom arrested.
		Along edges 3 and 4 (AD and BC) – Symmetry.
		Along stiffener positions (AD, EH, FG and BC) - U_z arrested.
2	BC2	Along edges 1 and 2 (AB and CD); U_x , U_y and U_z are arrested.
		Along edges 3 and 4 (AD and BC) – Symmetry.
		Along stiffener positions (AD, EH, FG and BC) - U_z arrested.

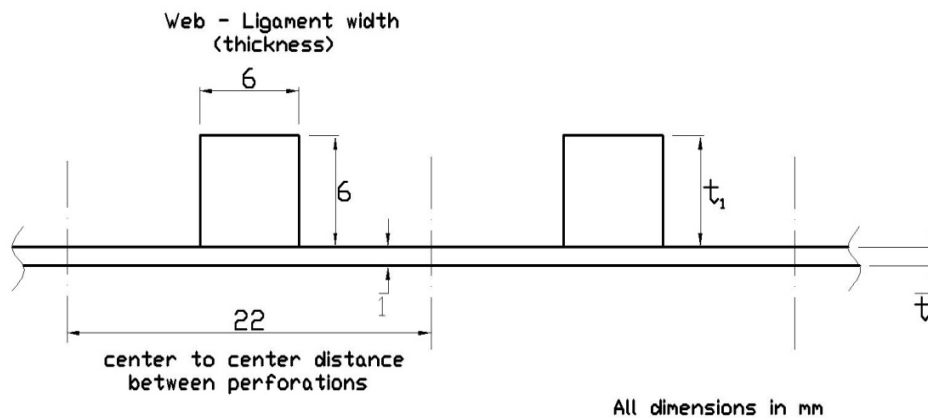
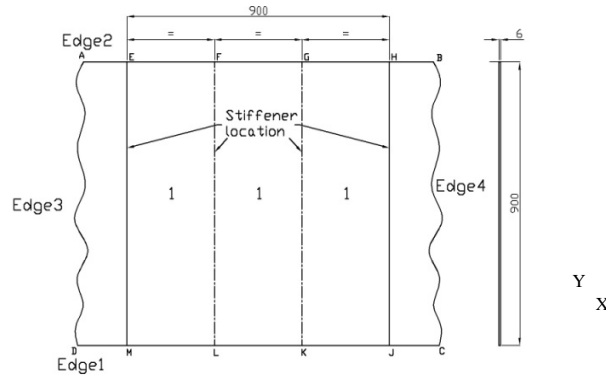


Fig. 3.3: Configuration of T beam of the PPL with Grillage Model

3.9 MATERIAL

The PPL that has been investigated in the present study is a part of a dome provided for protection of underwater transducers. For subsea applications generally, Titanium alloy material is used owing to the corrosion resistance and better strength to weight ratio. The material properties of Titanium alloy used in the present study is taken from the manufacturer test certificate supplied along with the material of PPL used for experimentation and given in Table 3.2.



Dimension in mm

Fig. 3.4: Schematic sketch of continuous plate considered for investigation to describe boundary conditions.

Table 3.2: Material properties of Titanium alloy

Material	Density (kg/m ³)	Poisson ratio	Youngs Modulus (MPa)	Yield stress (MPa)	Ultimate stress (MPa)
Titanium alloy	4500	0.3	1.1×10^5	930	1030

For linear structural analysis conducted in the present study, the plates have been analysed for a transverse distributed pressure of 1 Pa, so that it can be scaled for any load.

3.10 DESCRIPTION OF FINITE ELEMENT SOFTWARE

In this investigation, commercial software ANSYS (1992, 2004) and ANSYS LS-DYNA (2003) are used to carry out numerical analysis. ANSYS is a general purpose finite element software used for structural applications. Version 9.0 is used for this investigation. It supports seven analysis types viz., static, modal, harmonic, transient, spectrum, eigenvalue buckling and substructuring. This code solves problems from structural, thermal, electric, magnetic and fluid engineering disciplines. ANSYS element library has vast number of elements.

ANSYS LS-DYNA is developed by Livermore Software Technology Corporation and commercially available for use. It is a general purpose finite element code for analyzing

the large deformation, dynamic response of structures including structures coupled with fluids. The solution methodology is based on explicit time integration. It is more suitable for problems like Shock Analysis. It has eight different element types and all are 3-D, except the 2-D PLANE162 element (plane stress, axisymmetric or plane strain). Each explicit element type is valid for nearly all material models. Explicit elements support all nonlinear options. Elements have a linear displacement function. Each element uses single point integration and is extremely robust in large deformations.

3.11 DESCRIPTION OF FINITE ELEMENTS

A brief description of the finite element in the library of ANSYS and ANSYS LS-DYNA used in the present analysis has been given subsequently.

3.11.1 SHELL63 element

SHELL63 has both bending and membrane capabilities. Both in-plane and normal loads are permitted. The element has six degrees of freedom at each node: translations in the x, y, and z directions and rotations about the x, y, and z-axes. Stress stiffening and large deflection capabilities are included.

The geometry, node locations and the coordinate system are shown in Fig. 3.5. The element is defined by four nodes, four thicknesses, an elastic foundation stiffness, and the orthotropic material properties. The thickness is assumed to vary smoothly over the area of the element, with the thickness input at the four nodes. If the element has a constant thickness, only the thickness at one node need be input. Pressures may be input as surface loads on the element faces. Positive pressures act into the element. Nodal displacements and pressures, in-plane element forces, stresses and strain are the output of SHELL63.

3.11.2 SHELL93 element

SHELL93 is the element well suited to model curved shells. The geometry, node locations and the coordinate system are shown in Fig. 3.6. The element has six degrees

of freedom at each node. The deformation shapes are quadratic in both the in-plane directions. The element may have variable thickness capabilities.

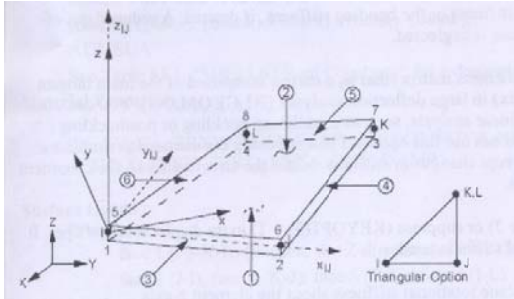


Fig. 3.5: Geometry & kinematics of SHELL63 element

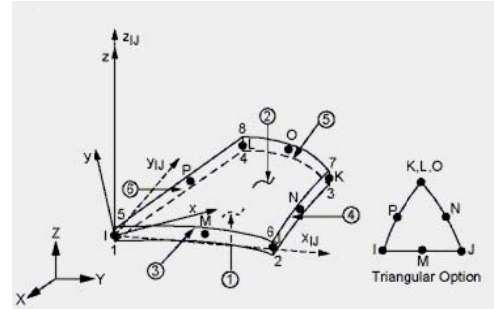


Fig. 3.6: Geometry & kinematics of SHELL93 element

3.11.3 SOLID45 element

This element is used for the 3D modeling of solid structures. The element is defined by eight nodes having three degrees of freedom at each node viz., translations in the nodal x , y , and z directions. The element has plasticity, creep, swelling, stress stiffening, large deflection, and large strain capabilities. Reduced integration option with hourglass control is available. The geometry, node locations and the coordinate system for this element are shown in Fig. 3.7. Pressures may be input as surface loads on the element faces. Positive pressures act into the element. Nodal displacements and pressures, stresses and strains are the important output parameters of SOLID45.

3.11.4 SOLSH190 element

SOLSH190 is used for simulating shell structures with a wide range of thickness (from thin to moderately thick). The element possesses the continuum solid element topology and features eight-node connectivity with three degrees of freedom at each node: translations in the nodal x , y , and z directions. Thus, connecting SOLSH190 with other continuum elements requires no extra efforts. The element formulation is based on logarithmic strain and true stress measures. The geometry, node locations, and the

coordinate system for this element are shown in Fig. 3.8. Pressures may be input as surface loads on the element faces. Positive pressures act into the element. The solution output is associated with the element and nodal displacements and pressures are included in the overall nodal solution.

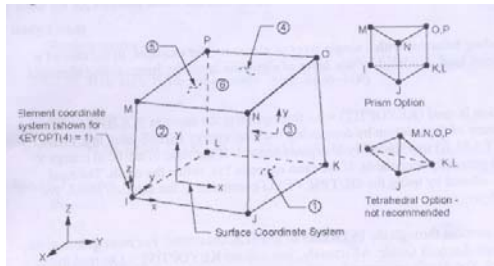


Fig. 3.7: Geometry & kinematics of SOLID45 element

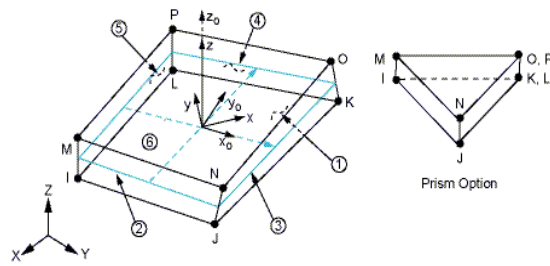


Fig. 3.8: Geometry & kinematics of SOLSH190 element

3.11.5 BEAM188 element

This element is suitable for analyzing slender to moderately thick beam structures, which is based on Timoshenko beam theory where shear deformation effects are included. BEAM188 can have six or seven degrees of freedom at each node. The seventh degree of freedom is to include warping magnitude if necessary. The element is well suited for linear, large rotation and large strain nonlinear applications. The geometry, node locations, and the coordinate system for this element are shown in Fig. 3.9.

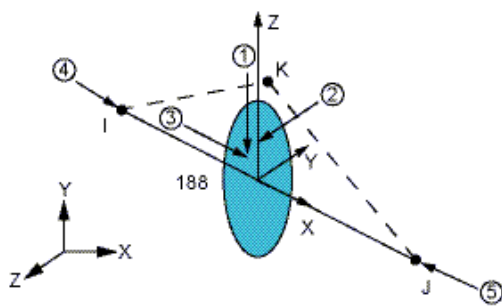


Fig. 3.9: Geometry & kinematics of BEAM188 element

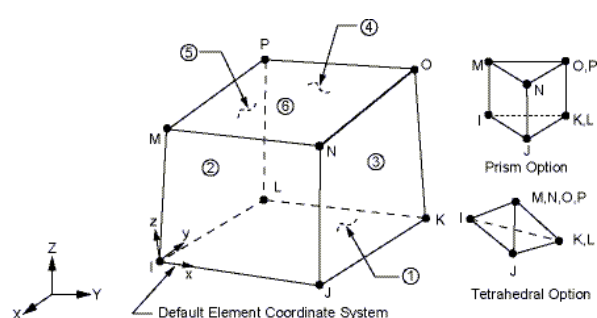


Fig. 3.10: Geometry & kinematics of FLUID30 element

3.11.6 FLUID30 element

FLUID30 is used for modeling the fluid medium and the interface in fluid / structure interaction problems. This element is based on a pressure formulation in which the element shape functions refer to the pressure variations associated with an acoustic wave. Typical applications include sound wave propagation and dynamics of submerged structure. The governing equation for acoustics, viz., the 3-D wave equation, has been discretized taking into account the coupling of acoustic pressure and structural motion at the interface. The element has eight corner nodes with four degrees of freedom per node viz., translations in the x, y and z directions and pressure. The translations, however, are applicable only at nodes that are on the interface. The geometry, node locations, and the coordinate system for this element are shown in Fig. 3.10. Fluid structure interfaces may be flagged by surface loads at the element faces. Specifying the FSI label will couple the structural motion and fluid pressure at the interface. The solution output is associated with the element and nodal displacements and pressures are included in the overall nodal solution.

3.11.7 SHELL163 element

SHELL163 has twelve formulations grouped into four. The four groups are: Belytschko-Tsay, Belyschko-Wong-Chiang, Belytschko-Leviathan and S/R Co-rotational Hughes-Liu. The first three use only one integration point in-plane, but the fourth one uses 4 integration point in-plane. In case of triangular shell element, two formulations are available. These are C^0 triangular shell which is based on Mindlin-Reissner plate theory and not recommended for entire mesh since formulation is stiff. The second one is BCIZ which is based on Kirchhoff plate theory. The geometry, node locations, and the coordinate system for this element are shown in Fig. 3.11.

3.11.8 SOLID164 element

This is an 8-node brick element for which Lagrangian and Arbitrary Lagrangian-Eulerian formulations are available. This element supports wide variety of material models. The

geometry, node locations, and the coordinate system for this element are shown in Fig. 3.12.

Features of finite elements described above are summarised and presented in Table 3.3.

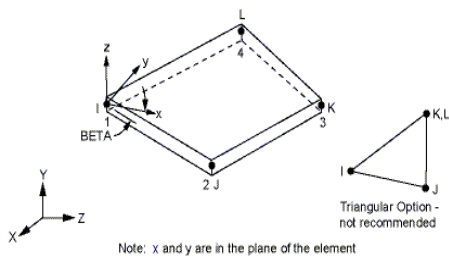


Fig. 3.11: Geometry & kinematics of SHELL163 element

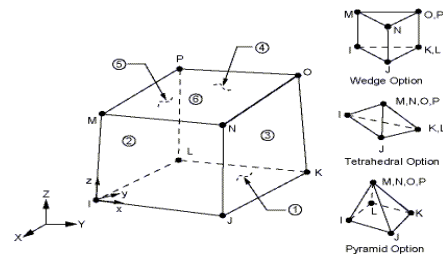


Fig. 3.12: Geometry & kinematics of SOLID164 element

Table 3.3: Element features

Element Description	Element name	No. of nodes	DOF at each node	Loading	Deformation shape
SHELL63	Elastic shell	4	6 ($U_x, U_y, U_z, \theta_x, \theta_y, \theta_z$)	Pressure	Linear
SHELL93	8 node structural shell	8	6 ($U_x, U_y, U_z, \theta_x, \theta_y, \theta_z$)	Pressure	Quadratic
SOLID45	3-D Structural Solid	8	3 (U_x, U_y, U_z)	Pressure	Linear
SOLSH190	3-D 8 node Solid Shell	8	3 (U_x, U_y, U_z)	Pressure	Linear
BEAM188	3-D Linear Strain Beam	2	6 / 7 ($U_x, U_y, U_z, \theta_x, \theta_y, \theta_z$)	Pressure	Linear
FLUID30	3D Acoustic Fluid	8	4 (U_x, U_y, U_z, p)	Pressure	Linear
SOLID163	Shell – Explicit	4	3 (translation, velocity, accelerations)	Pressure	Linear
SOLID164	3D Solid – Explicit	8	3 (translation, velocity, accelerations)	Pressure	Linear

3.12 SYSTEM CONFIGURATION

HP Precision workstation of model T5500 is used to carryout the analysis. The system has Intel Xeon processor with CPU 2.53 GHz, 4 GB RAM.

CHAPTER 4

LINEAR STATIC ANALYSIS OF UNIT CELL

4.1 INTRODUCTION

The scope and utility of unit cell for the static analysis have been investigated in this chapter. Linear static analysis of PP with SHP, SVP, EHP and EVP has been performed, besides the performance assessment of four finite elements available in the ANSYS library which can be used for the analysis of PP. The influence of release of rotation restraint has also been investigated. The finite element output is processed as Stress Concentration Factor (SCF) and Deflection Factor (DF) and useful conclusions are arrived at.

4.2 DESCRIPTION

Unit cell of the perforated plate is of dimension, 106 mm along the X axis and 194 mm along the Y axis. Thickness of the perforated plate is 6mm and the ligament width is 6 mm for SP and 6.25 mm for EP. The Coefficient of Perforation (COP) is 0.4552. Thus a factor “Coefficient of Area” (COA) is arrived, which is $(1 - COP)$ and equal to 0.5448. The ratio between the minimum dimension of perforation to the ligament width is 2.667. Unit cells of perforated plate of horizontal and vertical perforations of stadium and elliptical configurations as well as unit cell of perforated plate with lining are considered in the present analysis. Unit cell of NPP, same as that of perforated plate is analysed to serve as the bench mark for comparison. The unit cell of Perforated Plate with Lining (PPL) is devised by adding 1mm lining plate to the perforated plate.

4.3 FINITE ELEMENT ANALYSIS

The above mentioned unit cells are modeled using SHELL63, SHELL93, SOLID45 and SOLSH190 elements to realize the influence of finite element kinematics. The boundary conditions applied are given in Table 4.1. The Deflection (Def), von Mises Stress (VMS)

and Maximum Principal Stress (MPS) are evaluated at centroid, for four different mesh densities to fulfill the convergence studies for BC3 and BC4.

Table 4.1: Details of boundary conditions applied for unit cell

Sl.No.	Boundary condition	Constraints
1	BC3	All nodes along the four edges fixed
2	BC4	All nodes along the four edges: U_x , U_y and U_z are arrested.

4.3.1 Non Perforated Plate

The finite element model composed with SHELL63 element for mesh density 70×130 is shown in Fig. 4.1(a). This model has 9563 nodes and 9360 elements. The deflection, von Mises stress and maximum principal stress contours for this model for BC3 are shown in Figs. 4.1(b), 4.1(c) and 4.1(d) respectively. The same for BC4 are shown vide Figs. 4.1(e), 4.1(f) and 4.1(g).

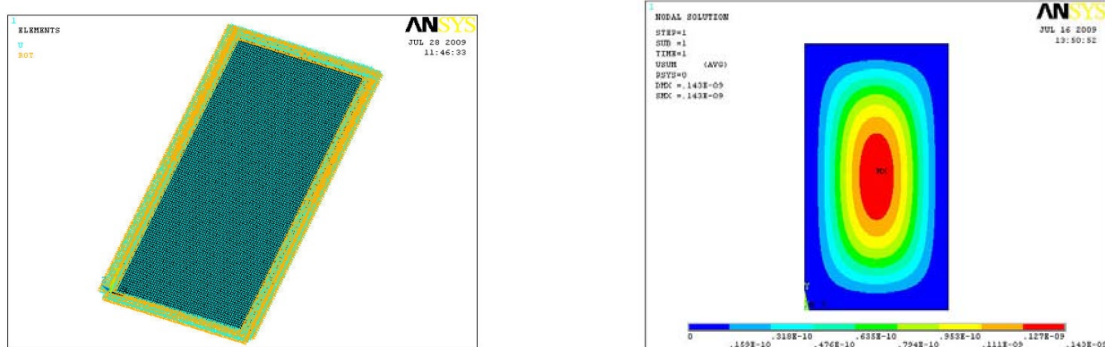
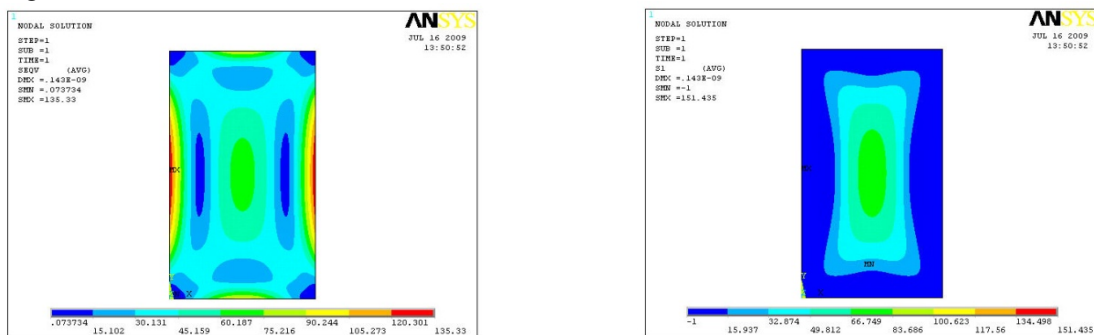


Fig. 4.1: (a)

(b)



(c)

(d)

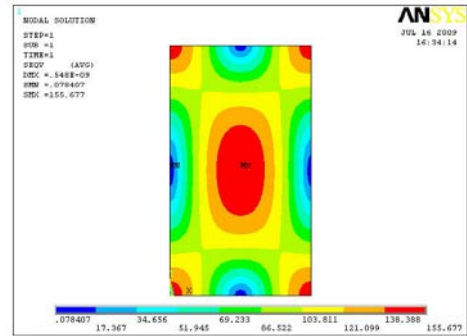
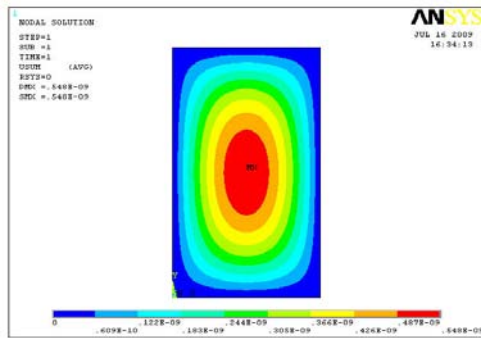
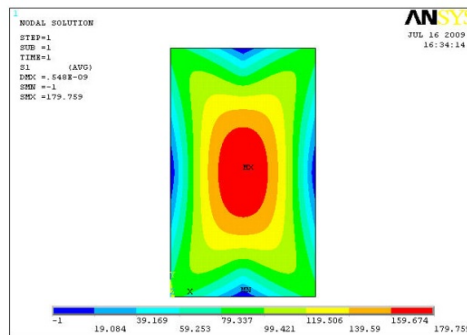


Fig. 4.1: (contd.) (e)

(f)



(g)

Fig. 4.1: (a) Finite Element Model of NPP with SHELL63 element for BC3, (b) Deflection Contour of NPP for 1Pa for BC3, (c) von Mises Stress Contour of NPP for 1Pa for BC3, (d) Maximum Principal Stress Contour of NPP for 1Pa for BC3, (e) Deflection Contour of NPP with SHELL63 element for BC4 and for 1 Pa, (f) von Mises Stress Contour of NPP for 1Pa for BC4 and (g) Maximum Principal Stress Contour of NPP for 1Pa for BC4.

The static structural responses of non perforated plate are given in Table 4.2. This table can be used to identify the convergence, comparison of performance of different finite elements and influence of boundary conditions.

Table 4.2: Details of finite element model and static structural responses of non perforated plate of unit cell for pressure of 1 Pa.

Non Perforated Plate			Number of nodes	Number of elements	at Centroid		
Element	BC	Mesh density			Deflection $\times 10^{-9}$ m	von Mises Stress, Pa	Maximum Principal Stress, Pa
SHELL63	BC3	38 x 70	2769	2660	0.1429	65.69	75.56
		52 x 96	5335	5184	0.1429	65.65	75.52
		70 x 130	9563	9360	0.1429	65.62	75.49
		98 x 178	17919	17640	0.1429	65.61	75.48
SHELL93		38 x 70	8197	2660	0.1495	65.73	75.64
		52 x 96	15853	5184	0.1495	65.69	75.59
		70 x 130	28485	9360	0.1495	65.67	75.56
		98 x 178	53477	17640	0.1495	65.66	75.55
SOLID45		38 x 70	11076	7980	0.1473	65.42	75.10
		52 x 96	21340	15552	0.1478	65.52	75.25
		70 x 130	47815	37440	0.1482	65.58	75.37
		98 x 178	125433	105840	0.1484	65.62	75.46
SOLSH190		38 x 70	11076	7980	0.1473	65.42	75.10
		52 x 96	21340	15552	0.1478	65.53	75.25
		70 x 130	47815	37440	0.1482	65.58	75.37
		98 x 178	125433	105840	0.1484	65.62	75.46
SHELL63	BC4	38 x 70	2769	2660	0.5481	155.70	179.78
		52 x 96	5335	5184	0.5482	155.68	179.77
		70 x 130	9563	9360	0.5483	155.68	179.76
		98 x 178	17919	17640	0.5483	155.67	179.75
SHELL93		38 x 70	8197	2660	0.5683	159.02	183.62
		52 x 96	15853	5184	0.5683	158.98	183.57
		70 x 130	28485	9360	0.5683	158.96	183.55
		98 x 178	53477	17640	0.5683	158.95	183.54

4.3.2 Stadium Horizontal Perforation

The finite element model composed with SHELL63 element for mesh density 78 x 156 is shown in Fig. 4.2(a). This model has 8803 nodes and 8008 elements. The deflection, von Mises stress and maximum principal stress contours for this model for BC3 are shown in Figs. 4.2(b), 4.2(c), and 4.2(d) respectively. The same for BC4 are shown in Figs. 4.2(e), 4.2(f) and 4.2(g).

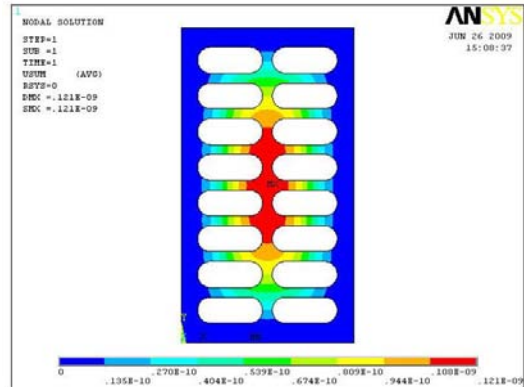
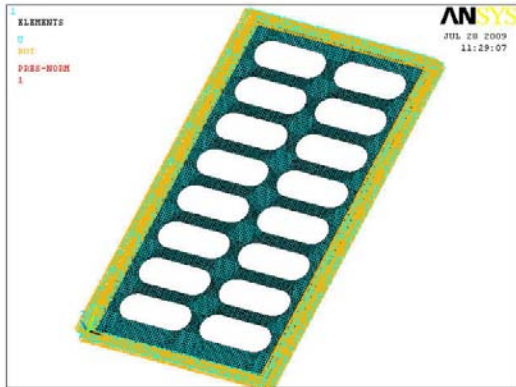
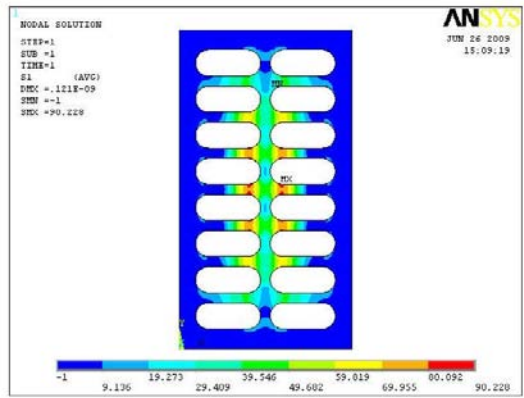
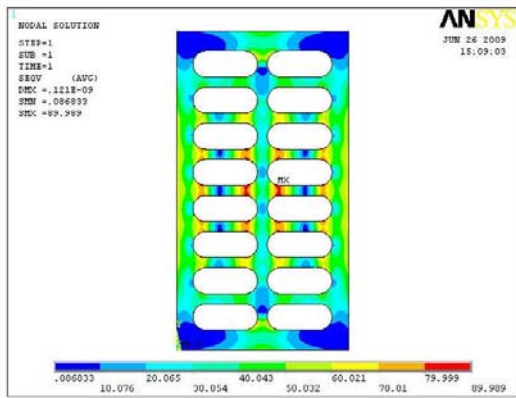


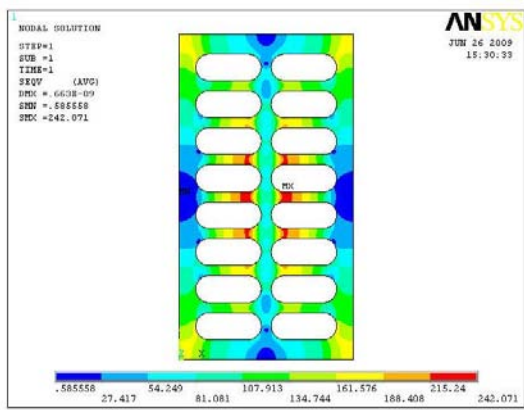
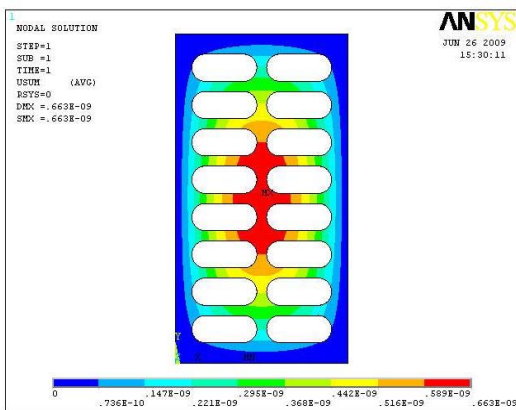
Fig. 4.2: (a)

(b)



(c)

(d)



(e)

(f)

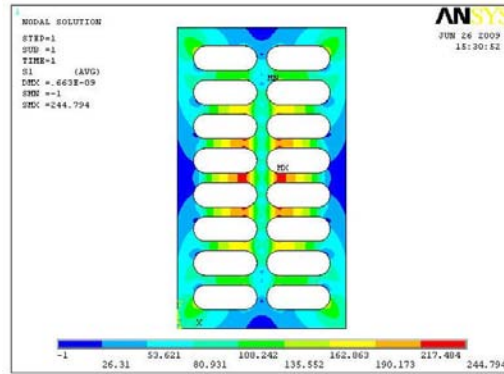


Fig. 4.2: (contd.) (g)

Fig. 4.2: (a) Finite Element Model of SHP with SHELL63 element for BC3, (b) Deflection Contour of SHP for 1Pa for BC3, (c) von Mises Stress Contour of SHP for 1Pa for BC3, (d) Maximum Principal Stress Contour of SHP for 1Pa for BC3, (e) Deflection Contour of SHP with SHELL63 element for BC4 and for 1 Pa, (f) von Mises Stress Contour of SHP for 1Pa for BC4 and (g) Maximum Principal Stress Contour of SHP for 1Pa for BC4.

The static structural responses of perforated plate with stadium horizontal perforation are given in Table 4.3.

Table 4.3: Details of finite element model and static structural responses of stadium horizontal perforation of unit cell for pressure of 1 Pa.

Stadium Horizontal Perforation			Number of nodes	Number of elements	at Centroid		
Element	BC	Mesh density			Deflection $\times 10^{-9}$ m	von Mises Stress, Pa	Maximum Principal Stress, Pa
SHELL63	BC3	44 x 88	2885	2432	0.1204	39.63	44.89
		60 x 122	5375	4760	0.1210	39.18	44.15
		78 x 156	8803	8008	0.1213	39.04	43.89
		102 x 194	14277	13260	0.1215	38.98	43.78
SHELL93		44 x 88	8217	2432	0.1393	51.45	53.96
		60 x 122	15525	4760	0.1393	51.32	53.90
		78 x 156	25629	8008	0.1393	51.37	53.87
		102 x 194	41829	13260	0.1393	51.36	53.86
SOLID45		42 x 86	8103	4536	0.1348	50.77	55.55
		60 x 122	21500	14280	0.1368	50.70	54.16
		78 x 156	44015	32032	0.1376	50.68	53.78
SOLSH190		102 x 194	99939	79560	0.1382	50.72	53.67
	42 x 86	8103	4536	0.1328	47.49	51.16	
	60 x 122	21500	14280	0.1349	47.48	50.01	

Table 4.3: (contd.)

Stadium Horizontal Perforation			Number of nodes	Number of elements	at Centroid		
Element	BC	Mesh density			Deflection $\times 10^{-9}$ m	von Mises Stress, Pa	Maximum Principal Stress, Pa
SOLSH190	BC3	78 x 156	44015	32032	0.1359	47.59	49.77
		102 x 194	99939	79560	0.1365	47.69	49.74
SHELL63	BC4	44 x 88	2885	2432	0.6601	93.51	107.89
		60 x 122	5375	4760	0.6620	91.44	105.58
		78 x 156	8803	8008	0.6628	90.74	104.78
		102 x 194	14277	13260	0.6632	90.42	104.41
SHELL93	BC4	44 x 88	8217	2432	0.7831	119.53	135.12
		60 x 122	15525	4760	0.7831	119.56	135.14
		78 x 156	25629	8008	0.7831	119.56	135.13
		102 x 194	41829	13260	0.7831	119.55	135.13

4.3.3 Stadium Vertical Perforation

The finite element model composed with SHELL63 element for mesh density 84 x 110 is shown in Fig. 4.3(a). This model has 6987 nodes and 6360 elements. The deflection, von Mises stress and maximum principal stress contours are shown for this model for BC3 in Figs. 4.3(b), 4.3(c) and 4.3(d) respectively. The same for BC4 are shown in Figs. 4.3(e), 4.3(f) and 4.3(g).

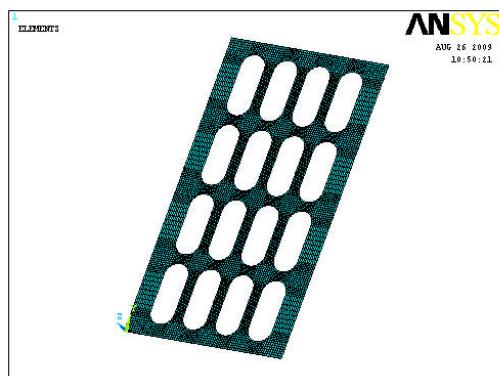
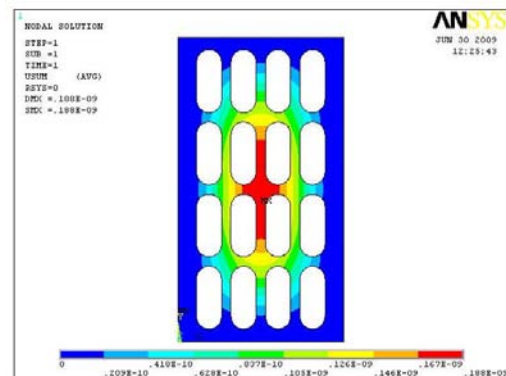


Fig. 4.3: (a)



(b)

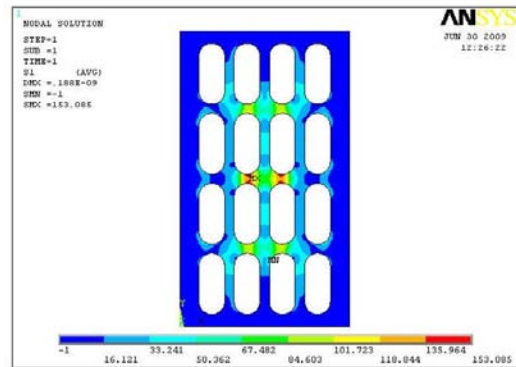
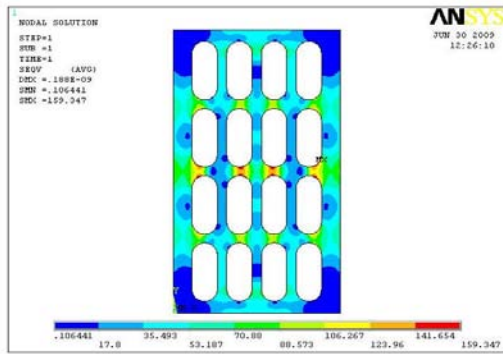
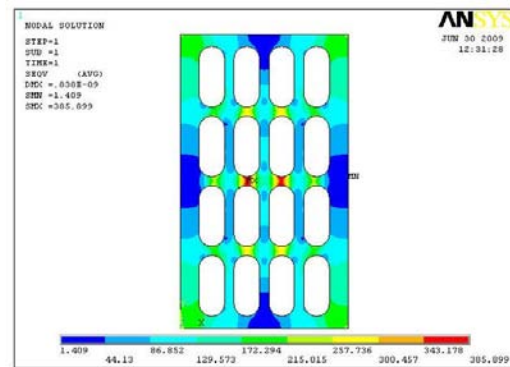
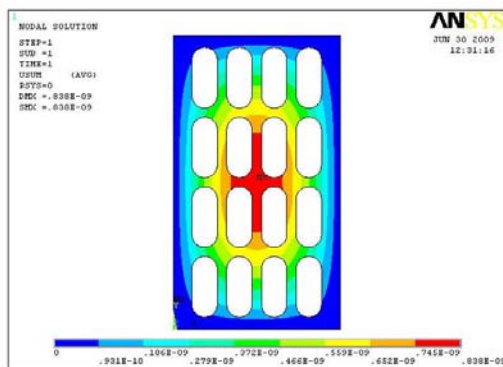


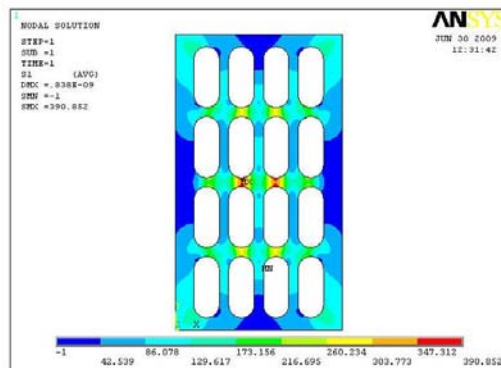
Fig. 4.3: (contd.) (c)

(d)



(e)

(f)



(g)

Fig. 4.3: (a) Finite Element Model of SVP with SHELL63 element for BC3, (b) Deflection Contour of SVP for 1Pa for BC3, (c) von Mises Stress Contour of SVP for 1Pa for BC3, (d) Maximum Principal Stress Contour of SVP for 1Pa for BC3, (e) Deflection Contour of SVP with SHELL63 element for BC4 and for 1 Pa, (f) von Mises Stress Contour of SVP for 1Pa for BC4 and (g) Maximum Principal Stress Contour of SVP for 1Pa for BC4.

The static structural responses of perforated plate with stadium vertical perforation are given in Table 4.4.

Table 4.4: Details of finite element model and static structural responses of stadium vertical perforation of unit cell for pressure of 1 Pa.

Stadium Vertical Perforation			Number of nodes	Number of elements	at Centroid		
Element	BC	Mesh density			Deflection $\times 10^{-9}$ m	von Mises Stress, Pa	Maximum Principal Stress, Pa
SHELL63	BC3	48 x 76	2753	2320	0.1856	67.40	73.64
		66 x 94	4797	4252	0.1868	66.87	72.51
		84 x 110	6987	6616	0.1874	66.71	72.13
		106 x 130	11289	10500	0.1877	66.66	71.97
SHELL93		48 x 76	7841	2320	0.2305	95.92	94.57
		66 x 94	13861	4252	0.2305	95.87	94.51
		84 x 110	21181	6616	0.2305	95.82	94.48
		106 x 130	33093	10500	0.2305	95.81	94.46
SOLID45		48 x 76	11012	6960	0.2228	94.34	96.56
		66 x 94	19188	12756	0.2253	93.97	94.45
		84 x 110	36375	26464	0.2271	94.05	93.91
		106 x 130	79023	63000	0.2282	94.19	93.78
SOLSH190		48 x 76	11012	6960	0.2201	89.09	88.91
		66 x 94	19188	12756	0.2224	88.76	86.81
		84 x 110	36375	26464	0.2241	88.97	86.41
		106 x 130	79023	63000	0.2252	89.21	86.40
SHELL63	BC4	48 x 76	2753	2320	0.8325	147.55	168.11
		66 x 94	4797	4252	0.8364	144.94	164.55
		84 x 110	6987	6616	0.8381	144.04	163.29
		106 x 130	11289	10500	0.8389	143.62	162.71
SHELL93		48 x 76	7841	2320	1.0470	210.89	223.22
		66 x 94	13861	4252	1.0470	211.04	223.33
		84 x 110	21181	6616	1.0470	211.00	223.30
		106 x 130	33093	10500	1.0470	211.03	223.32

4.3.4 Elliptical Horizontal Perforation

The finite element model composed with SHELL63 element for mesh density 47 x 112 is shown in Fig. 4.4(a). This model has 4081 nodes and 3584 elements. The deflection, von Mises stress and maximum principal stress contours for this model for BC3 are shown in Figs. 4.4(b), 4.4(c) and 4.4(d) respectively. The same for BC4 are shown vide Figs. 4.4(e), 4.4(f) and 4.4(g).

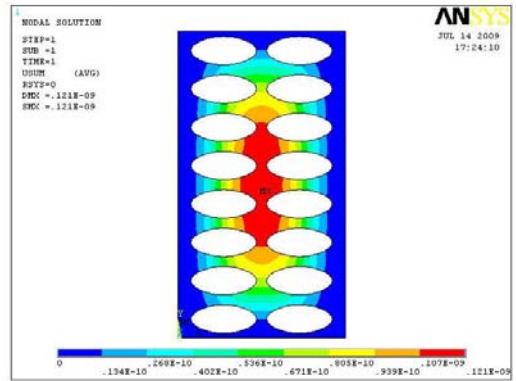
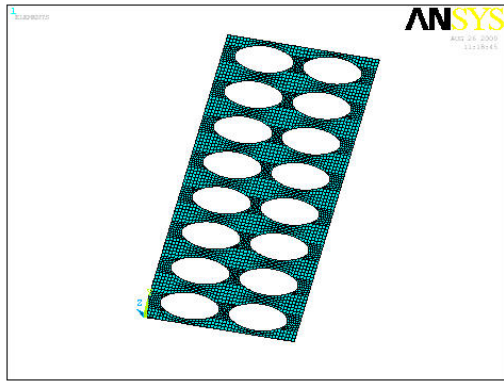
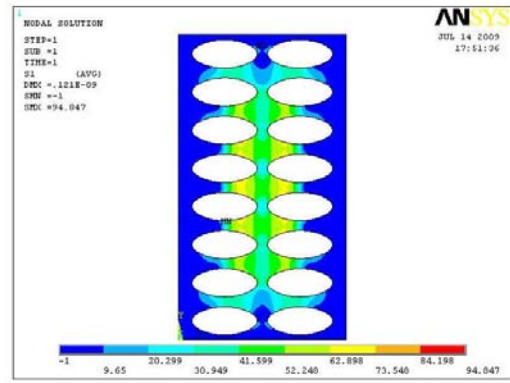
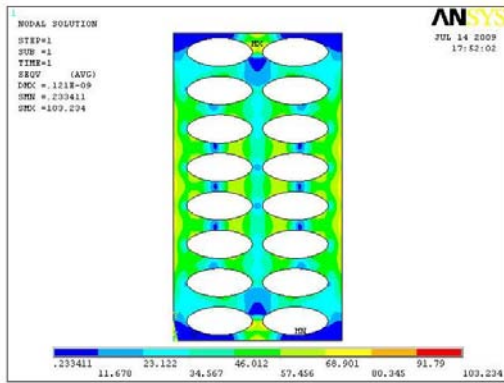


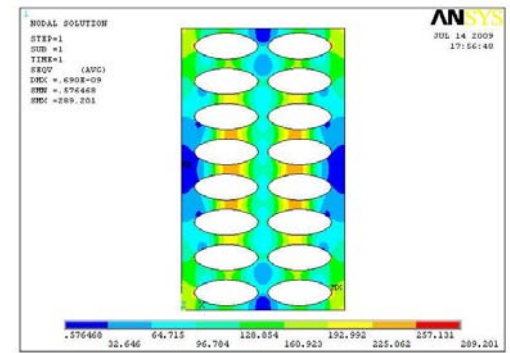
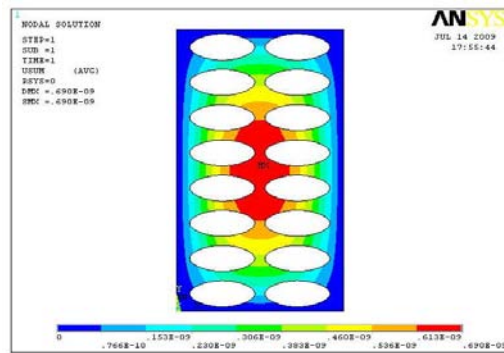
Fig. 4.4: (a)

(b)



(c)

(d)



(e)

(f)

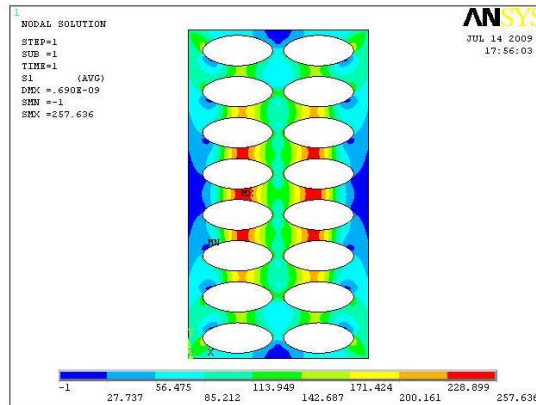


Fig. 4.4: (contd.) (g)

Fig. 4.4: (a) Finite Element Model of EHP with SHELL63 element for BC3, (b) Deflection Contour of EHP for 1Pa for BC3, (c) von Mises Stress Contour of EHP for 1Pa for BC3, (d) Maximum Principal Stress Contour of EHP for 1Pa for BC3, (e) Deflection Contour of EHP with SHELL63 element for BC4 and for 1 Pa, (f) von Mises Stress Contour of EHP for 1Pa for BC4 and (g) Maximum Principal Stress Contour of EHP for 1Pa for BC4.

The static structural responses of perforated plate with elliptical horizontal perforation are given in Table 4.5.

Table 4.5: Details of finite element model and static structural responses of elliptical horizontal perforation of unit cell for pressure of 1 Pa.

Elliptical Horizontal Perforation			Number of nodes	Number of elements	at Centroid		
Element	BC	Mesh density			Deflection $\times 10^{-9}$ m	von Mises Stress, Pa	Maximum Principal Stress, Pa
SHELL63	BC3	14 x 32	447	320	0.1164	46.65	53.32
		26 x 58	1257	996	0.1196	44.04	49.67
		47 x 112	4081	3584	0.1207	43.53	48.56
		88 x 201	12867	11952	0.1210	43.36	48.18
SHELL93		14 x 32	1229	320	0.1359	49.74	53.55
		26 x 58	3525	996	0.1360	49.54	53.12
		47 x 112	11761	3584	0.1360	49.72	53.21
SOLID45		88 x 201	37701	11952	0.1360	49.67	53.15
		14 x 32	894	320	0.1223	47.57	61.34
		28 x 58	4125	2224	0.1308	48.79	54.41
		47 x 112	16324	10752	0.1336	49.37	53.43

Table 4.5: (contd.)

Elliptical Horizontal Perforation			Number of nodes	Number of elements	at Centroid		
Element	BC	Mesh density			Deflection x 10 ⁻⁹ m	von Mises Stress, Pa	Maximum Principal Stress, Pa
SOLID45	BC3	88 x 201	77202	59760	0.1348	49.43	53.12
SOLSH190		14 x 32	894	320	0.1178	47.25	54.90
		28 x 58	4125	2224	0.1232	43.71	48.10
		47 x 112	16324	10752	0.1260	43.97	47.00
		88 x 201	77202	59760	0.1274	44.15	46.90
SHELL63	BC4	14 x 32	447	320	0.6622	114.15	131.64
		26 x 58	1257	996	0.6823	104.78	120.98
		47 x 112	4081	3584	0.6898	102.26	117.87
		88 x 201	12867	11952	0.6923	101.40	116.76
SHELL93		14 x 32	1229	320	0.8054	118.87	135.15
		26 x 58	3525	996	0.8108	120.91	137.16
		47 x 112	11761	3584	0.8113	121.93	138.08
		88 x 201	37701	11952	0.8113	121.84	137.99

4.3.5 Discussion on Convergence

The convergence plot for the four finite element types for deflection for BC3 is prepared for the NPP and shown in Fig. 4.5(a). The maximum deflection at the center of NPP as calculated by exact solution (Young, 1989) is 0.1429×10^{-9} m. Deflection at the center, obtained by finite element method using SHELL63 element converges with the exact solution for a mesh 38×70 . The deflection predicted by SHELL93 model of NPP with a mesh 38×70 converged to a value 4.6% higher than the exact solution. Similarly for SOLID45 and SOLSH190 models, the convergence of deflection occurred for a mesh of 70×130 at a value 3.7% higher than the exact solution.

The maximum deflection at the center of NPP has been evaluated for BC4 using SHELL63 and SHELL93 elements. Deflection predicted by the former converges for a 70×130 mesh to the value 2.16% higher than that is available as exact solution (Young, 1989) which is numerically equal to 0.5367×10^{-9} m. Deflections predicted by SHELL93 converges to a value 5.89% from the exact solution for the 38×70 mesh density.

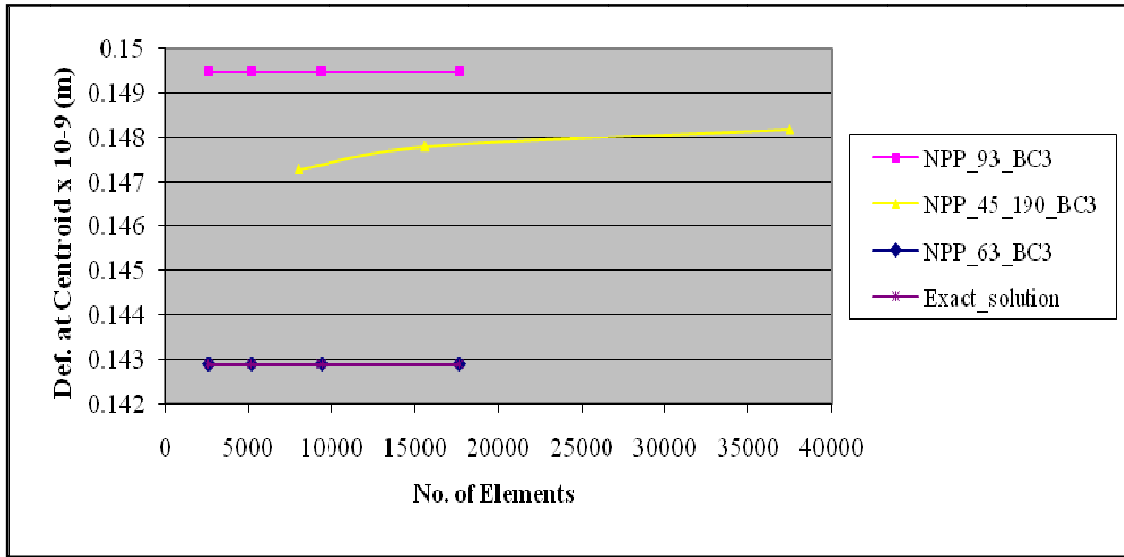


Fig. 4.5: (a)

Convergence plot for principal stress for BC3 for SHELL63, SHELL93, SOLID45 and SOLSH190 elements are shown vide Fig. 4.5(b) and Fig. 4.5(c). The principal stress at centroid of NPP for BC3 calculated from exact solution is 76.4672Pa. Finite element principal stress value of SHELL63 element converges with the exact solution for a mesh 70 x 130 by a value of 1.27% reduced than the exact solution. The convergence of principal stress predicted by SHELL93 model of the NPP occurred with a value of 1.20% reduced than the exact solution for a mesh 98 x 178. Similarly for SOLID45 and SOLSH190 models, the convergence of principal stress is predicted for a mesh of 98 x 178 with a value of 1.32% reduced than the exact solution.

The principal stress at centroid of NPP for BC4 as calculated by exact solution is 181.024Pa. Finite element principal stress value of SHELL63 element converges with the exact solution for a mesh 38 x 70 by a value of 0.687% reduced than the exact solution. The convergence of principal stress predicted by SHELL93 model of the NPP occurred with a value of 1.39% higher than the exact solution for a mesh 70 x 130.

Figs. 4.6 to 4.14 show the convergence plot for all the configurations of unit cell. Table 4.6 gives convergence of deflection, von Mises stress and maximum principal stress predicted for each configuration by the four elements.

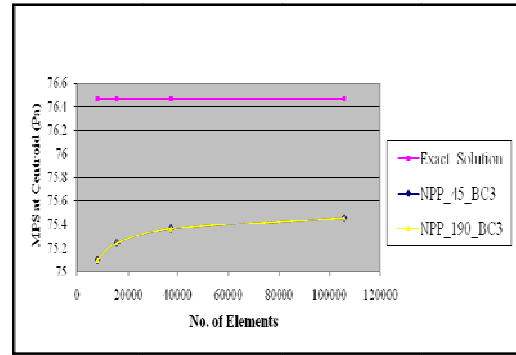
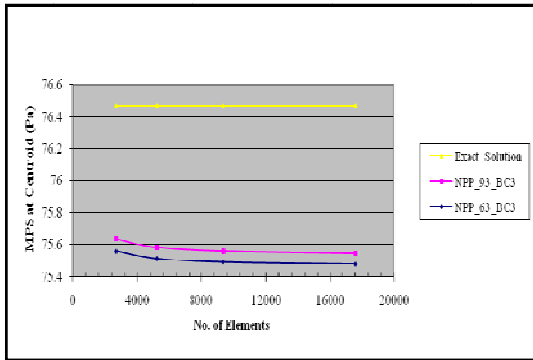


Fig. 4.5: (contd.) (b)

(c)

Fig. 4.5: (a) Convergence of deflection for NPP of different elements for BC3, (b) Convergence of maximum principal stress for NPP of SHELL63 and SHELL93 elements for BC3 and (c) Convergence study of maximum principal stress for NPP of SOLID45 and SOLSH190 elements for BC3.

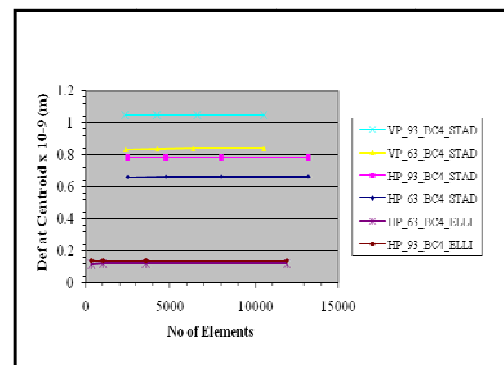
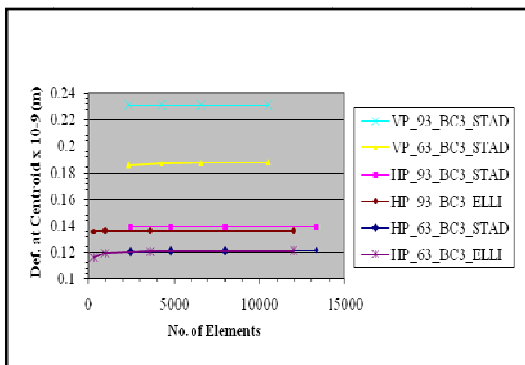


Fig. 4.6: Convergence of deflection for SHELL63 & SHELL93 elements for BC3

Fig. 4.7: Convergence of deflection for SHELL63 & SHELL93 elements for BC4

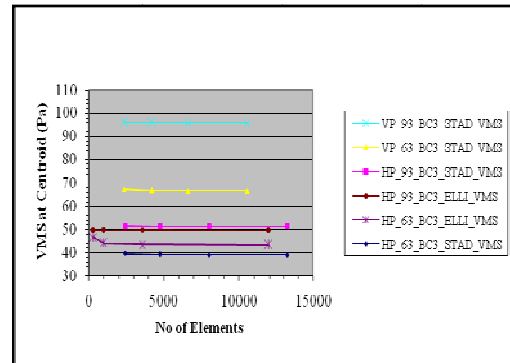
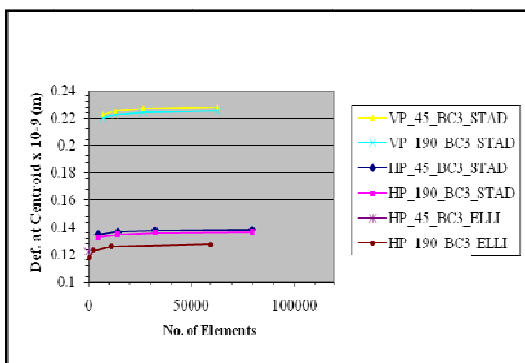


Fig. 4.8: Convergence of deflection for SOLID45 & SOLSH190 elements for BC3

Fig. 4.9: Convergence of VMS for SHELL63 & SHELL93 elements for BC3

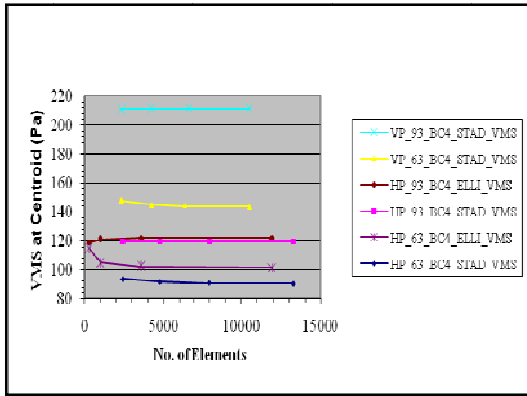


Fig. 4.10: Convergence of VMS for SHELL63 & SHELL93 elements for BC4

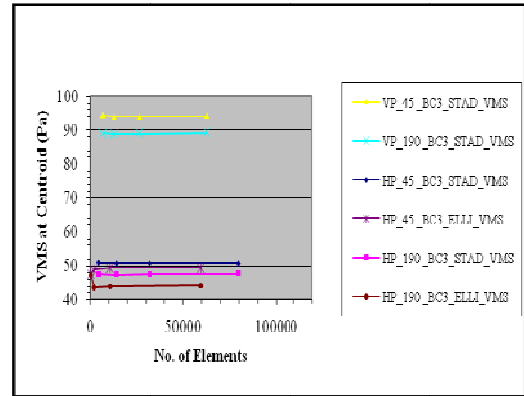


Fig. 4.11: Convergence of VMS for SOLID45 & SOLSH190 elements for BC3

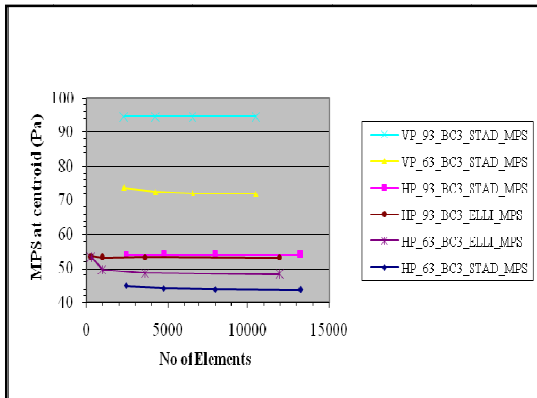


Fig. 4.12: Convergence of MPS for SHELL63 & SHELL93 elements for BC3

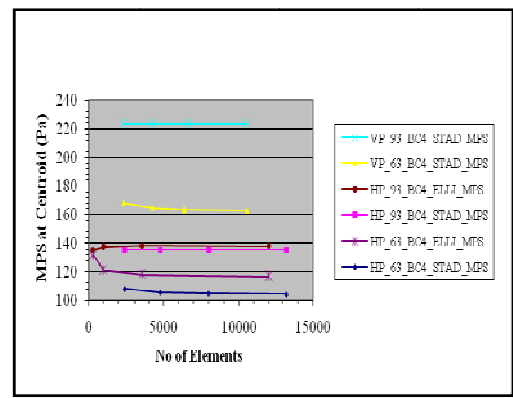


Fig. 4.13: Convergence of MPS for SHELL63 & SHELL93 elements for BC4

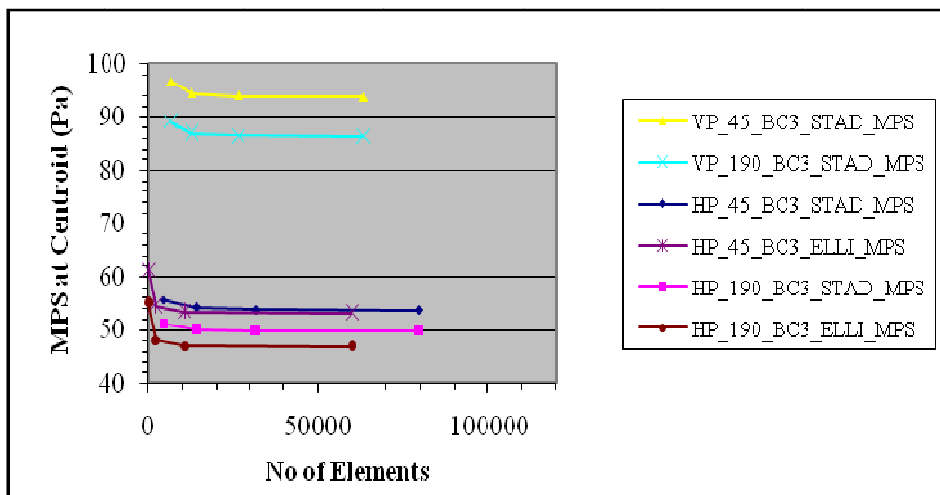


Fig. 4.14: Convergence of MPS for SOLID45 and SOLSH190 elements for BC3.

Table 4.6: Details of convergence of deflection, von Mises stress and maximum principal stress for various configurations.

Structural response	Configuration	Finite element	BC	Mesh density	No. of nodes	Reference Fig.
Deflection	SHP	SHELL63	BC3 and BC4	78 x 156	8803	4.6 and 4.7
	SVP			84 x 110	6987	
	EHP			47 x 112	4081	
	SHP	SHELL93	BC3	44 x 88	8217	4.6
	SVP			48 x 76	7841	
	EHP			26 x 58	3525	
	SHP	SHELL93	BC4	44 x 88	8217	4.7
	SVP			48 x 76	7841	
	EHP			47 x 112	11761	
	SHP	SOLID45 and SOLSH190	BC3	78 x 156	44015	4.8
	SVP			84 x 110	36375	
	EHP			47 x 112	16324	
von Mises Stress	SHP	SHELL63	BC3 and BC4	78 x 156	8803	4.9 and 4.10
	SVP			84 x 110	6987	
	EHP			47 x 112	4081	
	SHP	SHELL93	BC3	78 x 156	25629	4.9
	SVP			84 x 110	21181	
	EHP			47 x 112	11761	
	SHP	SHELL93	BC4	60 x 122	15525	4.10
	SVP			84 x 110	21181	
	EHP			47 x 112	11761	
	SHP	SOLID45	BC3	78 x 156	44015	4.11
	SVP			84 x 110	36375	
	EHP			47 x 112	16324	
	SHP	SOLSH190		42 x 86	8103	
	SVP			84 x 110	36375	
	EHP			47 x 112	16324	
Maximum Principal Stress	SHP	SHELL63	BC3 and BC4	78 x 156	8803	4.12 and 4.13
	SVP			84 x 110	6987	
	EHP			47 x 112	4081	
	SHP	SHELL93	BC3 and BC4	78 x 156	25629	4.12 and 4.13
	SVP			84 x 110	21181	
	EHP			47 x 112	11761	
	SHP	SOLID45 and SOLSH190	BC3	78 x 156	44015	4.14
	SVP			84 x 110	36375	
	EHP			47 x 112	16324	

Convergence has been achieved for mesh densities 78 x 156 for SHELL63, 44 x 88 for SHELL93, 78 x 156 for SOLID45 and SOLSH190. Based on the outcome of this analysis, and considering the perforated plate dimension under study, suitable mesh densities are arrived for further investigations on PP and PPL with stadium perforation.

4.3.6 Elliptical Vertical Perforation

Finite element model with SHELL63 of 92 x 138 mesh with elliptical vertical perforation is shown in Fig. 4.15(a). This finite element model has 9231 nodes and 8472 elements. The deflection, von Mises stress and maximum principal stress contours are shown in Figs. 4.15(b), 4.15(c), and 4.15(d) respectively.

The finite element model with SHELL93 element has 26949 nodes and 8472 elements whereas, with the SOLID45 and SOLSH190 have 46155 nodes and 33888 elements. Analyses are carried out for BC3 and BC4. The deflection, von Mises stress and maximum principal stress are shown in Table 4.7.

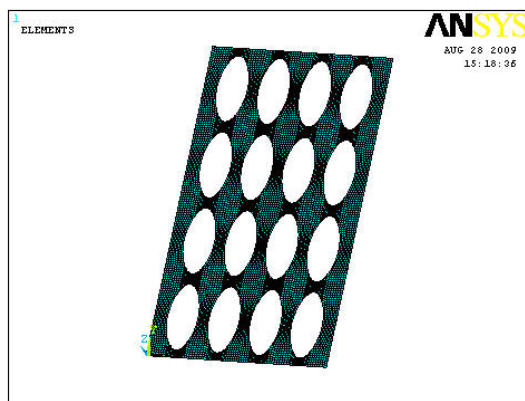
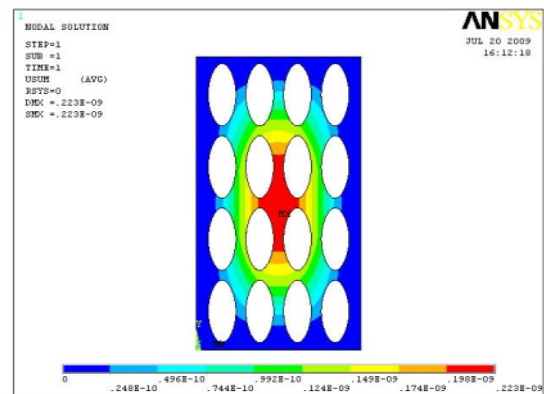


Fig. 4.15 (a)



(b)

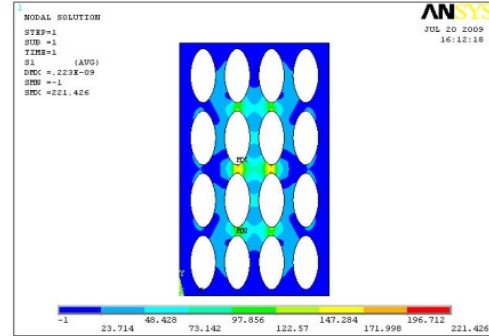
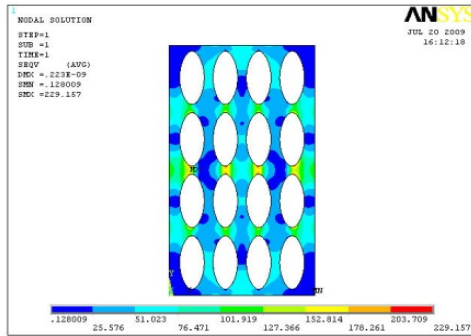


Fig. 4.15: (contd.) (c) (d)

Fig. 4.15: (a) Finite Element Model of EVP with SHELL63 element for BC3, (b) Deflection Contour of EVP for 1Pa for BC3, (c) von Mises Stress Contour of EVP for 1Pa for BC3, (d) Maximum Principal Stress Contour of EVP for 1Pa for BC3.

Table 4.7: Details of finite element model and static structural responses of elliptical vertical perforation of unit cell for pressure of 1 Pa.

Elliptical Vertical Perforation			Number of nodes	Number of elements	at Centroid		
Element	BC	Mesh density			Deflection $\times 10^{-9}$ m	von Mises Stress Pa	Maximum Principal Stress, Pa
SHELL63	BC3	92 x 138	9231	8472	0.2225	67.70	74.51
SHELL93			26949	8472	0.2743	90.60	93.24
SOLID45			46155	33888	0.2700	89.10	92.60
SOLSH190			46155	33888	0.2695	89.04	92.45
SHELL63	BC4		9231	8472	0.8997	142.97	163.50
SHELL93			26949	8472	1.1630	201.68	219.46

4.3.7 Stadium Horizontal Perforation of PPL

Finite element model of 78 x 156 mesh with SHELL63 element is shown in Fig. 4.16(a). This model has 25818 nodes and 24784 elements. The finite element model with SHELL93 element has 76426 nodes and 24784 elements whereas, with SOLID45 and SOLSH190 models have 69234 nodes and 48808 elements. Analyses are carried out for BC3 and BC4.

The deflection, von Mises stress and maximum principal stress contours for BC3 of SHELL63 are given in Figs. 4.16(b), 4.16(c) and 4.16(d) respectively. Figs. 4.16(e),

4.16(f) and 4.16(g) show the contour plots of deflection, von Mises stress and maximum principal stress respectively for the model with SHELL63 for BC4. The results for all the above cases are given in Table 4.8.

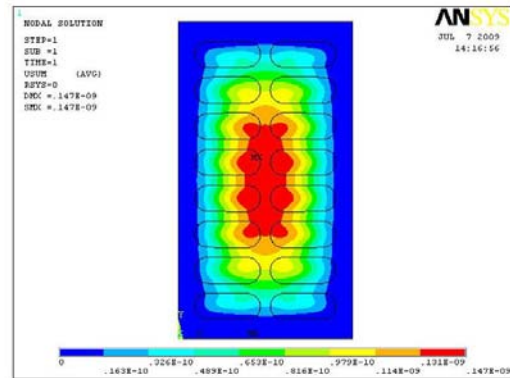
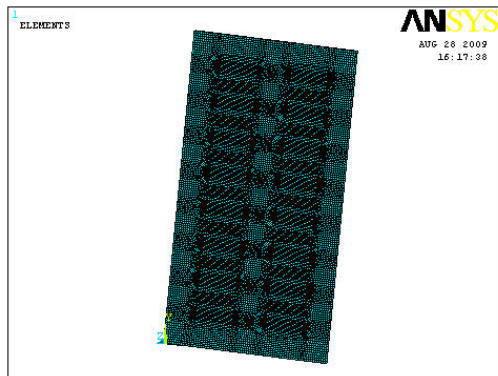
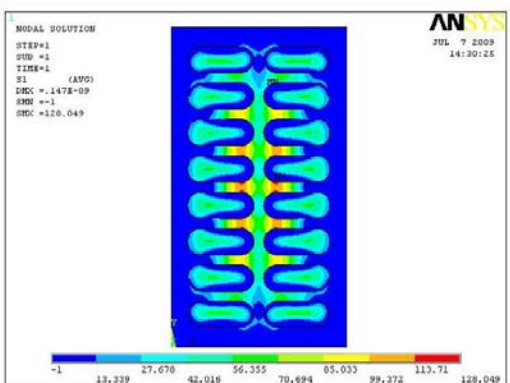
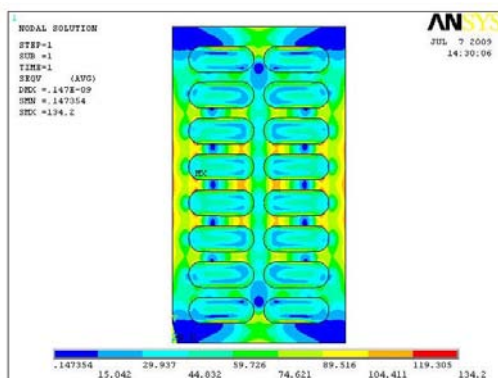


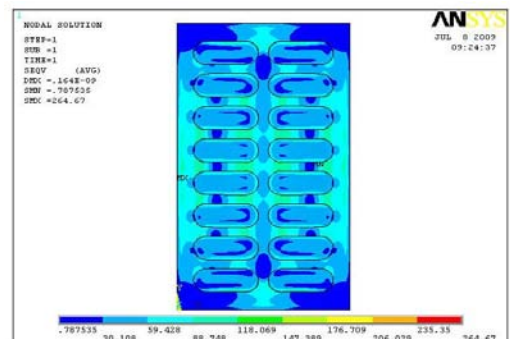
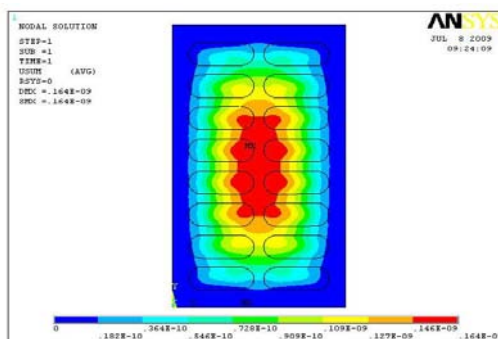
Fig. 4.16: (a)

(b)



(c)

(d)



(e)

(f)

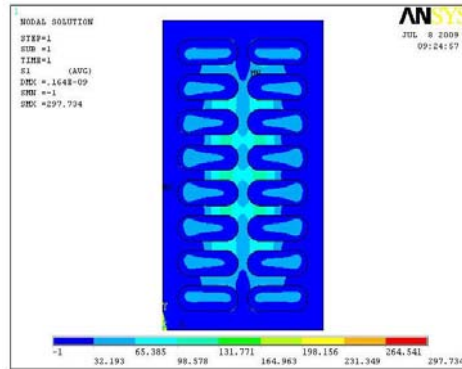


Fig. 4.16: (contd.) (g)

Fig. 4.16: (a) Finite Element Model of SHP of PPL with SHELL63 element for BC3, (b) Deflection Contour of SHP of PPL for 1Pa for BC3, (c) von Mises Stress Contour of SHP of PPL for 1Pa for BC3, (d) Maximum Principal Stress Contour of SHP of PPL for 1Pa for BC3, (e) Deflection Contour of SHP of PPL with SHELL63 element for BC4 for 1 Pa, (f) von Mises Stress Contour of SHP of PPL for 1Pa for BC4 and (g) Maximum Principal Stress Contour of SHP of PPL for 1Pa for BC4.

4.3.8 Stadium Vertical Perforation of PPL

Finite element model of 84 x 110 mesh with SHELL63 element is shown in Fig. 4.17(a). This model has 19110 nodes and 18288 elements. The finite element model with SHELL93 element has 56522 nodes and 18288 elements whereas, with SOLID45 and SOLSH190 models have 65442 nodes and 46456 elements. Analyses are carried out for BC3 and BC4.

The deflection, von Mises stress and maximum principal stress contours for BC3 of SHELL63 are given in Figs. 4.17(b), 4.17(c) and 4.17(d) respectively. Figs. 4.17(e), 4.17(f) and 4.17(g) show the contour plots of deflection, von Mises stress and maximum principal stress respectively for the model with SHELL63 for BC4. The results for all the above cases are given in Table 4.8.

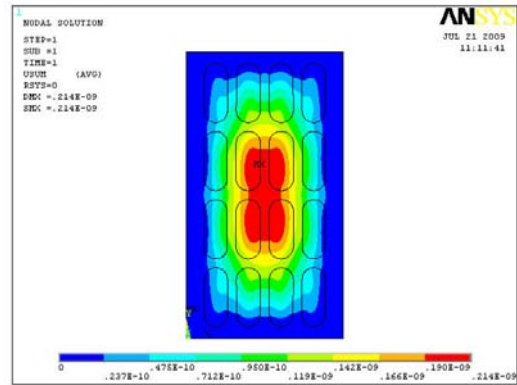
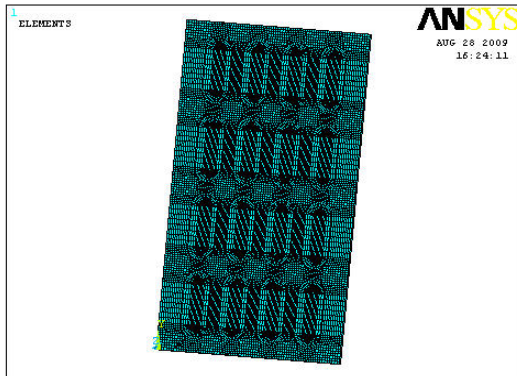
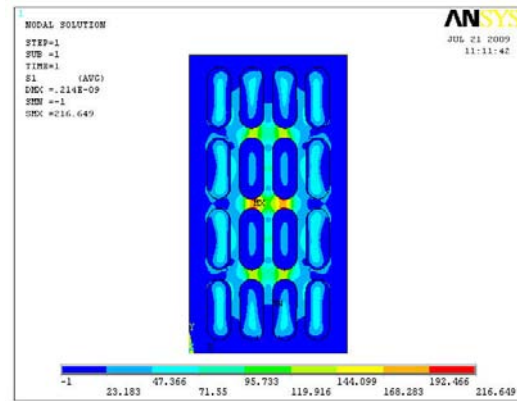
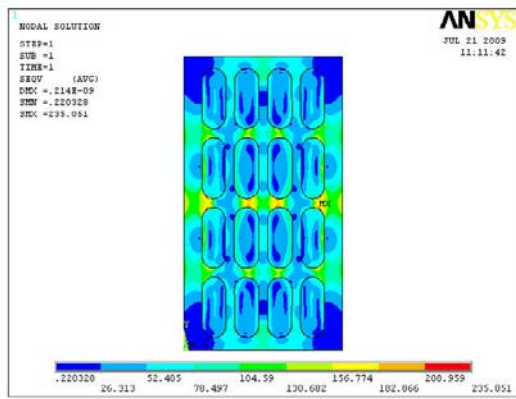


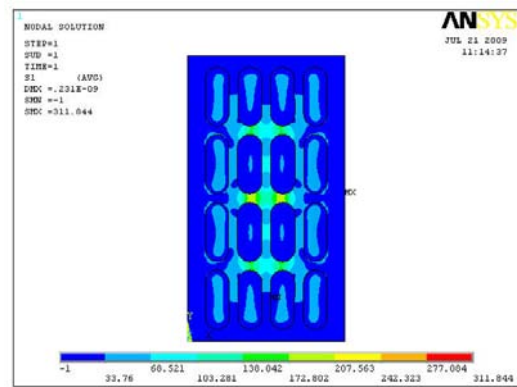
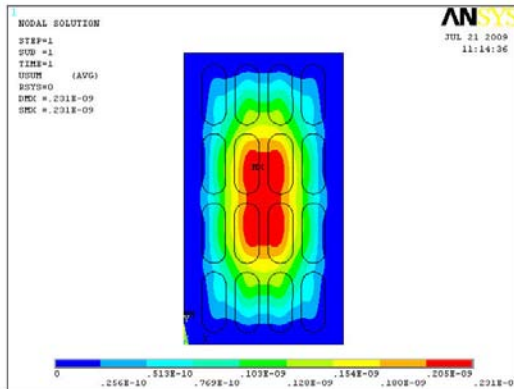
Fig. 4.17: (a)

(b)



(c)

(d)



(e)

(f)

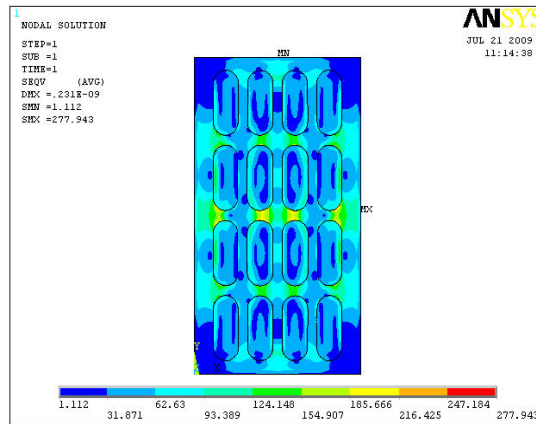


Fig. 4.17: (contd.) (g)

Fig. 4.17: (a) Finite Element Model of SVP of PPL with SHELL63 element for BC3, (b) Deflection Contour of SVP of PPL for 1Pa for BC3, (c) von Mises Stress Contour of SVP of PPL for 1Pa for BC3, (d) Maximum Principal Stress Contour of SVP of PPL for 1Pa for BC3, (e) Deflection Contour of SVP of PPL with SHELL63 element for BC4 for 1 Pa, (f) von Mises Stress Contour of SVP of PPL for 1Pa for BC4 and (g) Maximum Principal Stress Contour of SVP of PPL for 1Pa for BC4.

4.3.9 Elliptical Horizontal Perforation of PPL

Finite element model of 47 x 112 mesh with SHELL63 element is shown in Fig. 4.18 (a). This model has 11504 nodes and 10848 elements. The finite element model with SHELL93 element has 33870 nodes and 10848 elements whereas, with SOLID45 and SOLSH190 models have 26976 nodes and 17792 elements. Analyses are carried out for BC3 and BC4.

The deflection, von Mises stress and maximum principal stress contours for BC3 of SHELL63 are given in Figs. 4.18(b), 4.18(c) and 4.18(d) respectively. Figs. 4.18(e), 4.18(f) and 4.18(g) show the contour plots of deflection, von Mises stress and maximum principal stress respectively for the model with SHELL63 for BC4. The results for all the above cases are given in Table 4.8.

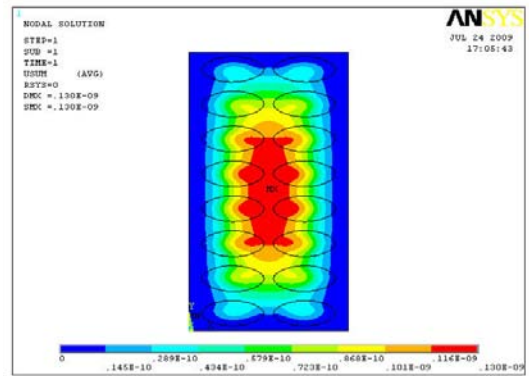
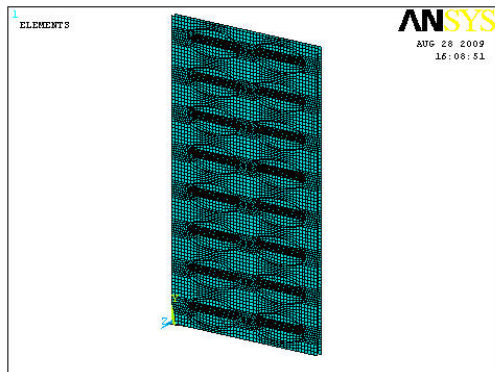
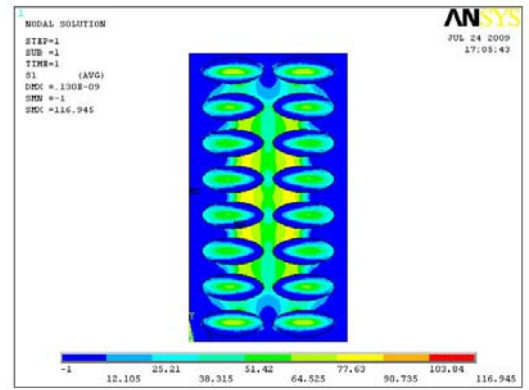
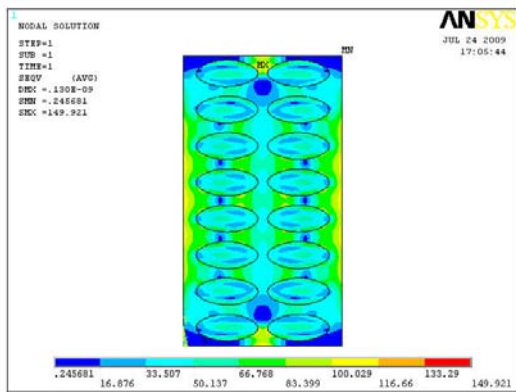


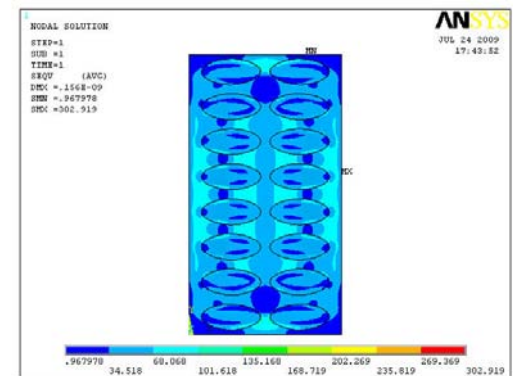
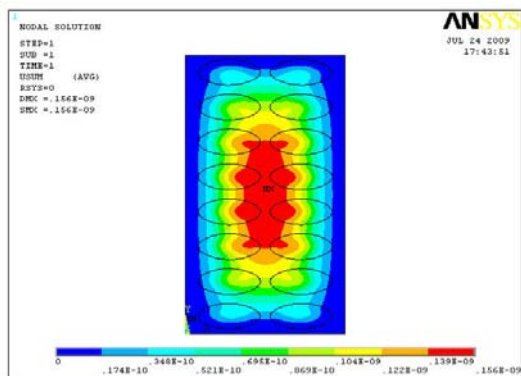
Fig. 4.18: (a)

(b)



(c)

(d)



(e)

(f)

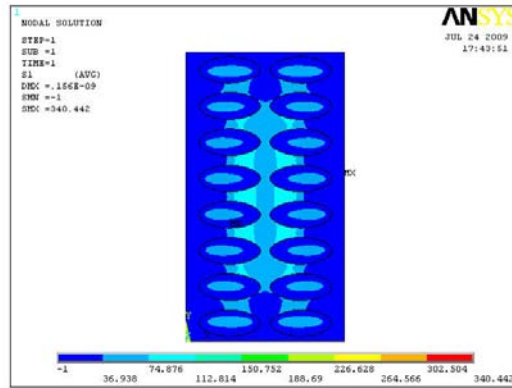


Fig. 4.18: (contd.) (g)

Fig. 4.18: (a) Finite Element Model of EHP of PPL with SHELL63 element for BC3, (b) Deflection Contour of EHP of PPL for 1Pa for BC3, (c) von Mises Stress Contour of EHP of PPL for 1Pa for BC3, (d) Maximum Principal Stress Contour of EHP of PPL for 1Pa for BC3, (e) Deflection Contour of EHP of PPL with SHELL63 element for BC4 for 1 Pa, (f) von Mises Stress Contour of EHP of PPL for 1Pa for BC4 and (g) Maximum Principal Stress Contour of EHP of PPL for 1Pa for BC4.

4.3.10 Elliptical Vertical Perforation of PPL

Finite element model of 92 x 138 mesh with SHELL63 element is shown in Fig. 4.19(a). This model has 27598 nodes and 26608 elements. The finite element model with SHELL93 element has 81818 nodes and 26608 elements whereas, with SOLID45 and SOLSH190 models have 81050 nodes and 56952 elements. Analyses are carried out for BC3 and BC4.

The deflection, von Mises stress and maximum principal stress contours for BC3 of SHELL63 are given in Figs. 4.19(b), 4.19(c), and 4.19(d) respectively. Figs. 4.19(e), 4.19(f) and 4.19(g) show the contour plots of deflection, von Mises stress and maximum principal stress respectively for the model with SHELL63 for BC4. The results for all the above cases are given in Table 4.8.

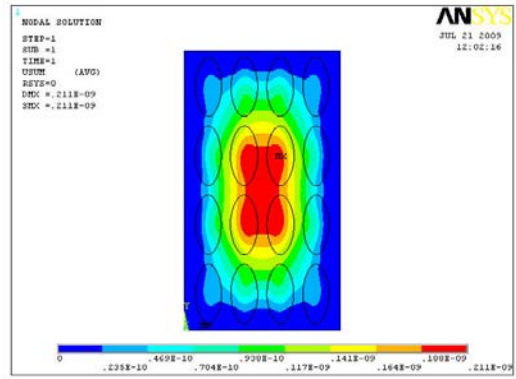
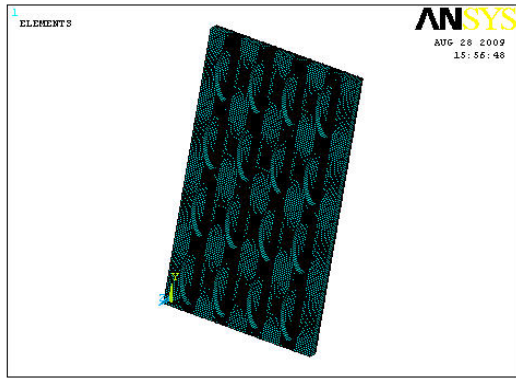
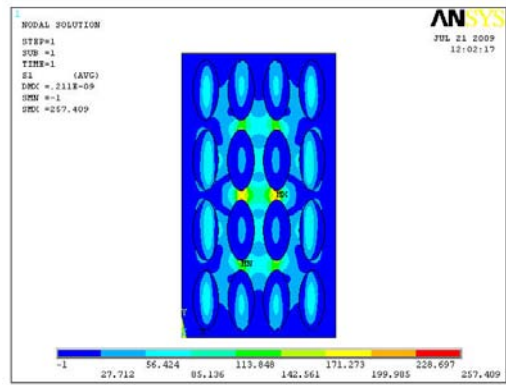
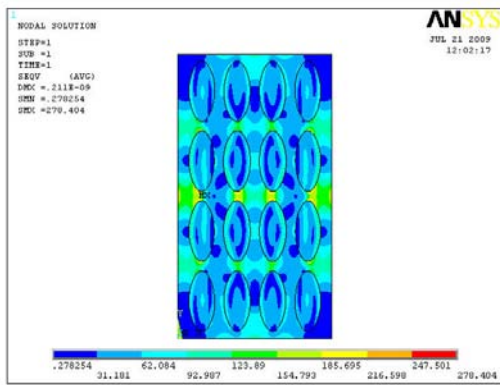


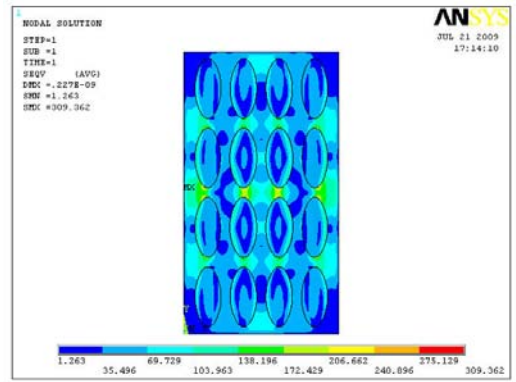
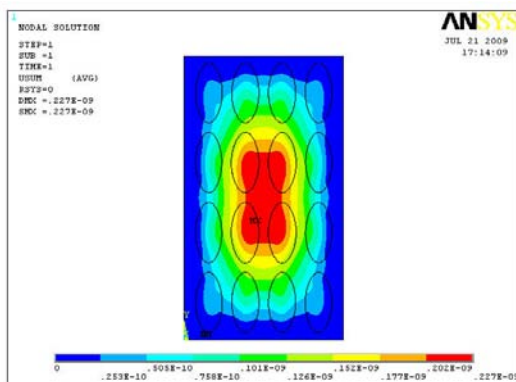
Fig. 4.19: (a)

(b)



(c)

(d)



(e)

(f)

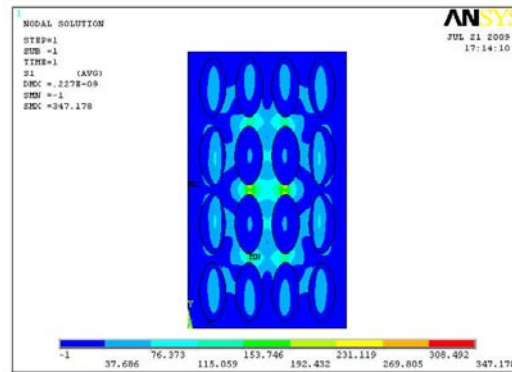


Fig. 4.19: (contd.) (g)

Fig. 4.19: (a) Finite Element Model of EVP of PPL with SHELL63 element for BC3, (b) Deflection Contour of EVP of PPL for 1Pa for BC3, (c) von Mises Stress Contour of EVP of PPL for 1Pa for BC3, (d) Maximum Principal Stress Contour of EVP of PPL for 1Pa for BC3, (e) Deflection Contour of EVP of PPL with SHELL63 element for BC4 for 1 Pa, (f) von Mises Stress Contour of EVP of PPL for 1Pa for BC4 and (g) Maximum Principal Stress Contour of EVP of PPL for 1Pa for BC4.

4.4 RESULTS AND DISCUSSION

The deflection, von Mises stress and maximum principal stress are arrived for various configurations of unit cell. The deflection obtained for NPP using finite element analysis for SOLID45 and SOLSH190 are found to be same for the respective mesh density.

4.4.1 Effect of lining plate

The variation in structural responses due to addition of 1mm lining plate is compiled and presented in Table 4.9. The response obtained from the analysis of PPL has been modified with COA and shown in this table so as to facilitate the comparison of this response with that of PP. It is observed that for BC3, the deflection is reduced by 35 to 50% and for BC4, deflection is reduced by 85%. For BC3, VMS is reduced by 15 to 27% and for BC4, the stress is reduced by 60%. For BC3, MPS is reduced by 10 to 34% and for BC4, it is reduced by 65%.

Table 4.8: Details of finite element model and static structural responses of various configurations of unit cell of perforated plate with lining for pressure of 1 Pa.

Perforated Plate with Lining				Number of nodes	Number of elements	at Centroid		
Config-uration	Element	BC	Mesh density			Deflection $\times 10^{-9}$ m	von Mises Stress Pa	Max. Principal Stress Pa
SHP	SHELL63	BC3	78 x 156	25818	24784	0.1452	60.83	68.64
	SHELL93			76426	24784	0.1677	72.45	78.61
	SOLID45			69234	48808	0.1673	73.34	79.93
	SOLSH190			69234	48808	0.1654	67.99	73.23
	SHELL63	BC4		25818	24784	0.1625	63.23	71.57
	SHELL93			76426	24784	0.1766	73.77	80.25
SVP	SHELL63	BC3	84 x 110	19110	18288	0.2073	114.16	117.33
	SHELL93			56522	18288	0.2488	147.97	142.10
	SOLID45			65442	46456	0.2494	149.83	144.53
	SOLSH190			65442	46456	0.2459	141.34	133.09
	SHELL63	BC4		19110	18288	0.2250	116.88	120.76
	SHELL93			56522	18288	0.2591	149.69	146.25
EHP	SHELL63	BC3	47 x 112	11504	10848	0.1302	55.57	62.78
	SHELL93			33870	10848	0.1493	67.04	60.75
	SOLID45			26976	17792	0.1472	61.27	68.18
	SOLSH190			26976	17792	0.1474	61.35	68.08
	SHELL63	BC4		11504	10848	0.1564	59.40	67.41
	SHELL93			33870	10848	0.1630	62.81	69.53
EVP	SHELL63	BC3	92 x 138	27598	26608	0.2039	100.20	104.33
	SHELL93			81818	26608	0.2440	124.86	123.18
	SOLID45			81050	56952	0.2447	125.56	124.63
	SOLSH190			81050	56952	0.2611	116.80	112.45
	SHELL63	BC4		27598	26608	0.2209	102.60	107.42
	SHELL93			81818	26608	0.2440	124.86	123.16
NPP	SHELL63	BC3	70 x 130	18602	18200	0.0900	48.24	55.49
	SHELL93			55402	18200	0.0956	48.25	55.53
	SOLID45			55806	45500	0.0947	48.22	55.42
	SOLSH190			55806	45500	0.0947	48.22	55.42
	SHELL63	BC4		18602	18200	0.1208	55.74	64.26
	SHELL93			55402	18200	0.1041	50.42	58.06

Table 4.9: Effect of lining plate on static structural responses for various configurations of unit cell in terms of percentage.

Config-uration	Perforated Plate with Lining			at Centroid for 1Pa.			at Centroid for (1 X 0.5448) Pa.			% Variation in VMS due to lining ((PPL-PP)/PP)*100	% Variation in MPS due to lining ((PPL-PP)/PP)*100
	Element	BC	Mesh density	Deflection x 10 ⁻⁹ m	von Mises Stress, Pa	Max. Principal Stress, Pa	Deflection x 10 ⁻⁹ m	von Mises Stress, Pa	Max. Principal Stress, Pa		
SHP	SHELL63			0.1452	60.83	68.64	0.0791	33.14	37.39	-34.8	-15.1
	SHELL93	BC3	78 x 156	0.1677	72.45	78.61	0.0914	39.47	42.83	-34.4	-23.2
	SOLID45			73.34	79.93	0.0911	39.96	43.55	-33.8	-21.2	
	SOLSH190	67.99		73.24	0.0901	37.04	39.90	-33.7	-22.0		
	SHELL63	63.23		71.57	0.0885	34.45	39.00	-86.6	-62.0		
	SHELL93	73.77		80.25	0.0962	40.19	43.72	-87.7	-66.4		
SHELL63	114.16	117.33		0.1129	62.20	63.92	-39.8	-6.8	-11.4		
SVP	SHELL93	BC3	84 x 110	0.2488	147.97	142.10	0.1355	80.61	77.42	-41.2	-15.9
	SOLID45			149.83	144.53	0.1359	81.63	78.74	-40.2	-13.2	
	SOLSH190	141.34		133.09	0.1340	77.00	72.51	-40.2	-13.5		
	SHELL63	116.88		120.76	0.1226	63.65	65.79	-85.4	-55.8		
	SHELL93	149.69		146.25	0.1412	81.55	79.68	-86.5	-61.4		
	SHELL63	55.57		62.78	0.0709	30.27	34.20	-41.3	-30.5	-29.6	
EHP	SHELL93	BC3	47 x 112	0.1493	67.04	60.75	0.0813	36.52	33.10	-40.2	-26.5
	SOLID45			61.27	68.18	0.0802	33.38	37.14	-40.0	-32.4	
	SOLSH190	61.35		68.08	0.0803	33.42	37.90	-36.3	-24.0		
	SHELL63	59.40		67.41	0.0852	32.36	36.72	-87.6	-68.4		
	SHELL93	62.81		69.53	0.0888	34.22	37.88	-89.1	-71.9		
	SHELL63	100.20		104.33	0.1111	54.59	56.84	-50.1	-19.4	-23.7	
EVP	SHELL93	BC3	92 x 138	0.2440	124.86	123.18	0.1329	68.02	67.11	-51.5	-24.9
	SOLID45			125.56	124.63	0.1333	68.41	67.88	-50.6	-23.2	
	SOLSH190	116.80		112.45	0.1422	63.63	61.26	-47.2	-28.5		
	SHELL63	102.60		107.42	0.1203	55.90	58.52	-86.6	-60.9		
	SHELL93	124.86		123.16	0.1329	68.02	67.10	-88.6	-66.3		
	SHELL63										

4.4.2 Effect of perforation orientation

The effect of orientation of perforation has been studied independently for stadium and elliptical geometries and the details are compiled and presented in Table 4.10. In case of stadium perforation, it is observed that deflection for BC3 is reduced by 55 to 65% in SHP compared to that of SVP. In BC4, the deflection for SHP is reduced by 26 to 33%. For SHP for BC3, the VMS is reduced by 70% for SHELL63 whereas for other elements the stress is reduced by about 85%. For BC4, the VMS in SHP are reduced by about 58 to 76%. Similar changes are seen for MPS also with slight reduction in percentage variation compared to VMS.

In general, SHP has displayed reduced deflection and stresses by more than 50% for all the four element types. However it is observed that 4 noded element shows reduced deflection and stresses, compared to 8 noded elements in corresponding SHP & SVP configuration.

It is observed that deflection for EHP is reduced by 84 to 113% for 4 different elements for BC3 whereas for BC4, EHP exhibits reduced deflection by 30 to 43% only to that of in BC4. The variation in deflection is plotted against the number of elements and shown in Fig. 4.20. However in case of VMS, the percentage variation between horizontal and vertical perforation is reduced by 55 to 102% for BC3 and for BC4 the percentage variation is reduced by 39 to 65%. In case of EHP, MPS is reduced by 53 to 96% for BC3 and for BC4, the stress is reduced by 38 to 58%. The percentage variation for all configurations is tabulated in Table 4.10. In general, in case of elliptical geometry, horizontal perforation is better on deflection and stresses compared to vertical perforation. It is evident from Table 4.8 that the elliptical horizontal orientation shows reduced deflection for PPL.

It can be observed that PP and PPL with HP has shown less deflection and stresses compared to VP. So plates with HP are recommended, unless otherwise required by specific reasons.

Table 4.10: Effect of orientation of perforation on static structural responses for various configurations of unit cell in terms of percentage.

		Orientation of perforation						
			SHP	SVP	% variation	EHP	EVP	% variation
Deflection X 10^{-9} m	BC3	SHELL63	0.1213	0.1874	-54.49	0.1207	0.2225	-84.34
		SHELL93	0.1393	0.2305	-65.47	0.1360	0.2743	-101.69
		SOLID45	0.1376	0.2271	-65.04	0.1336	0.2700	-102.10
		SOLSH190	0.1359	0.2241	-64.90	0.1260	0.2695	-113.89
	BC4	SHELL63	0.6628	0.8381	-26.45	0.6898	0.8997	-30.43
		SHELL93	0.7831	1.0470	-33.70	0.8113	1.1630	-43.35
VMS Pa	BC3	SHELL63	39.04	66.71	-70.88	43.53	67.70	-55.52
		SHELL93	51.37	95.82	-86.53	49.72	90.60	-82.22
		SOLID45	50.68	94.05	-85.56	49.37	89.10	-80.48
		SOLSH190	47.49	88.97	-87.33	43.97	89.04	-102.52
	BC4	SHELL63	90.74	144.04	-58.73	102.26	142.97	-39.81
		SHELL93	119.56	211.00	-76.48	121.93	201.68	-65.41
MPS Pa	BC3	SHELL63	43.89	72.13	-64.33	48.56	74.51	-53.42
		SHELL93	53.87	94.48	-75.38	53.21	93.24	-75.24
		SOLID45	53.78	93.91	-74.62	53.43	92.60	-73.32
		SOLSH190	49.77	86.42	-73.62	47.00	92.45	-96.70
	BC4	SHELL63	104.78	163.29	-55.84	117.87	163.50	-38.71
		SHELL93	135.13	223.30	-65.25	138.08	219.46	-58.94

4.4.3 Effect of release of rotation restraint at the boundary nodes

The effect of release of rotation restraint at the boundary nodes has been studied for all four configurations (SHP, SVP, EHP and EVP) by comparing the response predicted using SHELL63 and SHELL93 elements considering BC3 and BC4 along the nodes at the boundary edges. The percentage variation has been defined as the ratio of difference in the deflection for BC3 and BC4 to that for BC3.

It is observed that deflection for BC3 is reduced 300 to 500% when compared with BC4 and the same is shown in the Fig. 4.21. The reduction in stresses for BC3 has been found to be 110 to 160% with that for BC4. These percentage variations are arrived from the Tables 4.2 to 4.5 and presented in Table 4.11 for all the configurations.

Table 4.11: Effect of BC3 and BC4 boundary conditions on static structural responses for various configurations of unit cell in terms of percentage.

Effect of boundary conditions					
			BC3	BC4	% Variation
DEF x 10 ⁻⁹ (m)	SHELL63	SHP	0.1213	0.6628	-446.41
		SVP	0.1874	0.8381	-347.23
		EHP	0.1207	0.6898	-471.50
		EVP	0.2225	0.8997	-304.36
	SHELL93	SHP	0.1393	0.7831	-462.17
		SVP	0.2305	1.0470	-354.23
		EHP	0.1360	0.8113	-496.54
		EVP	0.2743	1.1630	-323.99
VMS (Pa)	SHELL63	SHP	39.04	90.74	-132.43
		SVP	66.71	144.04	-115.91
		EHP	43.53	102.26	-134.92
		EVP	67.70	142.97	-111.19
	SHELL93	SHP	51.37	119.56	-132.75
		SVP	95.82	211.00	-120.20
		EHP	49.72	121.93	-145.25
		EVP	90.60	201.68	-122.61
MPS (Pa)	SHELL63	SHP	43.89	104.78	-138.72
		SVP	72.13	163.29	-126.39
		EHP	48.56	117.87	-142.72
		EVP	74.51	163.50	-119.44
	SHELL93	SHP	53.87	135.13	-150.84
		SVP	94.48	223.30	-136.35
		EHP	53.20	138.08	-159.51
		EVP	93.24	219.46	-135.37

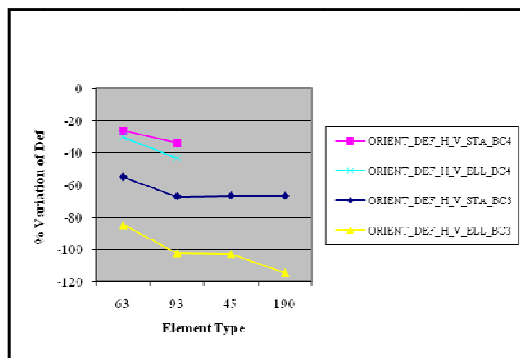


Fig. 4.20: Effect of perforation from horizontal to vertical orientation of unit cell for various elements on deflection represented in terms of percentage.

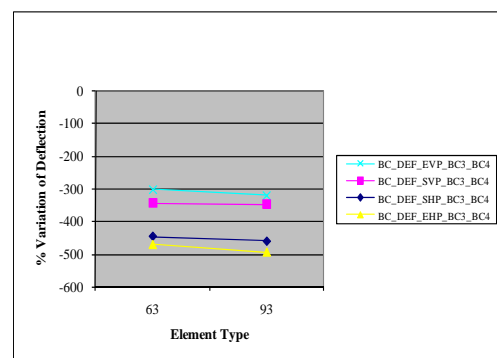


Fig. 4.21: Effect of boundary conditions BC3 and BC4 of unit cell for SHELL63 and SHELL93 elements on deflection represented in terms of percentage.

The dramatic increase in the deflection due to the release of rotation restraint is as seen in Fig. 4.21 and the increase is evident from Tables 4.1. to 4.4. Hence in practice, the boundary condition has to be seriously dealt with, in assuring the fixity along the edges.

4.4.4 Effect of perforation geometry

The structural responses are evaluated for stadium and elliptical geometry of perforations using SHELL63, SHELL93, SOLID45 and SOLSH190 elements by linear static analysis. The results are shown in Tables 4.1 to 4.4. The percentage variation for all the configurations is shown in Table 4.12.

It is observed from the above tables that the deflections predicted using the finite element models (made of 4 types of elements) of the stadium horizontal geometry and the elliptical horizontal geometry are compared. It has been found that the former exhibited higher deflection by 0.5 to 7% than the latter for BC3, and reduced by 3 to 4% for BC4 and has been shown in Fig.4.22.

From Table 4.12, it is observed that the von Mises stress for BC3 is reduced by 11% for SHELL63 in SHP compared to that in EHP. But the von Mises stresses are higher by 3 to 7% for 8 noded elements model of SHP compared to that of EHP. In BC4, von Mises stress is reduced by 13% for SHELL63 of SHP and reduced by 2% for SHELL93 in SHP.

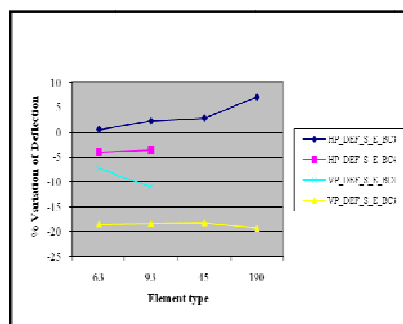


Fig.4.22: Effect of Geometry from stadium to elliptical perforation of unit cell for various elements and boundary conditions on deflection represented in terms of percentage.

Maximum principal stress for BC3 is reduced by 11% for SHELL63 model of SHP compared to that of EHP. But for 8 noded elements, the stress is higher by 1 to 5% in SHP compared to that for EHP. In BC4, the stress is reduced by 12% for SHELL63 model of SHP and reduced by 2% for SHELL93 model of SHP.

The deflections predicted using finite element models of stadium vertical geometry and elliptical vertical geometry are compared. The former shows 18% reduction than the latter for BC3 and 7 to 11% reduction for BC4 and these are shown in Fig.4.22.

From Table 4.12, it is observed that the von Mises stress for BC3 is reduced by 1.5% for SHELL63 model of SVP compared to that of EVP whereas for SOLSH190, there is a marginal decrease (0.08%) of stress in SVP. But the stresses are higher by 5 to 6% for SHELL93 and SOLID45 elements in SVP compared to that of corresponding elements in EVP. In BC4, von Mises stress is marginally higher (0.74%) in SHELL63 model of SVP and higher by 4% for SHELL93 model of SVP.

Table 4.12: Effect of stadium and elliptical geometry of perforation on static structural responses for various configurations of unit cell in terms of percentage.

		Geometry of perforation							
			SHP	EHP	% Variation		SVP	EVP	% Variation
Deflection X 10^{-9} (m)	BC3	SHELL63	0.1213	0.1207	0.49		0.1874	0.2225	-18.73
		SHELL93	0.1393	0.1360	2.37		0.2305	0.2743	-19.00
		SOLID45	0.1376	0.1336	2.91		0.2271	0.2700	-18.89
		SOLSH190	0.1359	0.1260	7.28		0.2241	0.2695	-20.26
	BC4	SHELL63	0.6628	0.6898	-4.07		0.8381	0.8997	-7.35
		SHELL93	0.7831	0.8113	-3.60		1.0470	1.1630	-11.08
VMS (Pa)	BC3	SHELL63	39.04	43.53	-11.50		66.71	67.70	-1.47
		SHELL93	51.37	49.72	3.22		95.82	90.60	5.45
		SOLID45	50.68	49.37	2.60		94.05	89.10	5.27
		SOLSH190	47.49	43.90	7.43		88.97	89.04	-0.08
	BC4	SHELL63	90.74	102.26	-12.69		144.04	142.97	0.74
		SHELL93	119.56	121.93	-1.98		211.00	201.68	4.42
MPS (Pa)	BC3	SHELL63	43.89	48.56	-10.64		72.13	74.50	-3.30
		SHELL93	53.87	53.20	1.23		94.48	93.24	1.31
		SOLID45	53.78	53.43	0.66		93.91	92.60	1.39
		SOLSH190	49.77	47.00	5.57		86.42	92.45	-6.98
	BC4	SHELL63	104.78	117.87	-12.49		163.29	163.50	-0.13
		SHELL93	135.13	138.08	-2.18		223.30	219.46	1.72

Similarly maximum principal stress for BC3 is reduced by 3% for SHELL63 model of SVP and has been reduced by 7% in SOLSH190 compared to that of EVP whereas for SHELL93 and SOLID45 elements, the stress is higher by 1 to 2% in SVP compared to the corresponding models of EVP. In BC4, the stress is marginally reduced by 0.13% for SHELL63 model of SVP and higher by 2% for SHELL93 model of SVP.

4.4.5 Effect of nodal rotational degrees of freedom of the elements

SHELL63 and SHELL93 elements have 3 translations and 3 rotations degree of freedom and SOLID45 and SOLSH190 elements have no nodal rotational degrees of freedom and basically have three translational characteristics only. The percentage variation of structural responses of SHP, SVP, EHP and EVP has been presented in Table 4.13. The percentage variation is calculated for models with SHELL63 and SHELL93 independently, comparing the corresponding values for SOLID45 and SOLSH190.

It is observed from Table 4.13 that the deflection is reduced by 12%, von Mises stress and maximum principal stress are reduced by 13 to 29% for SHP for BC3 with SHELL63 element compared to SOLID45 and SOLSH190 elements. In case of 8 noded SHELL93 element, the above responses are marginally higher than those in SOLID45 and SOLSH190 elements by 2%.

The percentage variation of deflection with respect to element type is shown in Fig. 4.23. In case of SVP and EVP, the deflection for SHELL63 is reduced by 20% compared to SOLID45 and SOLSH190 and for EHP the deflection is reduced by 5 to 10%. For SHELL93, the deflection for SVP, EHP and EVP is marginally higher by 2 to 7% compared to that of SOLID45 and SOLSH190.

In case of SVP and EVP, the stresses for SHELL63 are reduced by 20 to 40% compared to those for SOLID45 and SOLSH190 and for EHP the stresses are reduced by 1 to 13%. For SHELL93, the stresses for SVP, EHP and EVP are marginally higher by 1 to 11% compared to that of SOLID45 and SOLSH190.

Table 4.13: Effect of nodal rotational degrees of freedom of SHELL63 and SHELL93 for various configurations of unit cell on static structural responses in terms of percentage.

Effect of nodal rotational degrees of freedom of the elements						
	Configuration	Element No		Element No		% Variation
DEF x 10 ⁻⁹ (m)	SHP	SHELL63	0.1213	SOLID45	0.1376	-13.44
				SOLSH190	0.1359	-12.04
		SHELL93	0.1393	SOLID45	0.1376	1.22
				SOLSH190	0.1359	2.44
	SVP	SHELL63	0.1874	SOLID45	0.2271	-21.18
				SOLSH190	0.2241	-19.58
		SHELL93	0.2305	SOLID45	0.2271	1.48
				SOLSH190	0.2241	2.78
	EHP	SHELL63	0.1207	SOLID45	0.1336	-10.69
				SOLSH190	0.1260	- 4.39
		SHELL93	0.136	SOLID45	0.1336	1.76
				SOLSH190	0.1260	7.35
EVP	SHELL63	0.2225	SOLID45	0.2700	-21.35	
			SOLSH190	0.2695	-21.12	
	SHELL93	0.2743	SOLID45	0.2700	1.57	
			SOLSH190	0.2695	1.75	
VMS (Pa)	SHP	SHELL63	39.041	SOLID45	50.68	-29.82
				SOLSH190	47.49	-21.65
		SHELL93	51.369	SOLID45	50.68	1.33
				SOLSH190	47.49	7.54
	SVP	SHELL63	66.713	SOLID45	94.05	-40.97
				SOLSH190	88.97	-33.36
		SHELL93	95.821	SOLID45	94.08	1.85
				SOLSH190	88.97	7.15
	EHP	SHELL63	43.53	SOLID45	49.37	-13.41
				SOLSH190	43.97	- 1.00
		SHELL93	49.717	SOLID45	49.37	0.70
				SOLSH190	43.90	11.57
EVP	SHELL63	67.696	SOLID45	89.10	-31.61	
			SOLSH190	89.04	-31.53	
	SHELL93	90.596	SOLID45	89.10	1.66	
			SOLSH190	89.04	1.72	
MPS (Pa)	SHP	SHELL63	43.893	SOLID45	53.78	-22.53
				SOLSH190	49.77	-13.39
		SHELL93	53.87	SOLID45	53.78	0.17
				SOLSH190	49.77	7.61
	SVP	SHELL63	72.129	SOLID45	93.91	-30.20
				SOLSH190	86.41	-19.80
		SHELL93	94.477	SOLID45	93.91	0.60
				SOLSH190	86.19	8.54
	EHP	SHELL63	48.563	SOLID45	53.43	-10.02
				SOLSH190	47.00	3.22
		SHELL93	53.207	SOLID45	53.42	- 0.42
				SOLSH190	47.00	11.67
EVP	SHELL63	74.507	SOLID45	92.60	-24.29	
			SOLSH190	92.45	-24.08	
	SHELL93	93.241	SOLID45	92.60	0.68	
			SOLSH190	92.45	0.85	

4.4.6 Effect of higher order element

The performance of SHELL63 and SHELL93 in evaluating the structural responses of PP has been investigated on SHP, SVP, EHP and EVP for BC3 and BC4. The percentage variation for all configurations is tabulated in Table 4.14. The predicted deflection by SHELL63 is lower bound by 13 to 23% for BC3 and 17 to 29% for BC4 when compared with similar values predicted by SHELL93. Fig.4.24 shows the percentage variation of deflection with respect to perforation configuration. The reduction in stresses is found to be 10 to 43% for BC3 and 17 to 36% for BC4 when SHELL63 element is used.

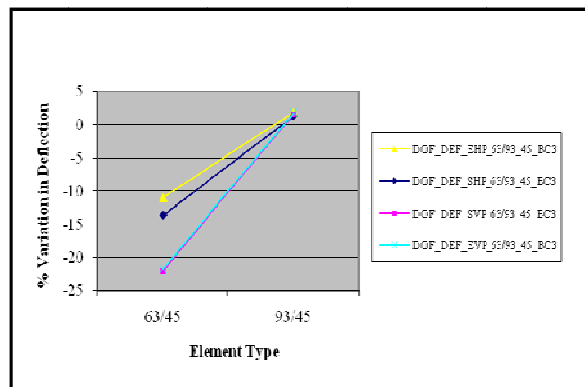


Fig.4.23: Effect of nodal DOF of SHELL & SOLID45 elements of unit cell on deflection represented in terms of percentage.

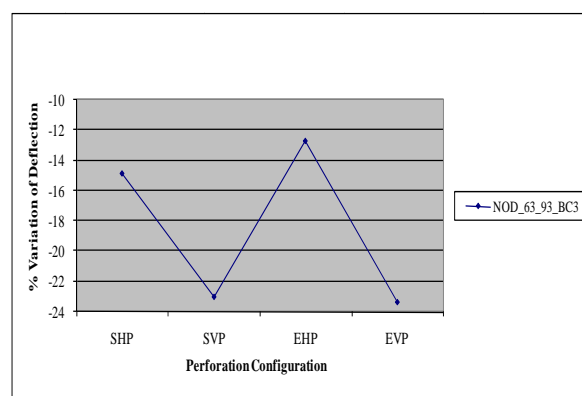


Fig.4.24: Effect of number of nodes of SHELL63 & SHELL93 elements of unit cell on deflection represented in terms of percentage.

Table 4.14: Effect of number of nodes in elements of SHELL63 and SHELL93 for various configurations of unit cell on static structural responses in terms of percentage.

Effect of number of nodes in elements							
		BC3			BC4		
		SHELL63	SHELL93	% Variation	SHELL63	SHELL93	% Variation
DEF $\times 10^{-9}$ (m)	SHP	0.1213	0.1393	-14.84	0.6628	0.7831	-18.15
	SVP	0.1874	0.2305	-23.00	0.8381	1.0470	-24.93
	EHP	0.1207	0.1360	-12.68	0.6898	0.8113	-17.61
	EVP	0.2225	0.2745	-23.37	0.8997	1.1630	-29.27
VMS (Pa)	SHP	39.04	51.37	-31.58	90.74	119.56	-31.76
	SVP	66.71	95.82	-43.63	144.04	211.00	-46.49
	EHP	43.53	49.72	-14.21	102.26	121.93	-19.24
	EVP	67.70	90.60	-33.83	142.97	201.68	-41.06
MPS (Pa)	SHP	43.893	53.87	-22.73	104.78	135.13	-28.97
	SVP	72.129	94.477	-30.98	163.29	223.30	-36.75
	EHP	48.563	53.207	-9.56	117.87	138.08	-17.15
	EVP	74.507	93.241	-25.14	163.50	219.46	-34.23

4.4.7 Evaluation of Stress concentration and Deflection factor

Stress Concentration Factor (SCF) and Deflection Factor (DF) are the two non dimensional parameter used in the present study to evaluate the effect of perforation in plate. The SCF is defined as the ratio of maximum principal stress at a location in perforated plate to the stress at the same point on non perforated plate. DF is defined as the ratio of the deflection at a position in perforated plate to that in non perforated plate at the same location.

The scope of the study cover the horizontal and vertical configuration of stadium and elliptical perforation for BC3 and BC4 using the four finite elements SHELL63, SHELL93, SOLID45 and SOLSH190. In each model quarter symmetry is utilized and the evaluation of SCF and DF have been carried out in perforations 1, 2, 3 and 4 shown in Figs. 3.2(a) to 3.2(d). The SCF and DF for PP and PPL have been evaluated from the linear static analysis and are given in Tables 4.15(a) to 4.15(p).

Table 4.15: (a) Stress concentration factor for SHP for BC3 and BC4.

Element	Perforation number							
	1		2		3		4	
	BC3	BC4	BC3	BC4	BC3	BC4	BC3	BC4
SHELL63	2.472	2.598	2.497	2.606	2.514	2.611	7.584	2.946
SHELL93	2.880	3.238	2.967	3.333	3.034	3.347	7.484	3.776
SOLID45	2.848	-----	2.927	-----	2.896	-----	7.011	-----
SOLSH190	3.033	-----	3.243	-----	3.592	-----	5.990	-----

Table 4.15: (b) Deflection factor for SHP for BC3 and BC4.

Element	Perforation number							
	1		2		3		4	
	BC3	BC4	BC3	BC4	BC3	BC4	BC3	BC4
SHELL63	1.575	2.182	1.592	2.240	1.632	2.250	1.604	2.210
SHELL93	1.730	2.541	1.772	2.553	1.804	2.583	1.772	2.496
SOLID45	1.730	-----	1.768	-----	1.796	-----	1.738	-----
SOLSH190	1.718	-----	1.747	-----	1.776	-----	1.733	-----

Table 4.15: (c) Stress concentration factor for SVP for BC3 and BC4.

Element	Perforation number							
	1		2		3		4	
	BC3	BC4	BC3	BC4	BC3	BC4	BC3	BC4
SHELL63	4.199	4.152	5.656	3.856	3.753	3.916	4.812	3.348
SHELL93	5.105	5.359	6.159	4.683	4.706	5.064	6.594	4.662
SOLID45	4.966	-----	7.029	-----	4.837	-----	7.228	-----
SOLSH190	4.076	-----	6.486	-----	4.184	-----	6.937	-----

Table 4.15: (d) Deflection factor for SVP for BC3 and BC4.

Element	Perforation number							
	1		2		3		4	
	BC3	BC4	BC3	BC4	BC3	BC4	BC3	BC4
SHELL63	2.618	2.826	2.118	2.864	2.290	2.761	1.960	2.769
SHELL93	2.919	3.420	2.551	3.325	2.627	3.311	2.257	3.304
SOLID45	2.904	-----	2.711	-----	2.515	-----	2.271	-----
SOLSH190	2.879	-----	2.498	-----	2.547	-----	2.220	-----

Table 4.15: (e) Stress concentration factor for EHP for BC3 and BC4.

Element	Perforation number							
	1		2		3		4	
	BC3	BC4	BC3	BC4	BC3	BC4	BC3	BC4
SHELL63	1.913	2.735	1.942	2.740	1.964	2.732	4.270	3.889
SHELL93	1.980	3.416	2.063	3.488	2.563	3.226	5.676	4.817
SOLID45	2.013	-----	2.090	-----	2.730	-----	4.366	-----
SOLSH190	3.613	-----	3.927	-----	4.503	-----	2.247	-----

Table 4.15: (f) Deflection factor for EHP for BC3 and BC4.

Element	Perforation number							
	1		2		3		4	
	BC3	BC4	BC3	BC4	BC3	BC4	BC3	BC4
SHELL63	1.573	2.334	1.639	2.356	1.807	2.366	1.956	2.507
SHELL93	1.702	2.660	1.799	2.714	1.956	2.804	2.171	2.968
SOLID45	1.684	-----	1.767	-----	1.902	-----	2.084	-----
SOLSH190	1.593	-----	1.695	-----	1.898	-----	2.101	-----

Table 4.15: (g) Stress concentration factor for EVP for BC3 and BC4.

Element	Perforation number							
	1		2		3		4	
	BC3	BC4	BC3	BC4	BC3	BC4	BC3	BC4
SHELL63	6.067	6.003	8.323	4.803	5.151	5.491	6.407	4.028
SHELL93	8.253	8.803	9.516	8.318	6.910	8.403	7.676	7.197
SOLID45	7.314	-----	10.254	-----	6.518	-----	9.304	-----
SOLSH190	7.505	-----	10.995	-----	6.466	-----	9.491	-----

Table 4.15: (h) Deflection factor for EVP for BC3 and BC4.

Element	Perforation number							
	1		2		3		4	
	BC3	BC4	BC3	BC4	BC3	BC4	BC3	BC4
SHELL63	2.970	3.046	2.693	3.150	2.625	3.120	2.500	2.966
SHELL93	3.518	3.830	3.222	3.968	3.012	3.802	2.745	3.692
SOLID45	3.472	-----	3.443	-----	2.948	-----	2.544	-----
SOLSH190	3.491	-----	3.445	-----	3.007	-----	2.544	-----

Table 4.15: (i) Stress concentration factor of PPL for SHP for BC3 and BC4.

Element	Perforation number							
	1		2		3		4	
	BC3	BC4	BC3	BC4	BC3	BC4	BC3	BC4
SHELL63	2.600	2.206	2.660	2.260	2.730	2.366	6.185	8.295
SHELL93	2.847	2.769	2.981	2.898	3.133	3.004	8.081	9.613
SOLID45	2.859	-----	2.981	-----	2.983	-----	5.998	-----
SOLSH190	3.058	-----	2.683	-----	2.755	-----	7.427	-----

Table 4.15: (j) Deflection factor of PPL for SHP for BC3 and BC4.

Element	Perforation number							
	1		2		3		4	
	BC3	BC4	BC3	BC4	BC3	BC4	BC3	BC4
SHELL63	1.738	1.343	1.658	1.362	1.681	1.380	1.725	1.363
SHELL93	1.797	1.731	1.790	1.744	1.834	1.768	1.914	1.821
SOLID45	1.783	-----	1.821	-----	1.852	-----	1.948	-----
SOLSH190	1.763	-----	1.800	-----	1.829	-----	1.880	-----

Table 4.15: (k) Stress concentration factor of PPL for SVP for BC3 and BC4.

Element	Perforation number							
	1		2		3		4	
	BC3	BC4	BC3	BC4	BC3	BC4	BC3	BC4
SHELL63	4.399	3.683	4.342	13.197	4.131	3.503	4.407	6.610
SHELL93	4.888	4.728	8.685	7.697	4.776	4.543	6.464	7.204
SOLID45	4.957	-----	6.962	-----	4.565	-----	6.765	-----
SOLSH190	4.203	-----	5.750	-----	4.300	-----	5.852	-----

Table 4.15: (l) Deflection factor of PPL for SVP for BC3 and BC4.

Element	Perforation number							
	1		2		3		4	
	BC3	BC4	BC3	BC4	BC3	BC4	BC3	BC4
SHELL63	2.426	1.931	2.283	1.639	2.189	1.765	1.832	1.406
SHELL93	2.762	2.636	2.644	2.513	2.439	2.336	2.210	2.249
SOLID45	2.793	-----	2.694	-----	2.385	-----	2.282	-----
SOLSH190	2.773	-----	2.667	-----	2.434	-----	2.228	-----

Table 4.15: (m) Stress concentration factor of PPL for EHP for BC3 and BC4.

Element	Perforation number							
	1		2		3		4	
	BC3	BC4	BC3	BC4	BC3	BC4	BC3	BC4
SHELL63	2.481	1.819	1.907	1.878	2.301	2.021	2.236	3.028
SHELL93	2.246	2.780	2.191	2.937	2.195	2.465	3.369	4.001
SOLID45	1.864	-----	1.974	-----	2.077	-----	2.810	-----
SOLSH190	1.683	-----	1.974	-----	2.464	-----	3.259	-----

Table 4.15: (n) Deflection factor of PPL for EHP for BC3 and BC4.

Element	Perforation number							
	1		2		3		4	
	BC3	BC4	BC3	BC4	BC3	BC4	BC3	BC4
SHELL63	1.466	1.300	1.513	1.327	1.602	1.427	1.947	1.480
SHELL93	1.578	1.580	1.621	1.639	1.802	1.743	2.179	2.084
SOLID45	1.576	-----	1.672	-----	1.775	-----	2.091	-----
SOLSH190	1.575	-----	1.634	-----	1.777	-----	2.082	-----

Table 4.15: (o) Stress concentration factor of PPL for EVP for BC3 and BC4.

Element	Perforation number							
	1		2		3		4	
	BC3	BC4	BC3	BC4	BC3	BC4	BC3	BC4
SHELL63	5.160	4.327	3.300	8.033	4.480	3.806	4.792	7.881
SHELL93	6.594	6.254	6.104	6.509	5.866	5.565	5.539	5.905
SOLID45	5.979	-----	3.914	-----	5.110	-----	4.628	-----
SOLSH190	3.865	-----	5.864	-----	4.078	-----	3.982	-----

Table 4.15: (p) Deflection factor of PPL for EVP for BC3 and BC4.

Element	Perforation number							
	1		2		3		4	
	BC3	BC4	BC3	BC4	BC3	BC4	BC3	BC4
SHELL63	2.538	1.902	2.389	1.664	2.120	1.714	1.800	1.297
SHELL93	2.745	2.517	2.776	2.478	2.314	2.213	2.131	1.884
SOLID45	2.732	-----	2.834	-----	2.415	-----	2.328	-----
SOLSH190	2.935	-----	2.976	-----	2.471	-----	2.253	-----

Stress concentration factor and deflection factor predicted using SHELL63 for stadium and elliptical geometry are compiled and presented in Table 4.16. This table can be used as a design support for ligament width of 6 mm since it is based upon underwater sonar application in India and Russia.

Table 4.16: SCF and DF of unit cell for various configurations using SHELL63 element.

SHELL63		Stress concentration factor				Deflection factor			
Config-uration	BC	Perforation number							
		1	2	3	4	1	2	3	4
SHP	BC3	2.472	2.497	2.514	7.584	1.575	1.592	1.632	1.604
	BC4	2.598	2.606	2.611	2.946	2.182	2.240	2.250	2.210
SVP	BC3	4.199	5.656	3.753	4.812	2.618	2.118	2.290	1.960
	BC4	5.359	3.856	3.916	3.348	2.826	2.864	2.761	2.769
EHP	BC3	1.913	1.942	1.964	4.270	1.573	1.639	1.807	1.956
	BC4	2.735	2.740	2.732	3.889	2.334	2.356	2.366	2.507
EVP	BC3	6.067	8.323	5.161	6.407	2.970	2.693	2.625	2.500
	BC4	6.003	4.803	5.491	4.028	3.046	3.150	3.120	2.966
SHP of PPL	BC3	2.600	2.660	2.730	6.185	1.738	1.658	1.681	1.725
	BC4	2.206	2.260	2.366	8.295	1.343	1.362	1.380	1.363
SVP of PPL	BC3	4.399	4.342	4.131	4.407	2.426	2.283	2.189	1.832
	BC4	3.683	13.20	3.503	6.610	1.931	1.639	1.765	1.406
EHP of PPL	BC3	2.481	1.907	2.301	2.236	1.466	1.513	1.602	1.947
	BC4	1.819	1.878	2.021	3.028	1.300	1.327	1.427	1.480
EVP of PPL	BC3	5.160	3.300	4.480	4.792	2.538	2.389	2.120	1.800
	BC4	4.327	8.033	3.806	7.881	1.902	1.664	1.714	1.297

Considering SCF and DF, it is to observe that for SHELL63 for BC3, EHP shows reduced stress concentration factor and SHP shows reduced deflection factor around its periphery of the perforation. It has been inferred from Table 4.15(a) to 4.15(p) that the addition of lining plate on PP, has marginal reduction on SCF and DF. This is due to the presence of geometric discontinuities existing at the locations of perforations in PPL.

4.4.8 Recommendations

1. Finite element results for NPP have been compared with the exact solution in section 4.3.5 and it is found that principal stress predicted by SHELL63 elements is lower by 1.27%. For the SHELL93, the reduction in stress is predicted by 1.2% compared to the exact solution. However the reduction in stress for the SOLID45 and SOLSH190, is

found to be 1.32% compared with the exact solution. There is only marginal difference in stress between SHELL63 and SHELL93. This implies that SHELL93, which is an eight noded element will lead to a finite element model of the plate with more number of nodes than SHELL63 which is a four noded element and the analysis if performed with SHELL63 will give somewhat the same quality results as SHELL93 at a reduced computational effort. Considering these facts, the number of nodes and elements and computational effort, SHELL63 is recommended for the analysis.

2. The static responses viz., deflection, VMS and MPS for SHP and EHP are lower than that of SVP and EVP, for both the boundary conditions and for all the four elements used in the modeling. Hence horizontal perforation orientation is recommended for application. The horizontal orientation should be along the smaller dimension of the plate as analysed in this investigation.

3. Deflection, VMS and MPS of SHP and EHP for BC3 are lower than the corresponding values of BC4. This state is as expected since BC3 has all the rotations restrained along with translations. The 5 to 10% variation in the deflection and stresses is likely to surface out, when the actual fixed edge cannot provide the full fixity expected from that as in the case of a defective weld.

4. Horizontal perforation and BC3 boundary condition are the recommended feature of the PP. SHP gives 5% higher deflection than EHP, whereas the VMS and MPS predicted in SHP is lower than that in EHP.

Based on the studies on unit cell of two configurations, two perforations and four types of elements, it is recommended to use SHP for the underwater applications and SHELL63 element for further numerical investigations.

CHAPTER 5

NUMERICAL INVESTIGATIONS ON PERFORATED PLATE

5.1 INTRODUCTION

The perforated plates while in underwater environment are subjected to a variety of static and dynamic loads: hydrostatic pressure, drag force, shock loads etc., are a few to mention. The scope of numerical investigations in such plates usually covers linear and nonlinear static and dynamic analysis. It is envisaged to conduct shock analysis of the PP, considering the defense application of such plates in underwater environment.

5.2 DESCRIPTION OF PERFORATED PLATE

The perforated plate with stadium horizontal perforation has been considered for the analysis. It is a thin continuous plate of uniform thickness 0.006 m with height 0.9 m and stiffened vertically at 0.3m interval. For the present analysis, a plate of 0.9 m x 0.9 m along the X and Y axes is carved out from the continuous plate. The coordinate directions, geometry and fine details of the perforations are shown in Fig. 5.1. There are 40 rows and 18 columns of perforations. The origin for the coordinate system is taken as left, bottom corner. The edge clearance at top and bottom is 13 mm and at the other two edges, the clearance is 15 mm. The COP and COA of the specimen plate for the present analysis have been worked out as 0.5201 and 0.4799 respectively.

The perforated plate is usually stiffened in order to restrict the transverse deflections. Stiffeners are not explicitly modeled in the present analysis, instead the transverse translation at the nodes along the stiffener line at $x = 0, 0.3 \text{ m}, 0.6 \text{ m}$ and 0.9 m are arrested. A non perforated plate of identical dimension as that of PP has been analysed for all the identical conditions in order to bring out the influence of perforations on the structural responses.

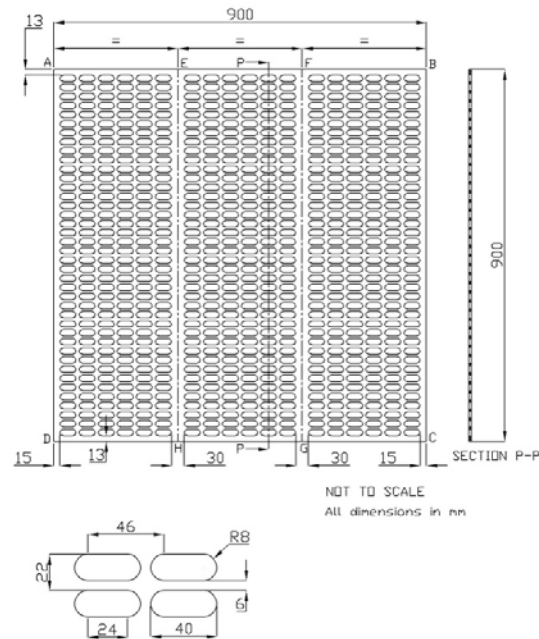


Fig. 5.1: Geometry of Perforated Plate considered for the investigation

5.3 LINEAR STATIC ANALYSIS

Plate model and solid model of PP have been generated as mentioned in section 3.5 and 3.6 and the elements mentioned previously are used for analysis. The details of these models are described subsequently.

5.3.1 Plate model

Plate models are generated with SHELL63 and SHELL93 elements. Both the finite element models have same appearance and shown in Fig. 5.2(a). The finite element model contains 13719 nodes and 10584 elements when modeled with SHELL63; and 38741 nodes and 10584 elements when modeled with SHELL93. The nodal values of deflection, von Mises stress and maximum principal stress are evaluated and presented in Table 5.1. Fig. 5.2(b) shows the deflection contour, Fig. 5.2(c) gives the contour of von Mises stress and Fig. 5.2(d) gives the maximum principal stress for BC1 and Figs. 5.2(e), 5.2(f) and 5.2(g) show the corresponding responses for BC2.

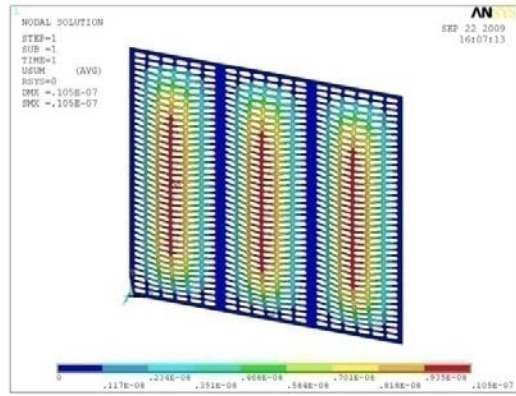
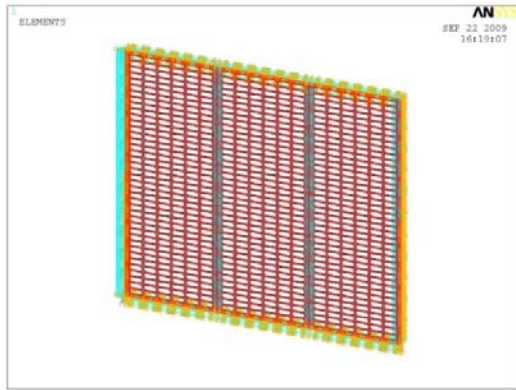
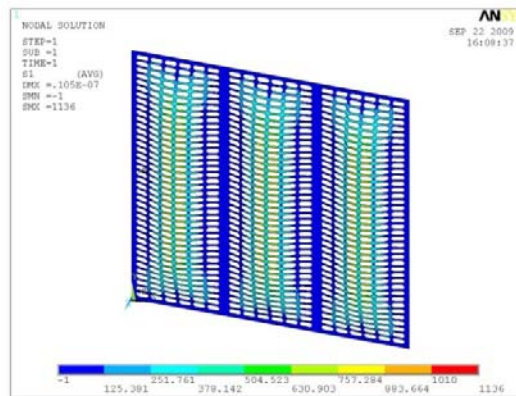
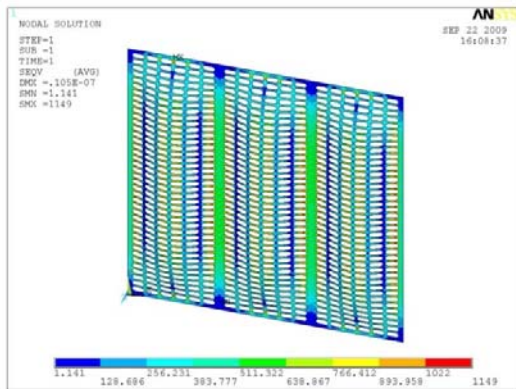


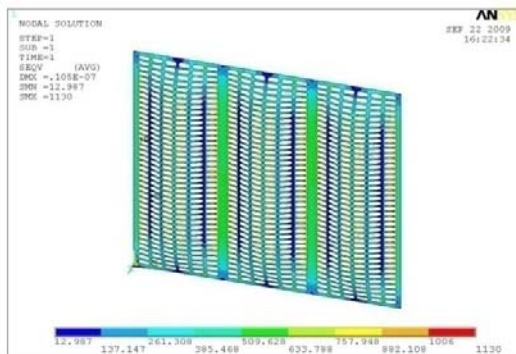
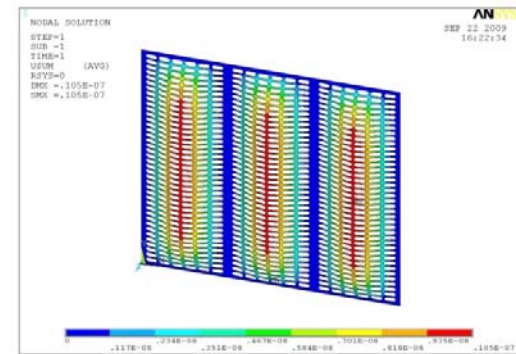
Fig. 5.2: (a)

(b)



(c)

(d)



(e)

(f)

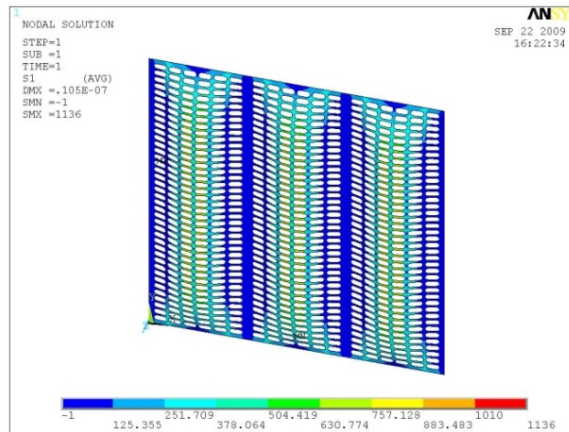


Fig. 5.2: (contd.) (g)

Fig. 5.2: (a) Finite Element Model of PP with SHELL63 element for BC1, (b) Deflection Contour of PP for 1Pa for BC1, (c) von Mises Stress Contour of PP for 1Pa for BC1, (d) Maximum Principal Stress Contour of PP for 1Pa for BC1, (e) Deflection Contour of PP with SHELL63 element for BC2 for 1 Pa, (f) von Mises Stress Contour of PP for 1Pa for BC2 and (g) Maximum Principal Stress Contour of PP for 1Pa for BC2.

5.3.2 Solid model

Solid models are generated with SOLID45 and SOLSH190 elements. The finite element models have same appearance and shown in Fig. 5.3(a). The model for each element contains 54876 nodes and 31752 elements. The nodal values of deflection, von Mises stress and maximum principal stress are presented in Table 5.1. Fig. 5.3(b) shows deflection contour, Fig. 5.3(c) shows von Mises stress contour and Fig. 5.3(d) shows the maximum principal stress contour for BC1 and Figs. 5.3(e), 5.3(f) and 5.3(g) are the corresponding figures for SOLSH190.

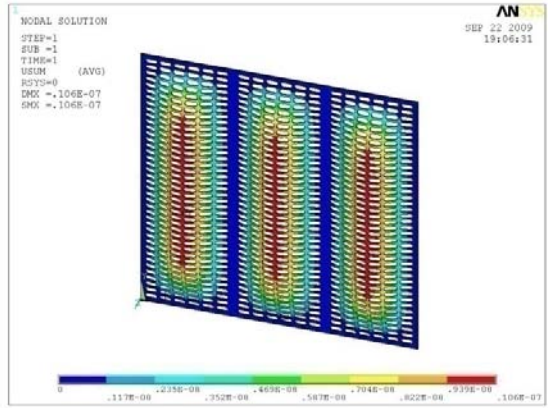
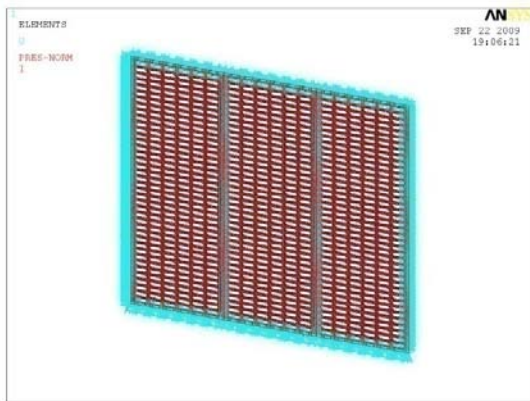
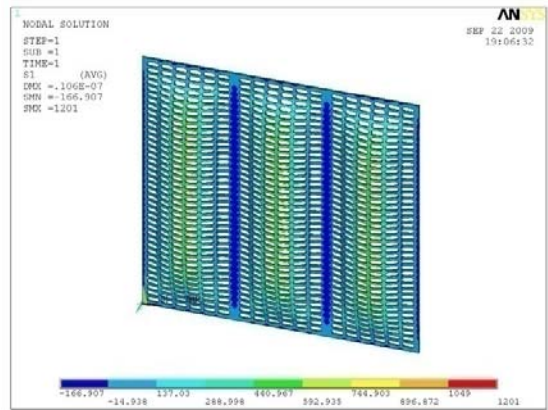
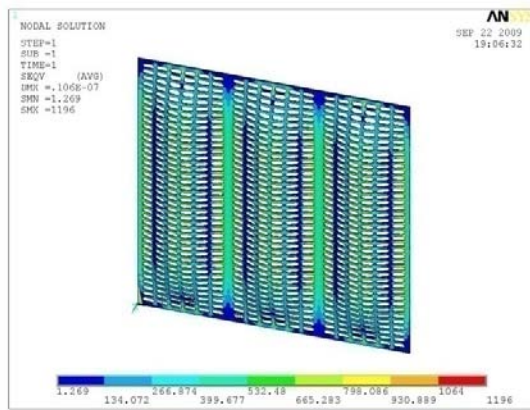


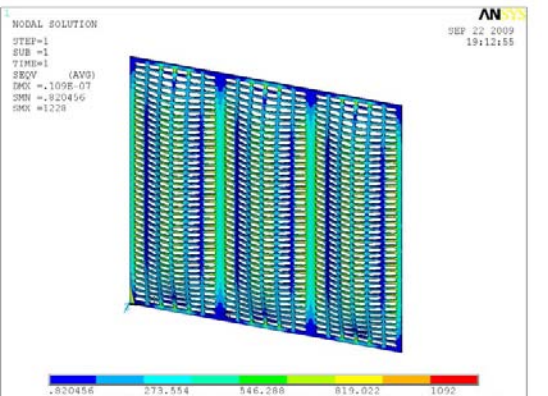
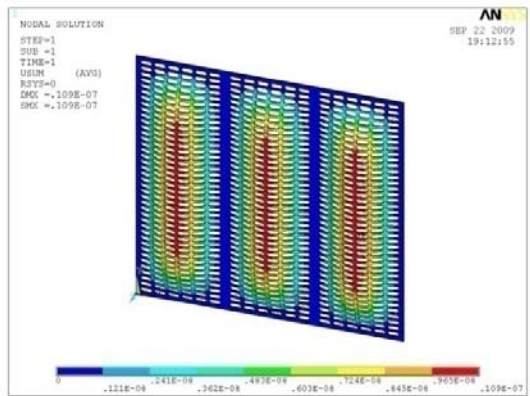
Fig. 5.3: (a)

(b)



(c)

(d)



(e)

(f)

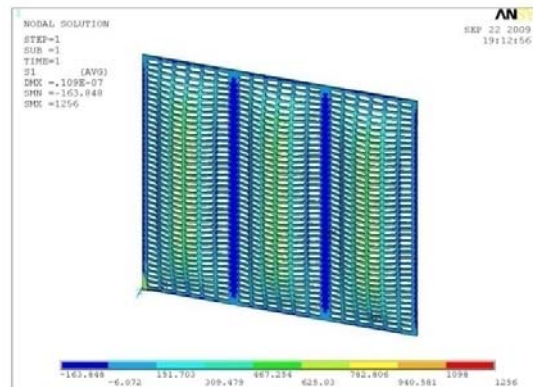


Fig. 5.3: (contd.) (g)

Fig. 5.3: (a) Finite Element Model of PP with SOLID45 element for BC1, (b) Deflection Contour of PP with SOLID45 element for 1Pa for BC1, (c) von Mises Stress Contour of PP with SOLID45 element for 1Pa for BC1, (d) Maximum Principal Stress Contour of PP for 1Pa for BC1, (e) Deflection Contour of PP with SOLSH190 element for BC1 for 1 Pa, (f) von Mises Stress Contour of PP with SOLSH190 element for 1Pa for BC1 and (g) Maximum Principal Stress Contour of PP with SOLSH190 element for 1Pa for BC1.

5.4 RESULTS AND DISCUSSION

The responses obtained from the analysis of NPP have been modified with COA and shown in Table 5.1 to facilitate the comparison of the PP response with that of NPP. The reference location for the comparison of the static response of PP and NPP has been chosen as the centroid of the corresponding plate.

In order to find out the influence of perforations on the strength and response of the plate, the percentage variation on structural responses is calculated and presented in Table 5.1. The variation is arrived by taking the ratio of difference in structural response between PP and NPP to that of NPP.

Table 5.1: Effect of perforation on NPP and PP of static structural responses of different models for BC1 and BC2.

Sl. No	Model	Boundary condition	Effect of Perforation between NPP and PP											
			Deflection X 10^{-7} (m) at Centroid				von Mises stress (Pa) at Centroid				Max. Principal stress (Pa) at Centroid			
			PP	NPP for 1Pa	NPP x COA	% Variation	PP	NPP for 1Pa	NPP x COA	% Variation	PP	NPP for 1Pa	NPP x COA	% Variation
1	Plate Model (SHELL 63)	BC1	0.1049	0.0978	0.0469	123.7	316	563.5	270.42	16.9	360.6	634.4	304.45	18.4
		BC2	0.1049	0.0977	0.0469	123.7	316	562.9	270.14	17.0	360.4	633.1	303.82	18.6
2	Plate Model (SHELL 93)	BC1	0.1104	0.098	0.047	134.9	393	569.4	273.26	43.8	402.2	641.1	307.66	30.7
		BC2	0.1102	0.0979	0.047	134.4	392	569	273.06	43.6	401.5	640	307.14	30.7
3	Solid Model (SOLID 45)	BC1	0.1032	0.0939	0.0451	128.8	433.8	535	256.75	69.0	492.7	602.9	289.33	70.3
		BC2	0.1046	0.094	0.0451	131.9	434.3	536.6	257.51	68.7	489.8	603.5	289.62	69.1

From the Table 5.1, it is evident that the effect of perforations is to increase the deflection by 120%, in all the four models studied. The plate models of the PP constituted with SHELL63 and SHELL93 elements go upper bound in the prediction of stresses by 17 to 19% and 30 to 43% respectively. However stresses predicted by solid model of the PP made with SOLID45 and SOLSH190 are higher by 70%.

The variations in the evaluation of stresses by the four elements used herein can be attributed to the nodal parameter of each of them. SHELL63 is a four noded element with linear shape function and SHELL93 an eight noded element with quadratic shape functions. Conformity characteristics of the elements may be the reason for the variations. SOLID45 and SOLSH190 are solid or brick element with translational degrees of freedom. The discrepancy in the stresses may be due to the lack of rotational degree of freedom of these elements which are employed for the prediction of stresses in the bending of plate. Based on the outcome of the analysis, it is recommended to use SHELL63 element.

5.5 GEOMETRIC NONLINEAR ANALYSIS

Geometric nonlinear analysis becomes necessary for structural systems which show large displacements and / or large strains. PP is prone to stress concentration and subsequently such structural system falls in the large strain category. Geometric nonlinear analysis of a structure is performed using finite element method as an iterative and incremental procedure. The displacements of a characteristic point at various load steps will be plotted and inferences are derived from this.

5.5.1 Description of finite element analysis

The plate models of NPP and PP with SHELL63 element which has been used for linear elastic analysis (Figs. 5.4 and 5.5) are used for geometric nonlinear analysis as well. Nonlinear static module of ANSYS has been used for the purpose. The maximum load for NPP and PP has been kept as 2000 and 1000 kPa respectively. This load is applied at 20 load steps. Deflections, VMS and MPS at each load step are made available.

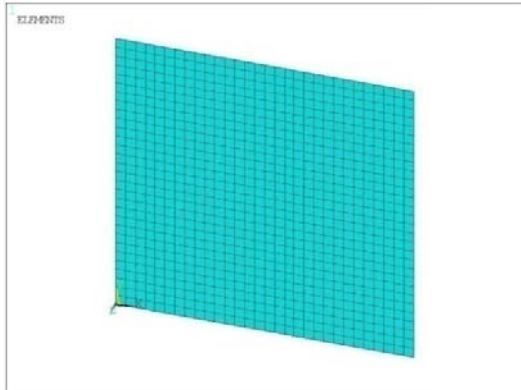


Fig. 5.4: Finite element model of NPP with SHELL63 element and BC1.

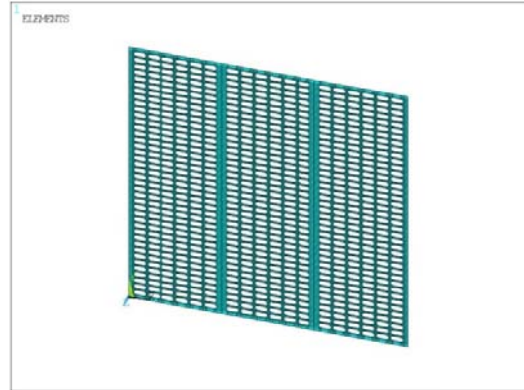


Fig. 5.5: Finite element model of PP with SHELL63 element and BC1.

5.5.2 Results and Discussion

The load deflection plot for NPP and PP are shown in Fig. 5.6 and deflection and stresses at a few load steps for NPP and PP are shown in Table 5.2. The initial portion of the plot is a straight line and becomes nonlinear at 500kPa for NPP. The intersection of tangent lines at the initial and final part of the plot, gives the load at which the nonlinearity is initiated. For PP, the nonlinearity starts when load is 380 kPa for a deflection of 3.45 mm.

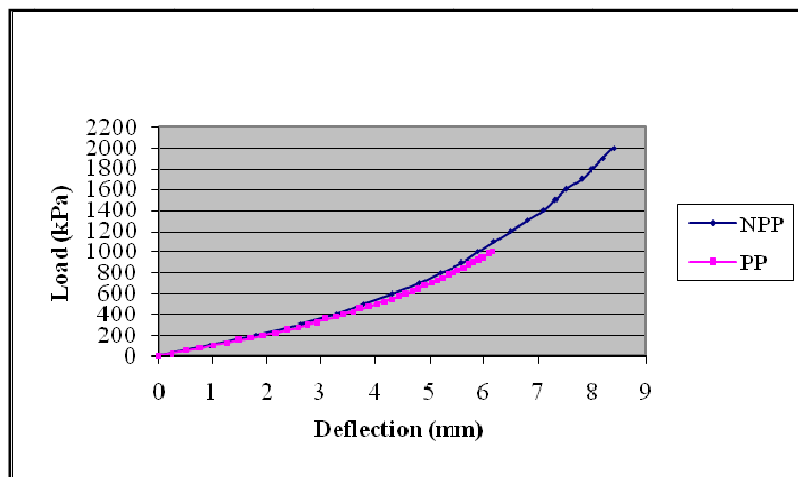


Fig. 5.6: Load – deflection plot for each load step for the configuration of NPP and PP

Table 5.2: Static structural responses of NPP and PP due to geometric nonlinearity of the plate for BC1.

Sl.No	Configuration	Load (kPa)	Deflection (mm)	VMS (MPa)	MPS (MPa)
1	NPP	300	2.6	310	348
		500	3.8	486	546
		1000	5.9	847	950
		2000	8.4	1400	1570
2	PP	500	4.03	530	532.9
		1000	6.17	937.7	955.3

5.6 FREE VIBRATION ANALYSIS

Considering its application for underwater platform, it is essential to study the behavior of the perforated plate immersed in the water medium. The presence of water medium and the effect of added mass are predominant factors in determining the natural frequency of the plate. The analysis carried out, considering water medium is termed as ‘water backed’ and without water medium is termed as ‘in vacuum’. The determination of free vibration characteristics of NPP and PP of 0.9 m x 0.9 m models ‘in vacuum’ and in water backed condition has been envisaged. The geometry and boundary condition are kept same as that of the plates for linear static analysis.

5.6.1 Description of finite element analysis

SHELL63 element is used to model NPP and PP and the fluid is with fluid acoustic element FLUID30. The thickness of the fluid element for modeling has been taken as forty times the plate thickness and this is divided into three layers. The stretch of the fluid domain and the number of layers has been arrived based on a number of trials carried out on NPP. The fluid region attached with the plate is assigned as “fluid with structure present” and the other two layers are assigned as “fluid with structure absent” for bringing the fluid structure interaction effect in the model. The outer boundaries of the element are of “fluid with structure absent”, with zero pressure. This simulates an infinite fluid region. The nodes of the fluid are coupled with the contact nodes on the plate. In each analysis, about 30 modes are evaluated to facilitate the natural frequency - modal index plot.

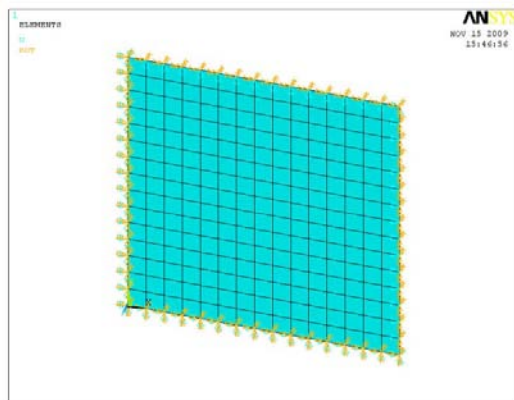
Since the NPP and PP possess the structural quarter symmetry, only one quarter of the plate has been modeled and symmetry boundary conditions are employed along the symmetry lines. For the other relevant locations, BC1 has been applied.

5.6.2 Validation

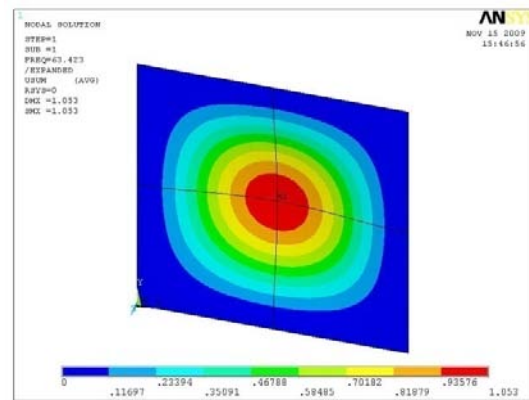
A simple case of NPP of dimension of 0.9 m x 0.9 m x 0.006 m with BC3 boundary condition is considered. Fundamental natural frequency is calculated using exact solution (Blevins, 1978) as 63.48 Hz. Analysis is carried out using four different finite elements. Fig. 5.7(a) gives the finite element model of NPP. Fig. 5.7(b) shows the mode shape with $m = 1$ and $n = 1$ of NPP. The results are tabulated in Table 5.3. It is seen that the variation between the finite element method and exact solution method is less than 0.2% for SHELL63 and SHELL93. However SHELL63 is recommended for further analysis.

Table 5.3: Comparison of natural frequency for various finite elements of NPP with BC3.

Natural frequency (Hz) for NPP							
SHELL 63	% Variation	SHELL 93	% Variation	SOLID 45	% Variation	SOLSH 190	% Variation
63.4	-0.12	63.44	-0.06	63.88	0.63	63.63	0.24



(a)



(b)

Fig. 5.7: (a) FE model of NPP with SHELL63 element for BC3, and (b) Mode shape for $m=1$ and $n=1$ of NPP for BC3.

5.6.3 Finite element model of Non Perforated Plate

Fig. 5.8(a) shows the finite element model of NPP. The finite element model has 256 nodes and 225 elements. The mode shape with modal index $m = 1$ and $n = 1$ is shown in Fig. 5.8(b). For the water backed plate, finite element model is shown in Fig. 5.9(a). This model has 2304 nodes and 2025 elements. The mode shape with modal index $m = 1$ and $n = 1$ is shown in Fig. 5.9(b).

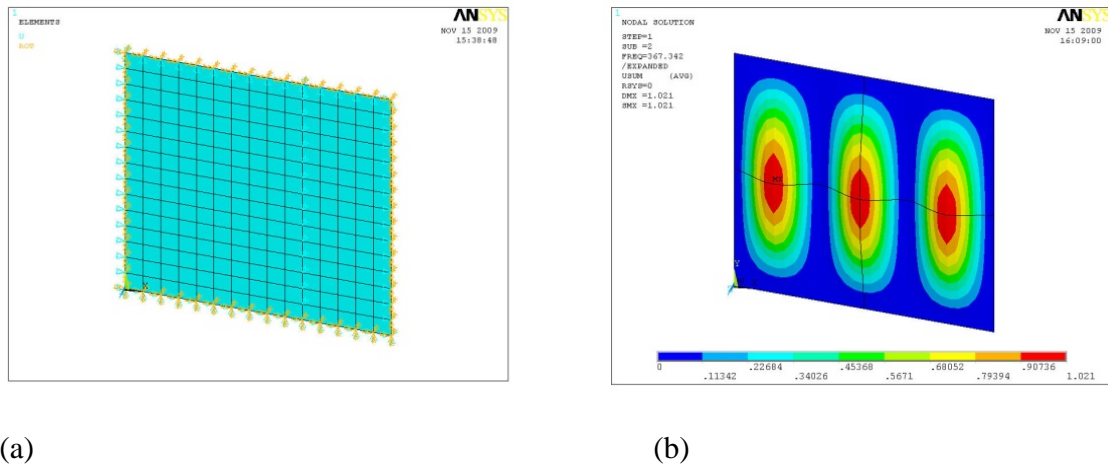


Fig. 5.8: (a) FE model of NPP with SHELL63 element for BC1, and (b) Mode shape for $m=1$ and $n=1$ of NPP for BC1.

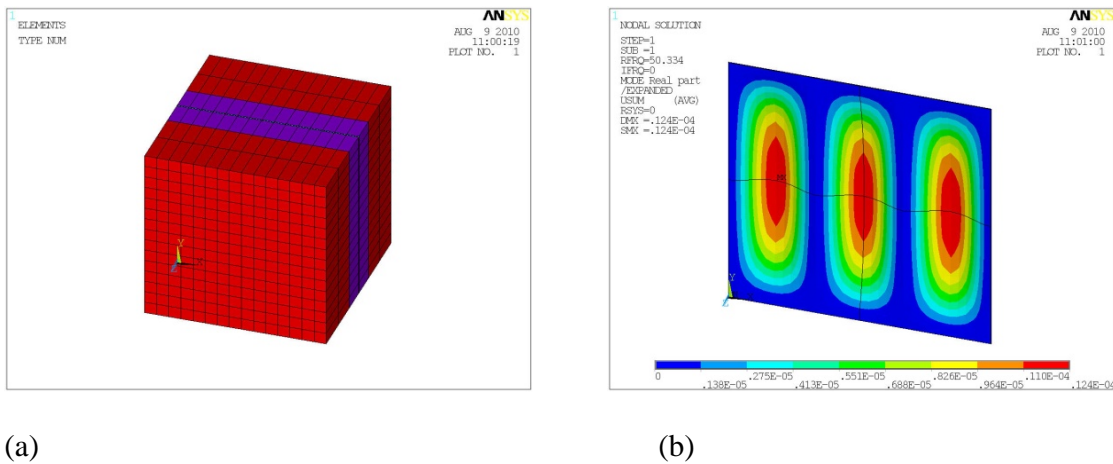
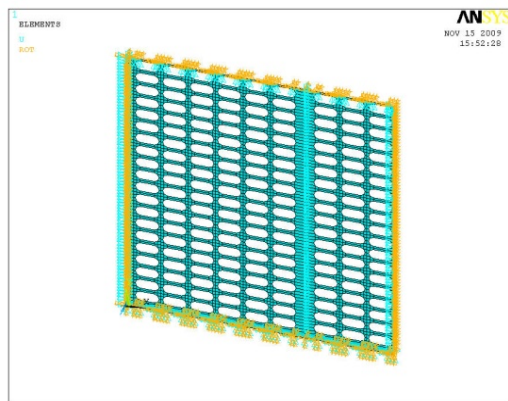


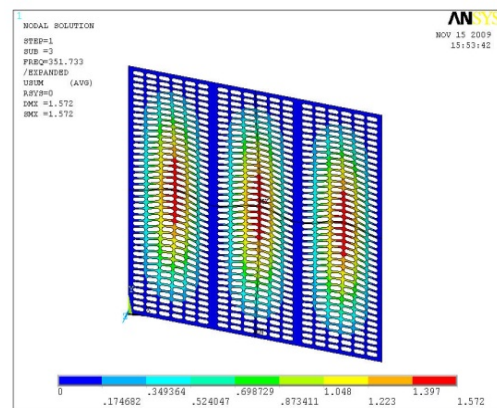
Fig. 5.9: (a) FE model of water backed NPP with SHELL63 element for BC1, and (b) Mode shape for $m=1$ and $n=1$ of water backed NPP for BC1.

5.6.4 Finite element model of Perforated Plate

Fig. 5.10(a) shows the finite element model of PP. The finite element model has 3494 nodes and 2646 elements. The mode shape with modal index $m = 1$ and $n = 1$ is shown in Fig. 5.10(b). For the water backed plate, finite element model is shown in Fig. 5.11(a). This model has 34686 nodes and 32454 elements. The mode shape for modal index $m=3$, $n=1$ gives the fundamental frequency and is shown in Fig. 5.11(b) and that of $m = 1$ and $n = 1$ is shown in Fig. 5.11(c). The frequencies for different modal indices are tabulated in Table 5.4.



(a)



(b)

Fig. 5.10: (a) FE model of PP with SHELL63 element for BC1, and (b) Mode shape for $m=1$ and $n=1$ of PP for BC1.

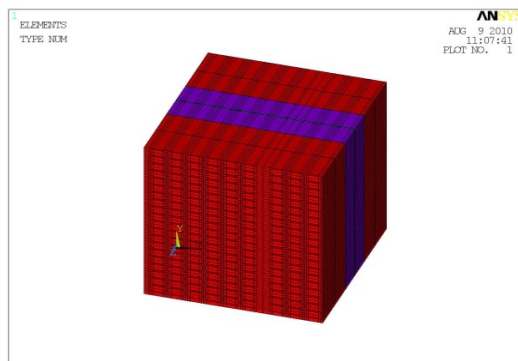
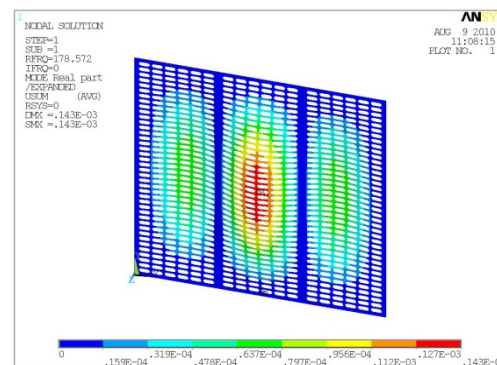


Fig. 5.11 (a)



(b)

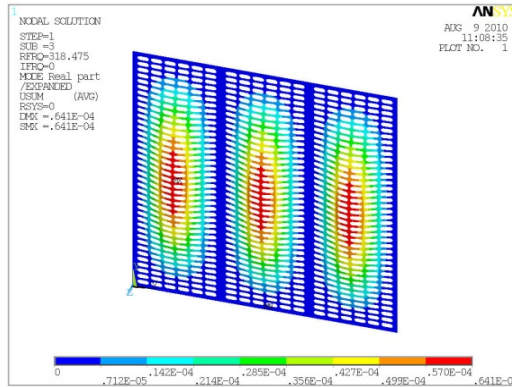


Fig. 5.11 (contd.) (c)

Fig. 5.11: (a) FE model of water backed PP with SHELL63 element for BC1, (b) Mode shape for $m=3$ and $n=1$ of PP for BC1, and (c) Mode shape for $m=1$ and $n=1$ of PP for BC1

5.7 RESULTS AND DISCUSSION

The natural frequency of NPP and PP are plotted independently against modal index 'n' 'in vacuum' and 'water backed condition' and shown in Fig. 5.12 and Fig. 5.13 and presented in Table 5.4. The natural frequency of NPP and PP 'in vacuum' and 'in water backed condition' are found to increase at a decreasing rate with increase in the model index (m). It is also found that the natural frequency of PP with water backed condition is higher than that of NPP.

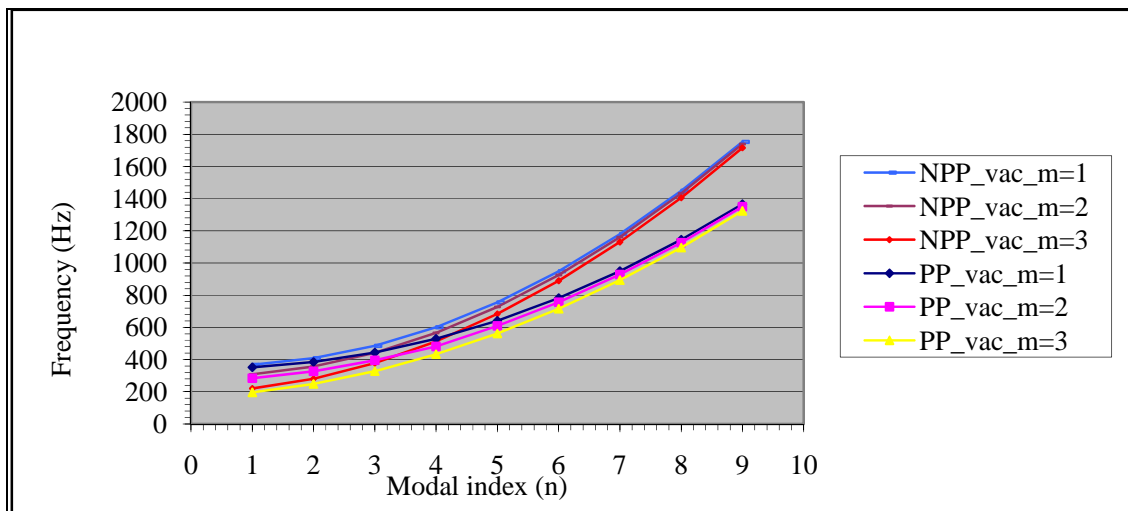


Fig. 5.12: Natural frequency of NPP and PP 'in vacuum' for modal index $m=1$ to $m=3$.

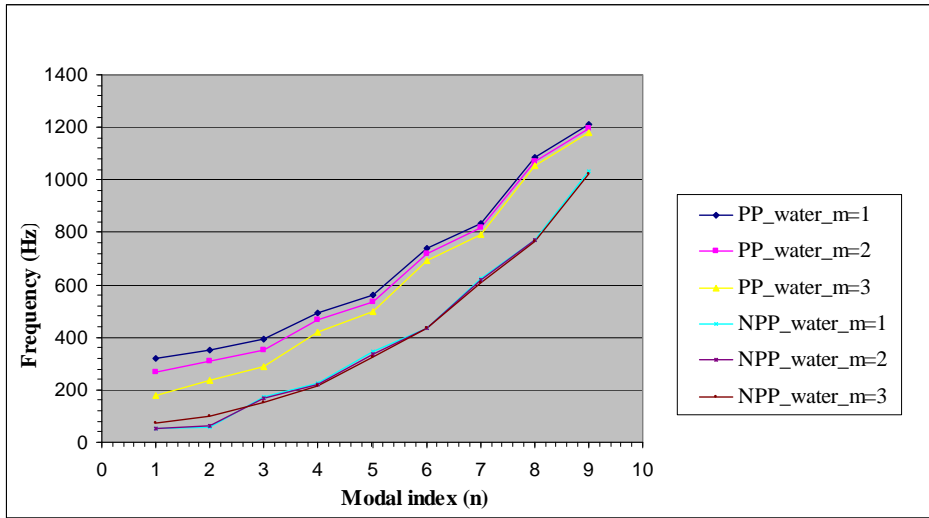


Fig. 5.13: Natural frequency of NPP and PP in water backed condition for modal index m=1 to m=3.

Table 5.4: Natural frequencies of NPP and PP ‘in vacuum’ and in water backed condition for SHELL63 element for BC1.

Modal index		SHELL63 – BC1			
		NPP		Stadium PP	
m	n	In vacuum	Water backed	In vacuum	Water backed
1	1	367.3	50.3	351.7	318.5
	2	408.8	58.5	385.1	352.4
	3	485.2	174.1	443.4	390.7
	4	600.3	225	528.6	492.4
	5	755.2	343.7	641.5	560.6
	6	948.9	434	782.1	738.4
	7	1180.3	622.5	950	835.5
	8	1448.5	772.6	1144.7	1084.7
	9	1752.7	1030.5	1365.9	1209.6
2	1	308.2	53	284.6	269.8
	2	356.7	62.9	326.6	310.2
	3	441.8	165.6	395	353.9
	4	565.3	220.8	481.4	464.3
	5	726.8	336.5	609.7	536.4
	6	925.9	434.3	756	719.8
	7	1160.7	618.8	928.3	819.1
	8	1432.4	771.4	1126.4	1071.4
	9	1738.9	-	1350.2	1197.3

Table 5.4: (contd.)

Modal index		SHELL63 – BC1			
		NPP		Stadium PP	
m	n	In vacuum	Water backed	In vacuum	Water backed
3	1	220.5	75	195.8	178.6
	2	279.9	98.1	248.2	235.1
	3	377.8	153.2	328.1	289.6
	4	512.7	214.4	432.9	417.5
	5	683.4	324.1	561.9	496
	6	889.4	433.9	715.3	691.1
	7	1130.2	608.4	893.2	793.9
	8	1405.6	767.2	1096.1	1053.7
	9	1715.7	1023	1323.8	1182

5.7.1 Effect of water backed condition on natural frequency

The change in natural frequency due to the presence of water medium around the plate has been calculated as the percentage of the ratio of the difference in natural frequency ‘in vacuum’ and water backed condition to that of the natural frequency ‘in vacuum’ for NPP as well as for PP. The percentage variation is plotted against the modal index ‘n’ and shown in Fig. 5.14 for NPP and in Fig. 5.15 for PP. It is observed that the variation in natural frequency due to the presence of water medium is a decrease of about 90% for NPP and in this case, the percentage reduces to 50 when the modal index ‘n’ increases from 1 to 9. For PP, the variation exhibits oscillations between 5 to 12% in the same range of modal index. Evidently, the reduction in natural frequency is due to the reduction in added mass owing to the partial transparency created by the presence of perforations.

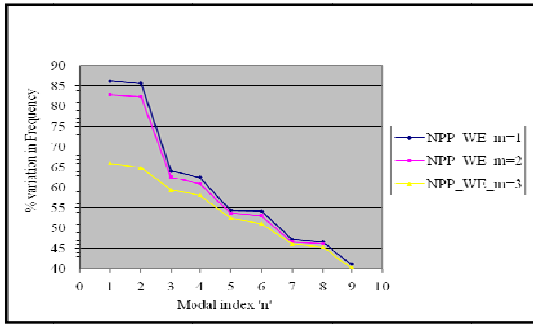


Fig. 5.14: Effect of water backed condition on natural frequency of NPP for modal index $m=1$ to $m=3$.

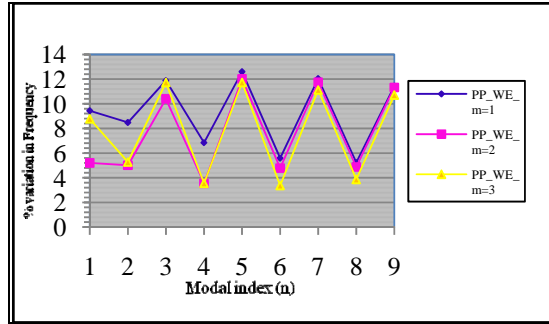


Fig. 5.15: Effect of water backed condition on natural frequency of PP for modal index $m=1$ to $m=3$.

5.7.2 Effect of perforation on natural frequency

In order to study the effect of perforation 'in vacuum' and in water backed condition, the natural frequencies of NPP and PP are compared. The variation in natural frequency is arrived by taking the ratio of the natural frequency between NPP and PP to that of NPP in the respective condition. This ratio is expressed in terms of percentage. The percentage variation is plotted against modal index 'n' and shown in Fig. 5.16 for 'in vacuum' condition and in Fig. 5.17 for water backed condition. It is observed that the percentage variation in natural frequency increases from 4 to 24% as the modal index 'n' increases 'in vacuum'. In water backed condition, the percentage variation in natural frequency exhibits a steep reduction from -500 to -100 between modal index $n = 2$ and 3 , and subsequently decays down to -5 as 'n' reaches the value 9. The minus (-) sign is due to the higher value of natural frequency of PP than that of NPP.

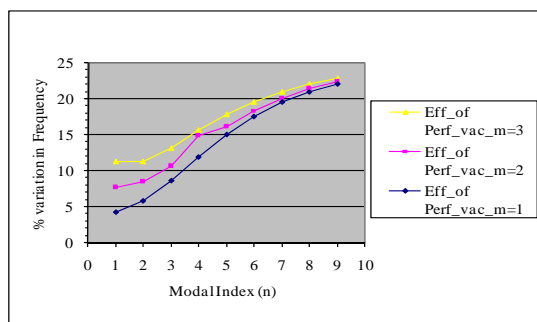


Fig. 5.16: Effect of perforation for 'in vacuum' condition on natural frequency for modal index $m=1$ to $m=3$.

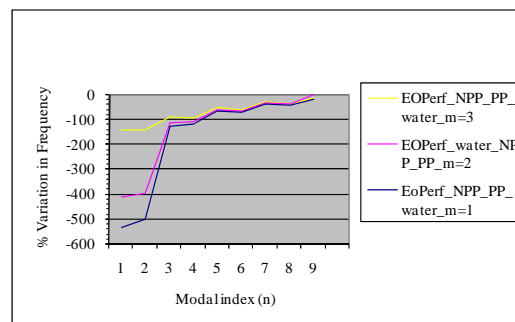


Fig. 5.17: Effect of perforation for water backed condition on natural frequency for modal index $m=1$ to $m=3$.

5.8 SHOCK ANALYSIS

The present study involves analysis of underwater plates subjected to noncontact underwater explosions as well. Arbitrary Lagrangian - Eulerian method has been used for obtaining the transient response of the structure subjected to the explosion. In the present analysis using ANSYS LS-DYNA, the approach is fairly elaborate bringing with modeling of the explosive, proceeding to modeling of the fluid structure interaction and ending with evaluation of free field pressure and structural response.

5.8.1 Calculation of pressure and explosive load

Various standards are being followed by the countries for the minimum shock resistance requirement of structure for underwater application. The explosive type, charge weight and stand off distance are the input parameters which decide the intensity of the pressure. For the water backed structures, one of the military standards (MIL-E-16400 G (Navy)) is taken as the reference in the present investigation. This standard stipulates minimum design requirement for the noncontact underwater explosion analysis. As per this standard, TNT is considered as the explosive with 55 lb charge weight and 30 feet as stand off distance.

As a result of underwater explosion, primary and secondary shock waves are formed. The primary shock waves are generated because of localized compression of surrounding water media. Secondary shock waves generated by the oscillating bubble of detonation products (gas bubble), are of low intensity but of longer durations. A detailed underwater explosion process is explained elsewhere (Cole, 1948). The pressure-time profile of shock waves in water is represented by an exponential function as given in eqn. 5.1,

$$p(t) = P_0 * (e^{-t/t_0}) \quad (5.1)$$

where $p(t)$ is the pressure at time (t) , P_0 is the initial peak pressure and t_0 is the time for pressure to reduce to P_0/e which is referred as time constant. The empirical correlation of primary shock pressure effects in terms of charge weight and standoff distance, for TNT as explosive, is as given in eqn. 5.2 (Cole, 1948).

$$P_0 = 21600 (w^{1/3} / R)^{1.13} \text{ psi} \quad (5.2)$$

where P_0 is the peak pressure in psi, w is the charge weight in pounds and R is the standoff distance in feet.

Explosive charge weight referred from the given military standard is 24947 gm of TNT. Experimentation with this much charge poses practical difficulties and subsequently same explosive is attempted with 1m stand off distance and the charge weight has been found approximately as 30gm. Other explosives commonly used as standard are Plastic Explosive Kirkee (PEK) and Composition 4 (C4). There is no direct equation available for the shock pressure estimation for PEK as in the case of TNT. However the procedure like the shock effect of PEK taken equal to 1.17 times of TNT (Rajendran and Narasimhan; Ramajeyathilagam) has been used in the present study to calculate the said value. Pressure estimated for TNT and PEK for specified charge weight and stand off distance are given in Table 5.5.

Table 5.5: Free field pressure estimation for given explosive, weight of explosive and stand off distance as per Cole's empirical formula.

Sl. No.	Explosive	w in lb (gm)	R in ft (m)	Pressure in psi (MPa)
1	TNT	55 (24947)	30 (9.15)	1650 (11.376)
2	TNT	0.06614 (30)	3.2808 (1)	2028 (13.984)
3	PEK*	0.06614 (30)	3.2808 (1)	2152 (14.838)

* - Shock effect of 1 gm of PEK = 1.17 gm of TNT (Rajendran and Narasimhan; Ramajeyathilagam) is applied.

The peak pressure arrived for 30 gm of PEK with 1 m as stand off is more severe than the specification given in the MIL standard. For all the numerical and experimental studies conducted herein, 30 gm of each of the explosive with 1m as stand off distance is considered.

5.9 FINITE ELEMENT ANALYSIS

Shock Analysis of NPP and PP of 0.9 m x 0.9 m have been carried out to study the response of them in terms of deflection, and principal stress for the specified explosive

details. The free field pressure at a stand off distance 1m is also estimated. The geometry of the NPP and PP are same as the one analysed for the free vibration analysis and full model has been used in shock analysis. The boundary condition BC1 is applied for the shock analysis as given in Table 3.1. The weight of the explosive material is 30 gm in each case. The height of the explosive in finite element model has been arrived at based on its density. The dimension of the PEK explosive model is 2 cm x 2 cm x 4.3352 cm. Keeping the section constant, the height of TNT is 4.717cm and that of C4 is 4.6846 cm.

5.9.1 Description of finite element analysis

For the analysis using ANSYS LS-DYNA, the explosive, structure and fluid are defined based on the Equation Of State (EOS) and material properties. LS-DYNA supports 15 different options for EOS and 20 different options for materials. The following options of EOS and materials mentioned in sections 5.9.2 to 5.9.5 are considered in this investigation due to their suitability for this application. The total time for analysis, time between each calculation and number of files to be written for results also form a part of the input in the analysis. Using ANSYS LS-DYNA solver module, 'k' (keyword) file is generated. This 'k' file is viewed using LSPREPOST.EXE file, to plot the responses at specified nodes / elements as a response history.

5.9.2 Equation Of State for explosive: JWL (Jones – Wilkens – Lee)

The JWL 'equation of state' is adapted for shock analysis in this investigation (Keith 2007, Kim 2008). It defines pressure as a function of relative volume 'V' and internal energy per initial volume 'E', as given in eqn. 5.3.

$$p = A \left[1 - \left(\frac{\omega}{R_1 V} \right) \right] e^{-R_1 V} + B \left[1 - \left(\frac{\omega}{R_2 V} \right) \right] e^{-R_2 V} + \frac{\omega E}{V} \quad (5.3)$$

where ω , A, B, R_1 and R_2 are user defined input parameters and constant for each type of explosives. This equation of state is normally used for determining the pressure of the detonation products of high explosives and also used with the 'Explosive Burn' (material model of explosive) which determines the lighting time for the explosive element.

5.9.3 Material model for explosive: Explosive Burn

Burn fractions, 'F', which multiply the equation of states for high explosives, control the release of chemical energy for simulating detonations. At any time, the pressure in a high explosive element is given by

$$p = Fp_{eos}(V, E) \quad (5.4)$$

where 'p_{eos}' is the pressure from the equation of state (from JWL). The details of EOS and material properties of explosives are given in Table 5.6.

Table 5.6: Details of EOS parameters and Material properties of PEK, TNT and C4 explosives.

Explosive Property EOS (JWL)				
Variables	Units	PEK	TNT	C4
A	Mbar	5.8683	3.712	6.0997
B	Mbar	0.10671	0.03231	0.1295
R1		4.4	4.15	4.5
R2		1.2	0.95	1.4
Ω		0.275	0.3	0.25
E ₀	Mbar	0.082	0.07	0.09
V ₀		1.0	1.0	1.0
Explosive Material Property (High_Explosive_Burn)				
P	gm /cc	1.73	1.59	1.6
Detonation Velocity	cm / μ sec	0.791	0.693	0.8193
PCJ	Mbar	0.285	0.21	0.28

5.9.4 Equation Of State for water: Gruneisen

The Gruneisen equation of state is used to calculate the internal characteristics of water in this investigation (Keith 2007, Kim 2008). This EOS can properly handle shock wave propagation in an underwater explosion event. Gruneisen EOS with cubic shock velocity - particle velocity defines pressure for compressed material as

$$p = \frac{\rho_0 C^2 \mu \left[1 + \left(1 - \frac{\gamma_0}{2} \right) \mu - \frac{a}{2} \mu^2 \right]}{\left[1 - (S_1 - 1) \mu - S_2 \frac{\mu^2}{\mu + 1} - S_3 \frac{\mu^3}{(\mu + 1)^2} \right]^2} + (\gamma_0 + a \mu) E \quad (5.5)$$

where E is the internal energy per initial volume, C is the intercept of the v_s - v_p curve, S_1 , S_2 , and S_3 are the coefficients of the slope of the $v_s - v_p$ curve, γ_0 is the Gruneisen gamma, and a is the first order volume correction to γ_0 and $\mu = \frac{\rho}{\rho_0} - 1$

5.9.5 Material model for water: Null Material

For solid elements, equation of state can be called through this model to avoid deviatoric stress calculations. A pressure cutoff may be specified to set a lower bound on the pressure. It is advantageous to model contact surfaces via shell elements which are not part of the structure, but are necessary to define areas of contact within or between nodal rigid bodies. Beams and shells that use this material type are completely bypassed in the element processing. The Young's modulus and Poisson's ratio are used for setting the contact interface stiffness. The details of EOS and material properties of water are given in Table 5.7.

Table 5.7: Details of EOS parameters and Material properties of water

Equation of State (EOS) – Gruneisen		
Property	Units	Water
C	cm / μ sec	0.15
S1		1.41
S2		0
S3		0
Gammao (γ_0)		1
A		0
E ₀	Mbar	0.0000189
Material Property (Null)		
ρ	gm / cc	1.025
Pressure cutoff		0

5.9.6 Description of finite element model

The geometric models of NPP and PP are generated using ANSYS software. Each model is analysed for three explosives (TNT, PEK and C4) as well as the fluid. SHELL163 element is used for the geometry and SOLID164 is used for explosive and fluid. The finite element model of NPP and PP are shown in Fig. 5.18(a) and Fig. 5.21(a) respectively.

5.9.7 Units

Consistent set of units are used in the ANSYS LS-DYNA analysis. The unit for Length is 'cm', for Time is μsec and for Pressure is Mbar. Similarly the Density is specified in g/cc and Modulus of Elasticity is in Mbar. The material property of Titanium alloy is tabulated in Table 5.8.

Table 5.8: Material properties of Titanium alloy for shock analysis

Material Plastic_Kinematic_Title		
Property	Units	Titanium alloy
ρ	gm / cc	4.5
E	Mbar	1.1
M		0.3
σ_y	Mbar	0.0097
E TAN	Mbar	0.00112
BETA		1.0

5.10 RESULTS AND DISCUSSION

The free field pressure at a distance of 1m from detonation point as time history plots are given in the Figs. 5.18(b), 5.19(a) and 5.20(a) due to explosions of PEK, TNT and C4 respectively for NPP. The deflection and principal stress are calculated on the plate. The time history curve for the deflection is shown in Figs. 5.18(c), 5.19(b) and 5.20(b) due to explosions of PEK, TNT and C4 respectively for NPP. The time history curves for the

principal stress are shown in Figs. 5.18(d), 5.19(c) and 5.20(c) for explosions PEK, TNT and C4 respectively for NPP. The duration of the plot is 2000 microsec.

The free field pressure at a distance of 1m from explosion point as time history plots are given in the Figs. 5.21(b), 5.22(a) and 5.23(a) for explosions PEK, TNT and C4 respectively for PP, and the deflection and principal stress are calculated on the plate. The time history curves for the deflection are shown in Figs. 5.21(c), 5.22(b) and 5.23(b) due to explosions of PEK, TNT and C4 respectively for PP. The time history curves for the principal stress are shown in Figs. 5.21(d), 5.22(c) and 5.23(c) due to explosions of PEK, TNT and C4 respectively for PP.

The maximum peak values obtained at each case is shown in Table 5.9. It is observed that the pressure in the free field close to NPP shows two peak pulses of almost equal magnitude for all the explosive modeling and analysis. This may be due to reflective pulse from NPP. The similar phenomenon is observed in the analysis of PP but the magnitude of second and subsequent pulses is less than the primary pulse. This phenomenon is noticed for PEK and C4. However for TNT, a marginal change in magnitude in second pulse has been noticed. The presence of perforations in the plate has brought out such changes in the free field pressure pulses since all other conditions are kept same.

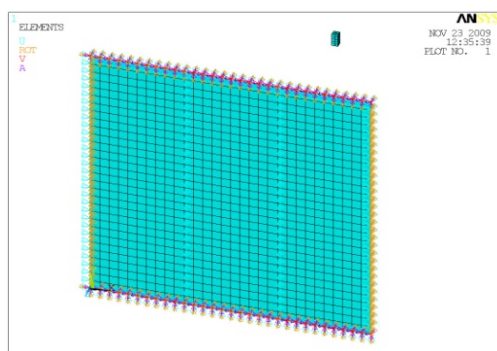
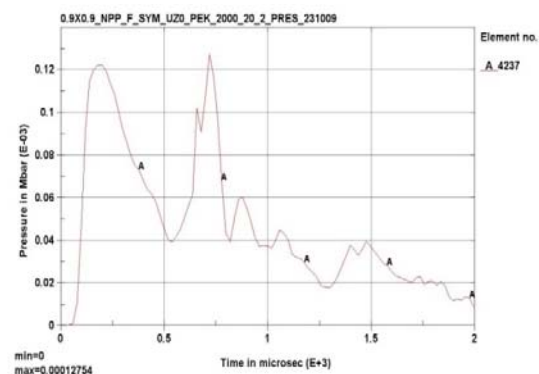


Fig.5.18: (a)



(b)

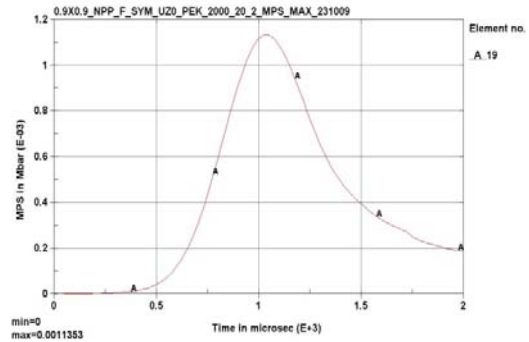
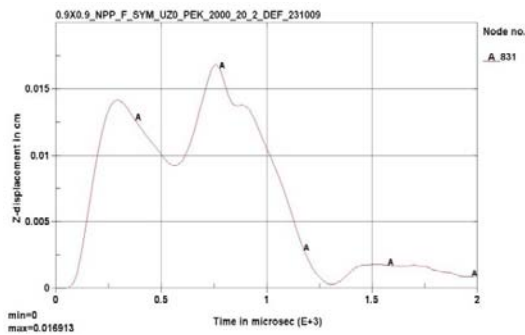


Fig.5.18: (contd.) (c)

(d)

Fig.5.18: (a) Finite Element model of NPP with SHELL163 element for geometry and SOLID164 element for PEK explosive and fluid for BC1, (b) Free field pressure history plot in front of Lining Plate for NPP due to explosion of PEK, (c) Deflection history plot for NPP due to explosion of PEK, and (d) Principal Stress history plot for NPP due to explosion of PEK.

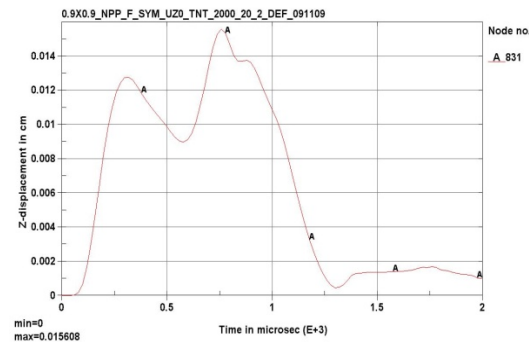
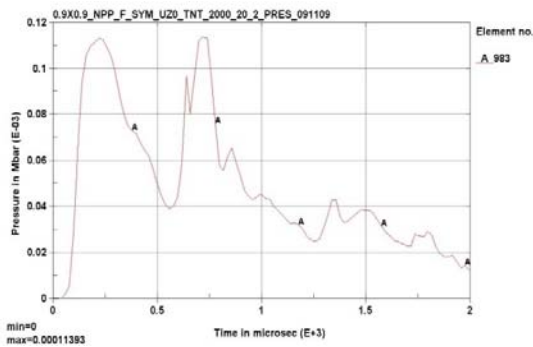


Fig.5.19: (a)

(b)

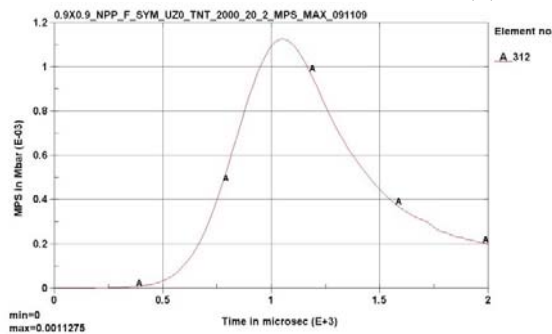
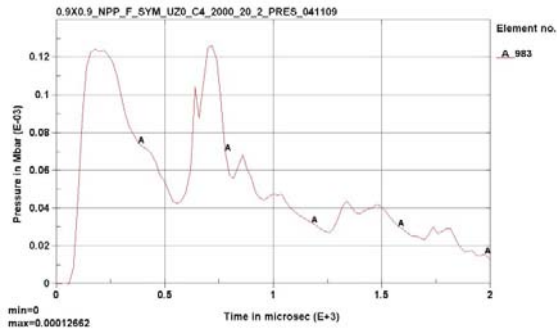
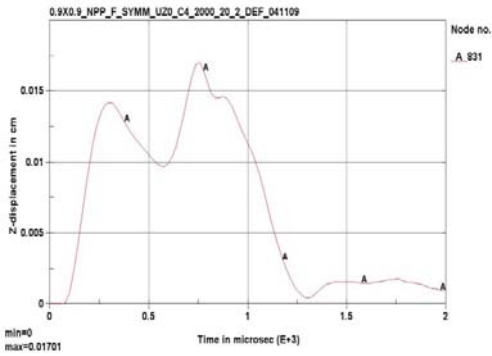


Fig.5.19: (contd.) (c)

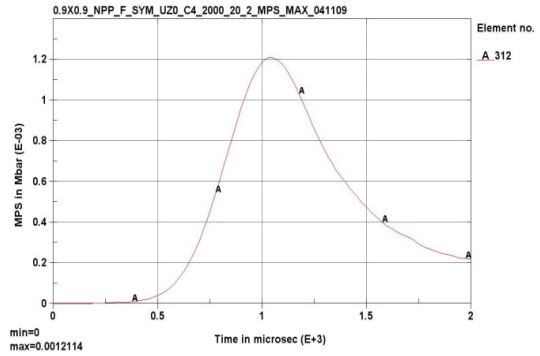
Fig.5.19: (a) Free field pressure history plot in front of Lining Plate for NPP due to explosion of TNT for BC1, (b) Deflection history plot for NPP due to explosion of TNT, and (c) Principal Stress history plot for NPP due to explosion of TNT.



(a)



(b)



(c)

Fig.5.20: (a) Free field pressure history plot in front of Lining Plate for NPP due to explosion of C4 for BC1, (b) Deflection history plot for NPP due to explosion of C4, and (c) Principal Stress history plot for NPP due to explosion of C4.

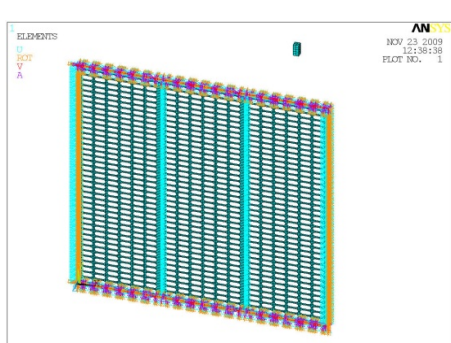
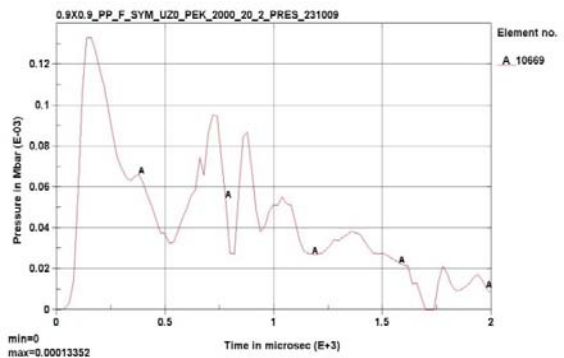


Fig.5.21: (a)



(b)

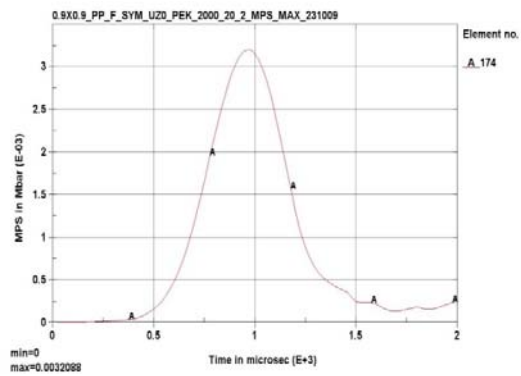
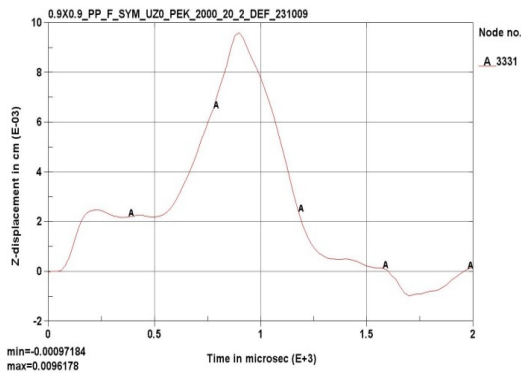


Fig.5.21: (contd.) (c)

(d)

Fig.5.21: (a) Finite Element model of PP with SHELL163 element for geometry and SOLID164 element for PEK explosive and fluid for BC1, (b) Free field pressure history plot in front of Lining Plate for PP due to explosion of PEK, (c) Deflection history plot for PP due to explosion of PEK, and (d) Principal Stress history plot for PP due to explosion of PEK.

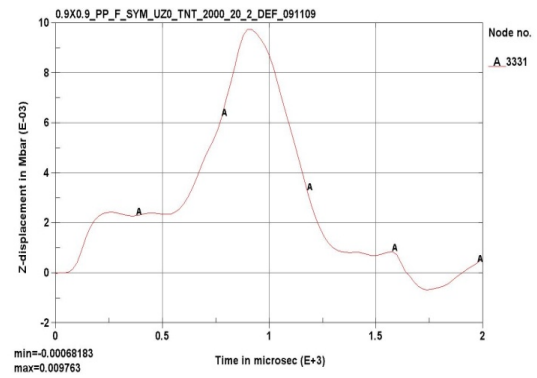
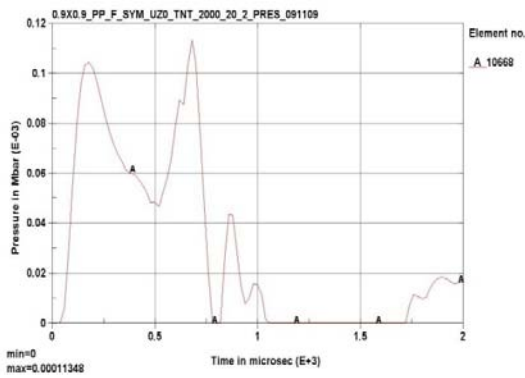


Fig.5.22: (a)

(b)

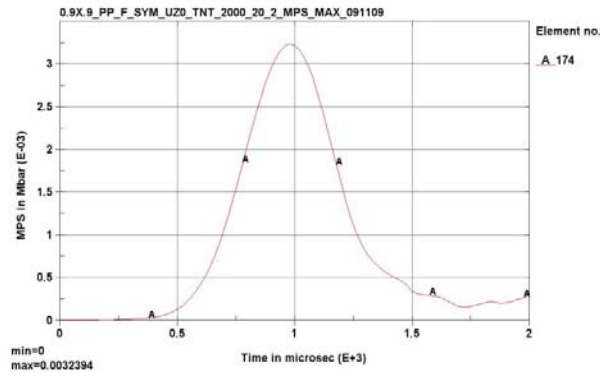


Fig.5.22: (contd.) (c)

Fig.5.22: (a) Free field pressure history plot in front of Lining Plate for PP due to explosion of TNT for BC1, (b) Deflection history plot for PP due to explosion of TNT, and (c) Principal Stress history plot for PP due to explosion of TNT.

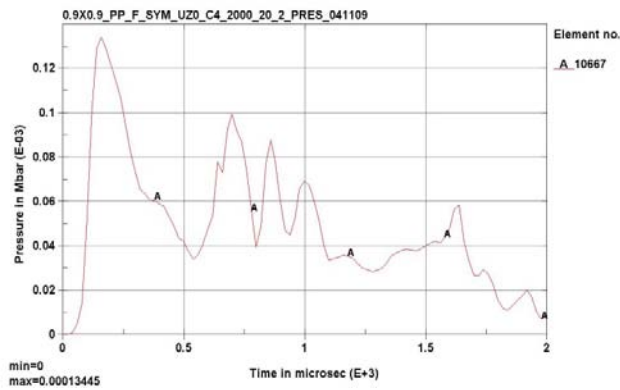


Fig.5.23: (a)

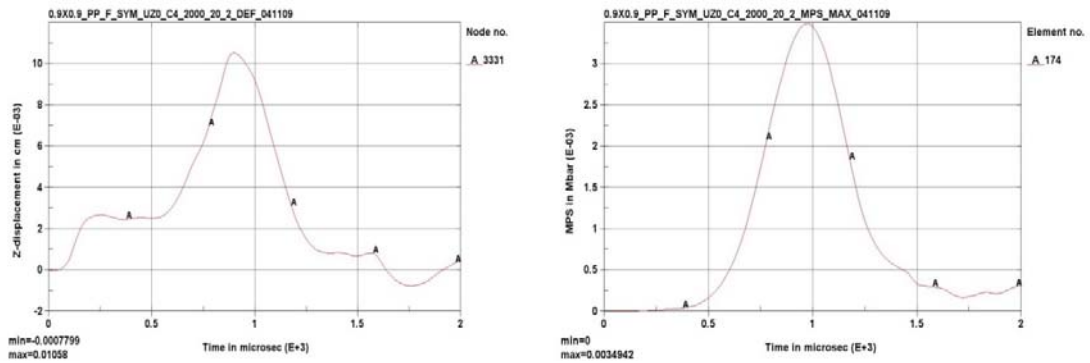


Fig.5.23: (contd.) (b)

(c)

Fig.5.23: (a) Free field pressure history plot in front of Lining Plate for PP due to explosion of C4 for BC1, (b) Deflection history plot for PP due to explosion of C4, and (c) Principal Stress history plot for PP due to explosion of C4.

Table 5.9: Free field pressure and structural responses of NPP and PP due to 30gm weight and 1m stand off distance for explosions of PEK, TNT and C4 for BC1.

Configuration (Stand off Distance R = 1m; charge weight w = 30 gm; Boundary condition = BC1)	Towards Explosion side				
	Free field pressure (MPa)	Deflection (mm) of plate		MPS (MPa) of plate	
		Close to Centre of plate	Maximum	at Centroid	Maximum
<u>NPP</u> Explosive: PEK	12.75	0.169	0.169	113.5	54
Explosive: TNT	11.39	0.16	0.16	113	51
Explosive: C4	12.66	0.17	0.17	121	55
<u>PP</u> Explosive: PEK	13.4	0.096	0.096	320.8	78.9
Explosive: TNT	11.3	0.10	0.10	324	73
Explosive: C4	13.4	0.11	0.11	349	81

Table 5.10: Variation of deflection and principal stress in percentage due to the perforation for PEK, TNT and C4 explosives

Effect of perforation in percentage				
Explosive	Deflection		Principal stress	
	Maximum	at Centroid	Maximum	at Centroid
PEK	-76	-76	64.6	31.6
TNT	-60	-60	65	30
C4	-54.5	-54.5	65.3	32.1

For NPP, the deflection at centroid of the plate is maximum and the stress is less than that of expected maximum stress. In case of PP, the same phenomenon is observed and the principal stress values are high due to the perforation on the plate.

In order to estimate the effect of perforation over NPP, on deflection and stress on each explosive, it is worked out by taking ratio of difference in each parameter of PP and NPP to that of PP. This ratio is expressed as percentage and presented in Table 5.10. The free field pressure at the same location is within 5% (from Table 5.9) and the variation in pressure time history plot is due to the presence of perforations. Theoretically for the given configuration of the structure, the pressures in the free field at a specific distance should have been equal due to same explosive of same weight of charge.

NPP shows high deflection of the order 54 to 76% more in PP. But the maximum value of principal stress in PP is 60% more than that of NPP and the principal stress value at the centroid of the plate is higher by 30% than that of NPP. The perforations cause the reduction of load and this may be the reason for reduced deflection. The geometric discontinuity in the form of perforations is the reason for increase in the stress value.

CHAPTER 6

NUMERICAL INVESTIGATIONS ON PERFORATED PLATE WITH LINING

6.1 INTRODUCTION

Underwater acoustic domes are generally composed with a hydrodynamically shaped thin plate strengthened with another perforated plate. Structurally this component behaves as a perforated plate with lining. Linear static, geometric nonlinear, free vibration and shock analysis of PPL have been envisaged in the present study.

6.2 DESCRIPTION OF PERFORATED PLATE WITH LINING

The perforated plate with lining of dimension 0.9 m x 0.9 m x 0.007 m is taken for analysis. It is considered as the modification of 0.006 m thick perforated plate with addition of 0.001 m thick lining plate. In order to control the deflections due to the hydrodynamic loads, the PPL is usually stiffened. Geometry of the PPL, analysed in the present study is shown in Fig. 6.1. The geometric details of the perforated plate remain same as that of earlier one. The lining plate is welded with the perforated plate and complete compatibility is anticipated.

6.3 LINEAR STATIC ANALYSIS

Plate model, solid model and grillage model of PPL are generated for analysis. Boundary conditions BC1 and BC2 are considered for the analysis. The finite elements SHELL63, SHELL93, SOLID45, SOLSH190 and BEAM188 are used on the various analysis. In finite element model of PPL, the nodes of lining plate and perforated plate are joined together using constraint equation method available in ANSYS to simulate the resistance welding of perforated plate and lining. This ensures the sharing of load by both the perforated plate and lining plate. The details of these models are described subsequently.

6.3.1 Plate model

Two plate models are generated with SHELL63 and SHELL93 elements respectively. The finite element model made of SHELL63 element is shown in Fig. 6.2(a). This finite element model contains 28878 nodes and 25488 elements. Fig. 6.2(b) shows the deflection contour, Fig. 6.2(c) gives the contour of von Mises stress and Fig. 6.2(d) gives the maximum principal stress for BC1 and Figs. 6.2(e), 6.2(f) and 6.2(g) show the corresponding contours for BC2. Similarly the plate model made of SHELL93 contains 83962 nodes and 25488 elements. The nodal values of deflection and von Mises stress and maximum principal stress are presented in Table 6.1.

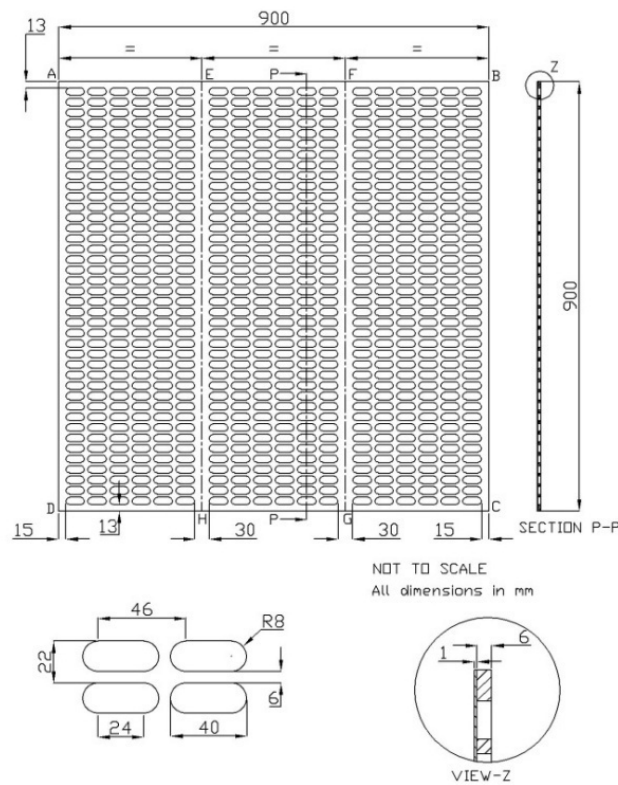


Fig. 6.1: Geometry of Perforated Plate with Lining

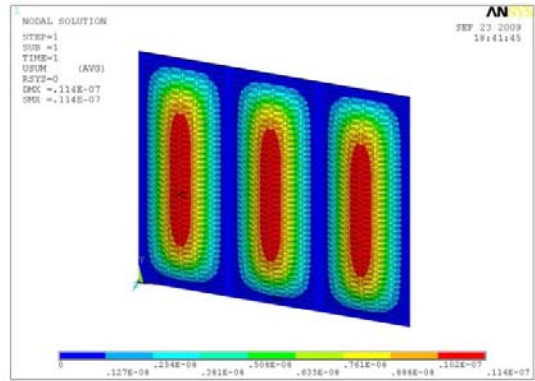
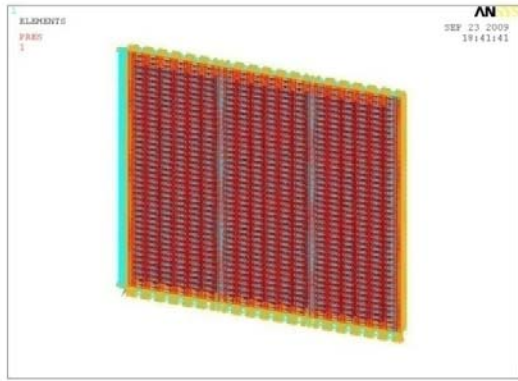
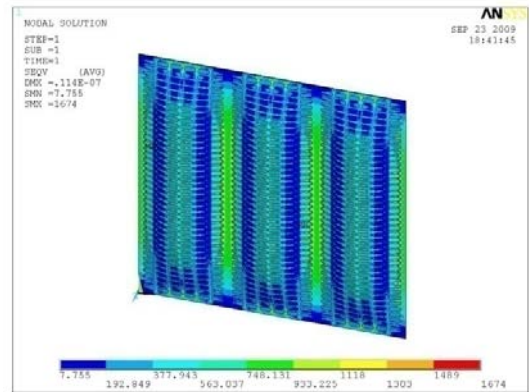
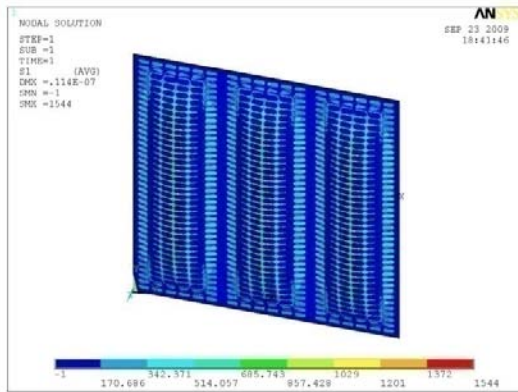


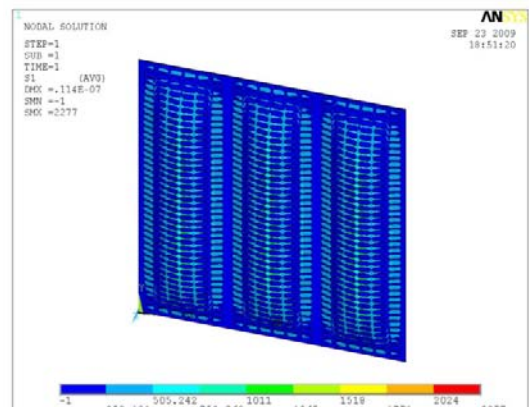
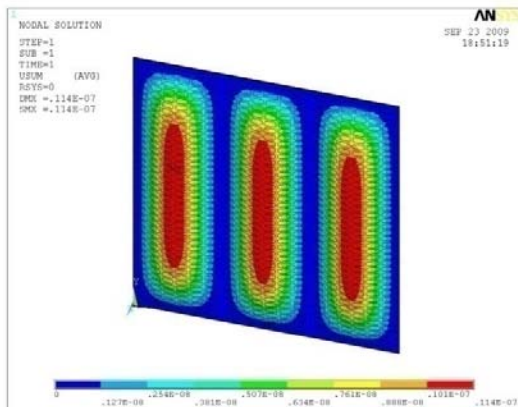
Fig. 6.2: (a)

(b)



(c)

(d)



(e)

(f)

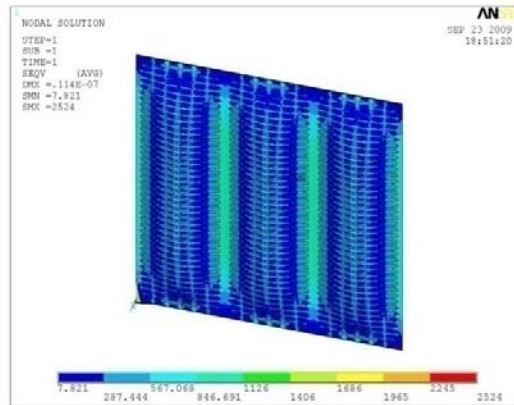


Fig. 6.2: (contd.) (g)

Fig. 6.2: (a) Finite Element Model of PPL with SHELL63 element for BC1, (b) Deflection Contour of PPL for 1Pa for BC1, (c) von Mises Stress Contour of PPL for 1Pa for BC1, (d) Maximum Principal Stress Contour of PPL for 1Pa for BC1, (e) Deflection Contour of PPL with SHELL63 element for BC2 for 1 Pa, (f) von Mises Stress Contour of PPL for 1Pa for BC2 and (g) Maximum Principal Stress Contour of PPL for 1Pa for BC2.

6.3.2 Solid model

Two solid models are generated with SOLID45 and SOLSH190 elements respectively. The finite element model made of SOLID45 element is shown in Fig. 6.3(a). Each model contains 71475 nodes and 46656 elements. Fig. 6.3(b) shows deflection contour, Fig. 6.3(c) shows von Mises stress contour and Fig. 6.3(d) shows the maximum principal stress contour for BC1 and Figs. 6.3(e), 6.3(f) and 6.3(g) show the corresponding values for SOLSH190 for BC1. The nodal values of deflection, von Mises stress and maximum principal stress are presented in Table 6.1.

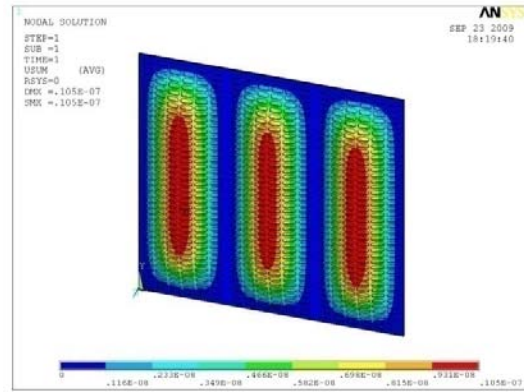
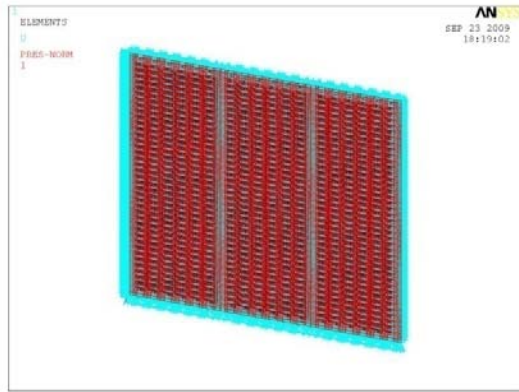
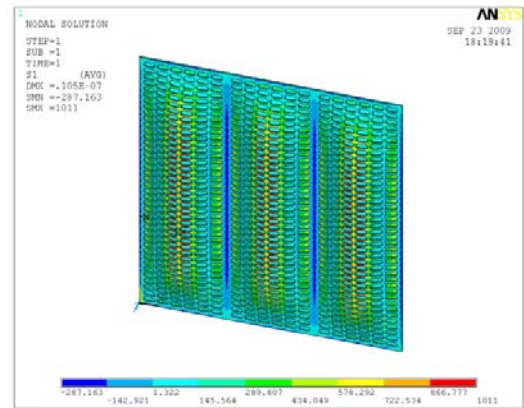
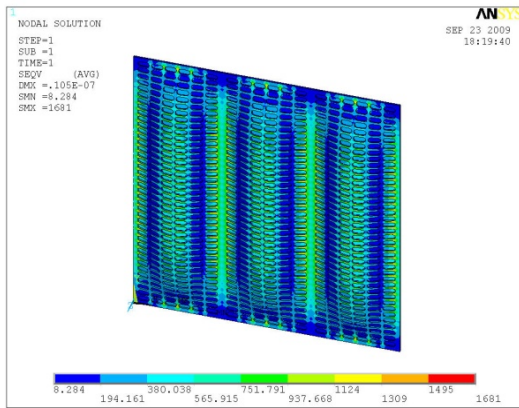


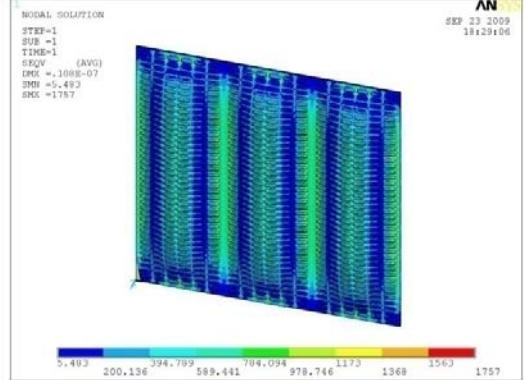
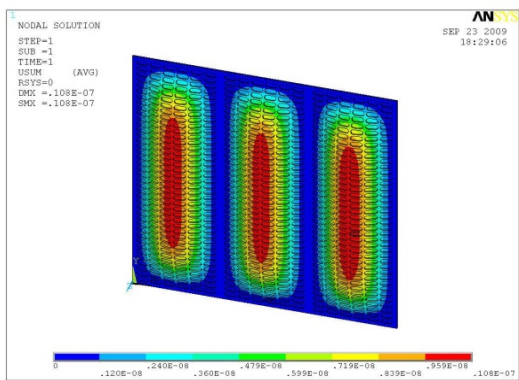
Fig. 6.3: (a)

(b)



(c)

(d)



(e)

(f)

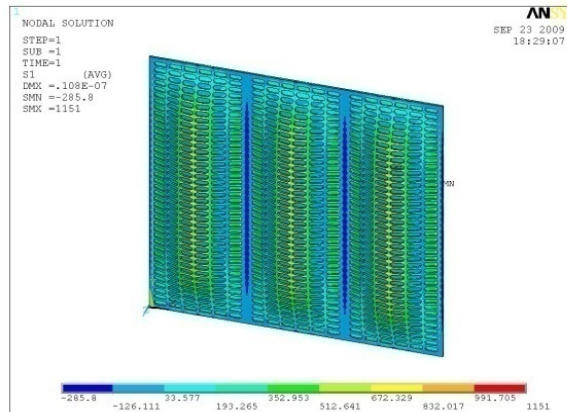
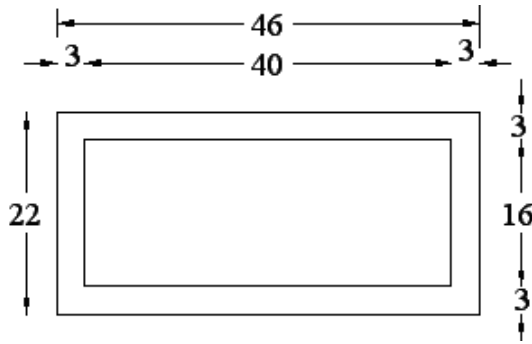


Fig. 6.3: (contd.) (g)

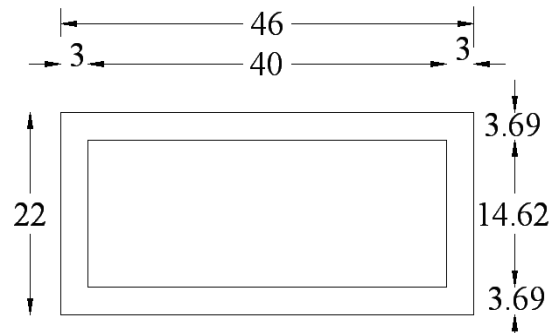
Fig. 6.3: (a) Finite Element Model of PPL with SOLID45 element for BC1, (b) Deflection Contour of PPL with SOLID45 element for 1Pa for BC1, (c) von Mises Stress Contour of PPL with SOLID45 element for 1Pa for BC1, (d) Maximum Principal Stress Contour of PPL with SOLID45 element for 1Pa for BC1, (e) Deflection Contour of PPL with SOLSH190 element for BC1 for 1 Pa, (f) von Mises Stress Contour of PPL with SOLSH190 element for 1Pa for BC1 and (g) Maximum Principal Stress Contour of PPL with SOLSH190 element for 1Pa for BC1.

6.3.3 Grillage model

The grillage model of PPL is constructed by approximating the geometry of the stadium perforation as a rectangle circumscribing the stadium geometry (referred as type1) and as a rectangle of the same area as the stadium geometry (referred as type2). The dimensions of two geometric approximations are shown in Figs. 6.4(a) and 6.4(b) respectively. The grillage model is composed with of BEAM188 element. Fig. 6.5(a) shows the finite element model. The geometric properties of the beam element are taken as that of a beam with ‘T’ cross section. The model is same for type1 and type2, except the input of geometric properties of the beam cross section. The finite element model consists of 1801 nodes and 2520 elements.



(Dimension in mm)



(Dimension in mm)

Fig. 6.4: (a)

(b)

Fig. 6.4: (a) Approximated geometry of the perforation to rectangular configuration – type1, and (b) Approximated geometry of the perforation to rectangular configuration – type2.

For type1 and BC1, the deflection, von Mises stress and maximum principal stress contours are plotted in Figs. 6.5(b), 6.5(c) and 6.5(d). Similarly for BC2, the corresponding contours are plotted in Figs. 6.5(e), 6.5(f) and 6.5(g).

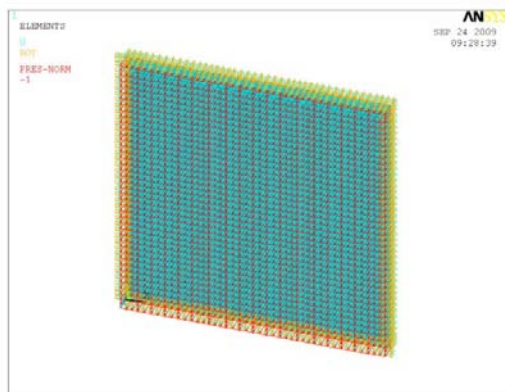
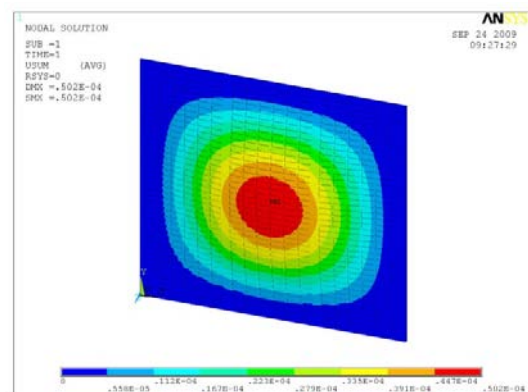


Fig. 6.5: (a)



(b)

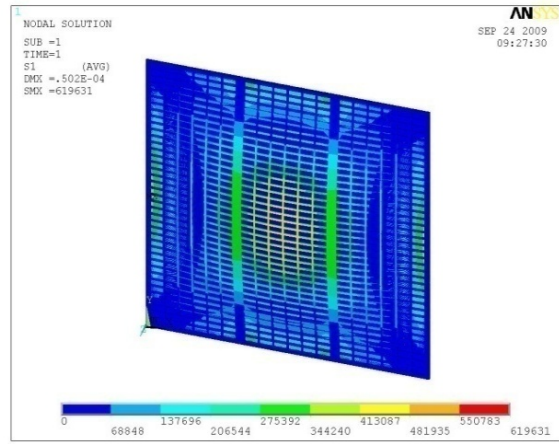
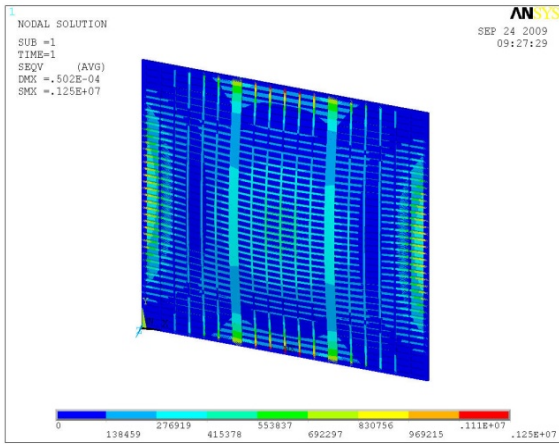
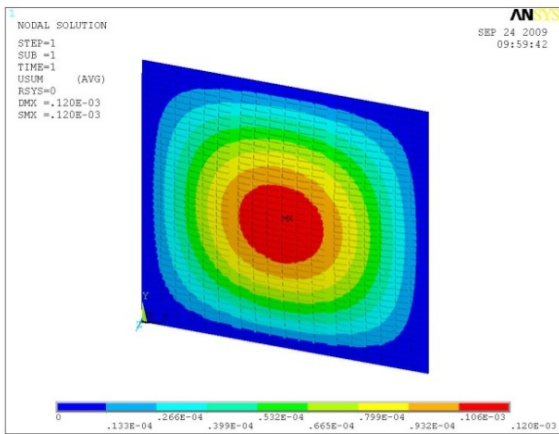
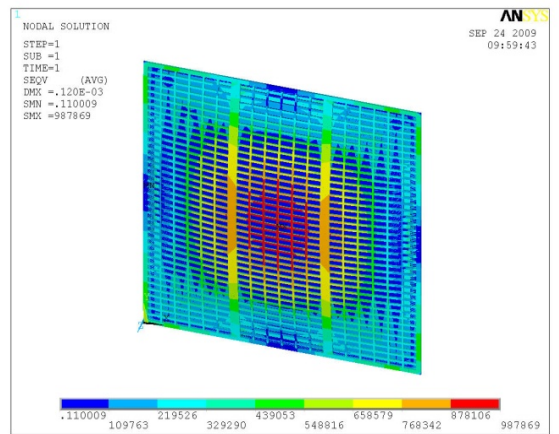


Fig. 6.5: (contd.) (c)

(d)



(e)



(f)

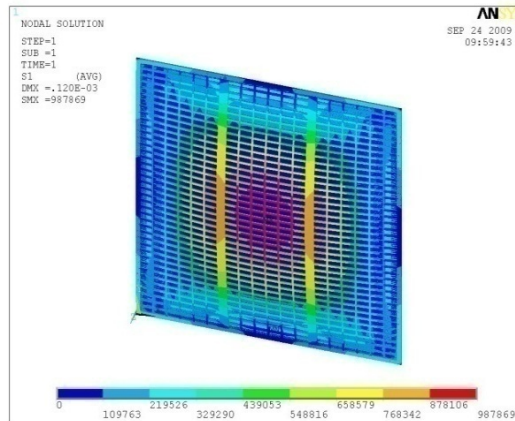


Fig. 6.5: (contd.) (g)

Fig. 6.5: (a) Finite Element Model of PPL with type1 perforation configuration, BEAM188 element for BC1, (b) Deflection Contour of PPL for 1Pa for BC1, (c) von Mises Stress Contour of PPL for 1Pa for BC1, (d) Maximum Principal Stress Contour of PPL for 1Pa for BC1, (e) Deflection Contour of PPL with type1 perforation configuration, BEAM188 element for BC2 for 1 Pa, (f) von Mises Stress Contour of PPL for 1Pa for BC2 and (g) Maximum Principal Stress Contour of PPL for 1Pa for BC2.

For type2 and BC1, the maximum deflection, von Mises stress and maximum principal stress contours are plotted in Figs. 6.6(a), 6.6(b) and 6.6(c). Similarly for BC2, the corresponding contours are plotted in Figs. 6.6(d), 6.6(e) and 6.6(f). The values are presented in Table 6.1.

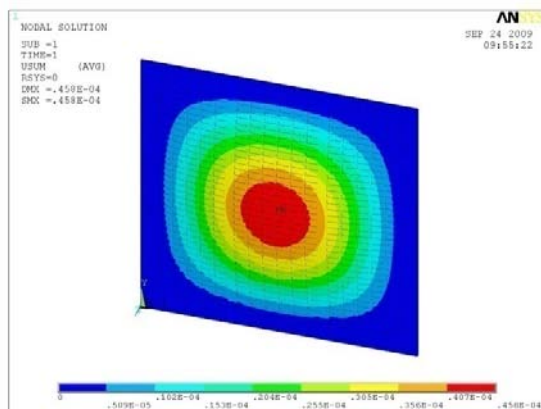
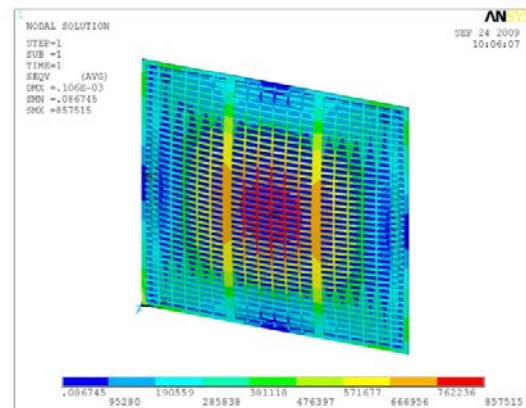


Fig. 6.6: (a)



(b)

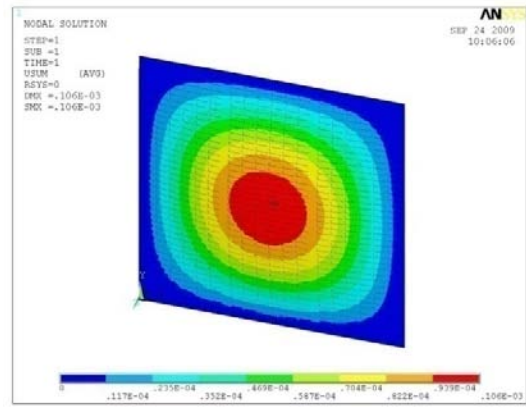
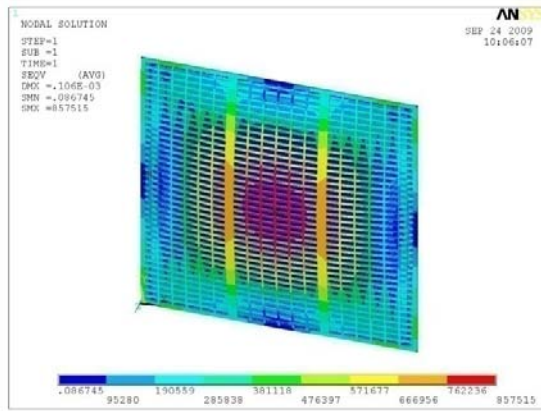
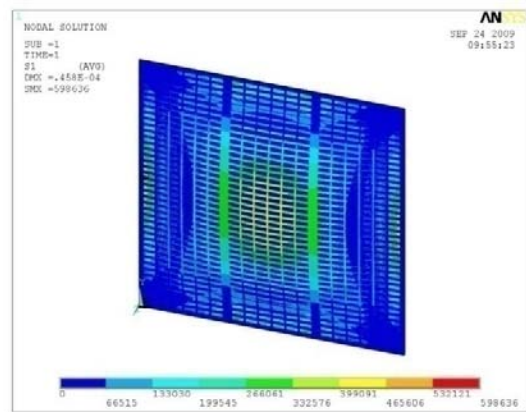
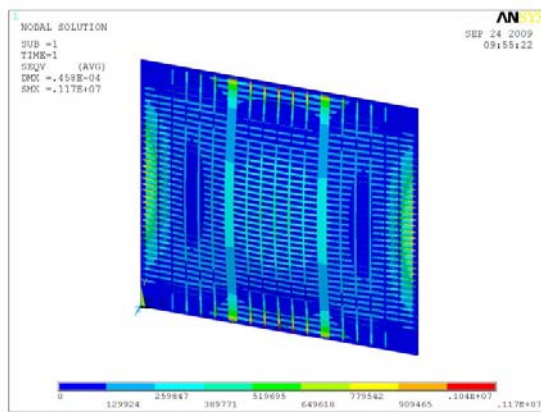


Fig. 6.6: (contd.) (c)

(d)



(e)

(f)

Fig. 6.6: (a) Deflection Contour of PPL with type2 perforation configuration, BEAM188 element for BC1 for 1 Pa, (b) von Mises Stress Contour of PPL for 1Pa for BC1, (c) Maximum Principal Stress Contour of PPL for 1Pa for BC1, (d) Deflection Contour of PPL for 1Pa for BC2, (e) von Mises Stress Contour of PPL for 1Pa for BC2 and (f) Maximum Principal Stress Contour of PPL for 1Pa for BC2.

6.3.4 Results and Discussion

Lower bound deflections are predicted by solid elements whereas deflections are upper bound for grillage model. This may be justified since rotational degrees of freedom are

absent in the solid elements and subsequently resulting in a softer finite element model. The discrete element modeling of the continuous domain to constitute a grillage may be the reason for the latter one. The response predicted by the grillage model is unrealistic.

In order to find out the influence of lining plate over PP, the percentage variation is calculated and is given in Table 6.2. The structural response of PPL has been multiplied with COA for the sake of achieving equivalence. The centroid of PP or PPL has been taken reference point for the response.

Table 6.1: Static structural responses of PPL for different finite element models and for BC1 and BC2 at centroid for 1 Pa.

FE model for PPL	BC	Deflection x 10 ⁻⁷ (m)	VMS (Pa)	MPS (Pa)
		(at Centroid)	(at Centroid)	(at Centroid)
Plate model (SHELL63)	BC1	0.1130	512	579
	BC2	0.1130	512	579
Plate model (SHELL93)	BC1	0.1154	651	665
	BC2	0.1153	653	665
Solid model (SOLID45)	BC1	0.1026	671	746
Solid model (SOLSH190)	BC1	0.1048	656	719
Grillage model Type1 (BEAM188)	BC1	502.4	471 x 10 ³	471 x 10 ³
	BC2	1198.0	988 x 10 ³	988 x 10 ³
Grillage model Type2 (BEAM188)	BC1	458.0	419 x 10 ³	419 x 10 ³
	BC2	1056.0	858 x 10 ³	858 x 10 ³

The release of rotation restraint is found to have negligible influence (less than 1%) on the structural response for the plate model studied here. The effect of lining plate on deflection is about 50% reduction for all the four cases. Regarding the prediction of stresses a decrease of 22% has been shown by the plate elements and 29% by the solid elements. Within the plate models 2% variation in stress has been noticed for SHELL63 and SHELL93 elements.

6.4 GEOMETRIC NONLINEAR ANALYSIS

PPL is modeled with SHELL63 element and it has 28878 nodes and 25488 elements and finite element model is shown in Fig. 6.2(a). A distributed load of intensity 500 kPa has been applied in 20 steps. The deflection, VMS and MPS at each load step have been estimated.

The load deflection curve is plotted and shown in Fig. 6.7(a). The initial portion of the plot is straight line and after certain loading, the deflection tends to be nonlinear. The load at which the linearity of the plate is disturbed has been identified as the intersection of tangent lines at the initial and final part of the plot. In this study, the linearity changes at a load of 240 kPa and deflection at that point is 2.6 mm. Deflection and stresses are obtained for PPL at this load as well as for the last load step and are shown in Table 6.3.

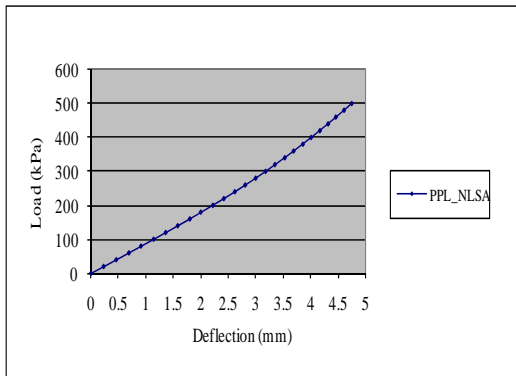
In order to compare the behavior of NPP, PP and PPL, their load deflection curves are plotted together and shown in Fig. 6.7(b). The intensity of nonlinear behavior is in the ascending order for NPP, PP and PPL. The same order is maintained regarding MPS which is evident on comparison of values from Table 5.2 and 6.3.

6.5 FREE VIBRATION ANALYSIS

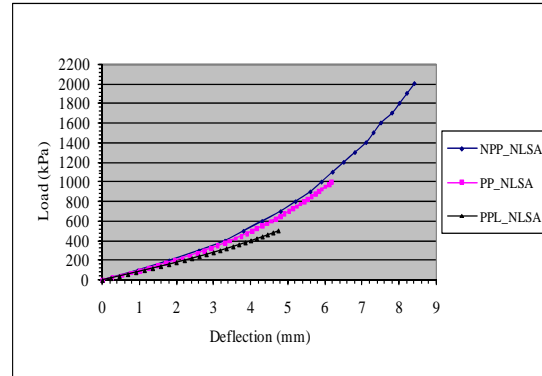
Free vibration analysis of the PPL is carried out in ‘in vacuum’ condition and in ‘water backed condition’. In both cases the quarter model of the structure has been used. Fig. 6.8(a) shows the finite element model of PPL for the ‘in vacuum’ condition, using SHELL63 element. The finite element model has 11202 nodes and 10098 elements. The mode shape for modal index $m=3$, $n=1$ is shown in Fig. 6.8(b) and that of $m = 1$ and $n = 1$ is shown in Fig. 6.8(c). In this case, the fundamental mode is exhibited in $m=3$ and $n=1$. Similarly for the water backed plate, finite element model is shown in Fig. 6.9(a). This model has 34686 nodes and 33534 elements.

Table 6.2: Effect of lining plate on PP and PPL of static structural responses of different models for BC1 and BC2 for an equivalent load (PPL * COA)

Sl No	Configuration	Boundary condition	Effect of Perforation between PP and PPL														
			Deflection X 10 ⁻⁷ (m) at Centroid						von Mises stress (Pa) at Centroid						Max. Principal stress (Pa) at Centroid		
			PP	PPL	PPL x COA	% Variation	PP	PPL	PPL x COA	% Variation	PP	PPL	PPL x COA	PP	PPL	PPL x COA	% Variation
1	Plate model (SHELL 63)	BC1	0.1049	0.113	0.0542	48.3	316	511.7	245.6	22.3	360.6	578.5	277.6	23			
		BC2	0.1049	0.113	0.0542	48.3	315.9	511.9	245.7	22.2	360.4	578.4	277.6	23			
2	Plate model (SHELL 93)	BC1	0.1104	0.1154	0.0554	49.8	393	651.23	312.5	20.5	402.2	664.66	319	20.7			
		BC2	0.1102	0.1153	0.0553	49.8	392.1	652.86	313.3	20.1	401.5	665.14	319.2	20.5			
3	Solid model (SOLID45)	BC1	0.1032	0.1026	0.0492	52.3	433.8	671.4	322.2	25.7	492.7	746.1	358.1	27.3			
		BC2	0.1046	0.1048	0.0503	51.9	434.3	655.6	314.6	27.6	489.8	719.5	345.3	29.5			



(a)



(b)

Fig. 6.7: (a) Load – Deflection plot for each load step for the configuration of PPL, and (b) Load – Deflection plot for each load step for the configuration of NPP, PP and PPL.

Table 6.3: Static structural responses of PPL from the geometric nonlinear analysis for BC1.

Type of plate	Load (kPa)	Deflection (mm)	VMS (MPa)	MPS (MPa)
PPL	240	2.61	362.0	412.6
	500	4.75	771.1	870.8

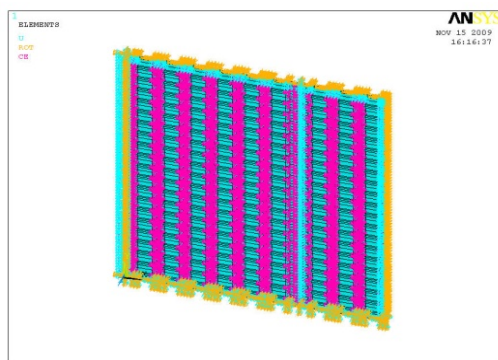
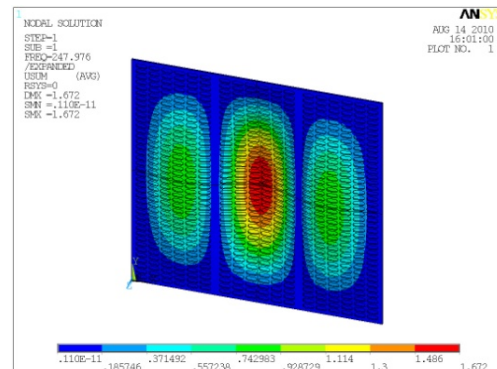


Fig. 6.8: (a)



(b)

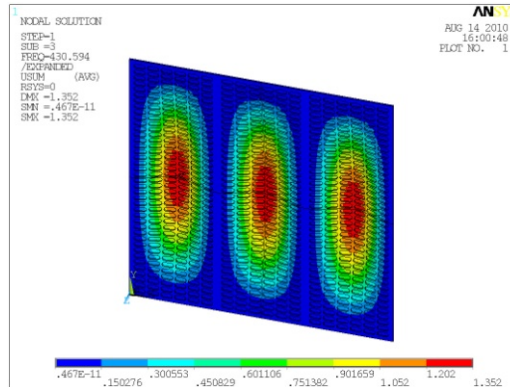


Fig. 6.8: (contd.) (c)

Fig. 6.8: (a) FE model of PPL ‘in vacuum’ with SHELL63 element for BC1, (b) Mode shape for $m=3$ and $n=1$ of PPL for BC1, and (c) Mode shape for $m=1$ and $n=1$ of PPL for BC1.

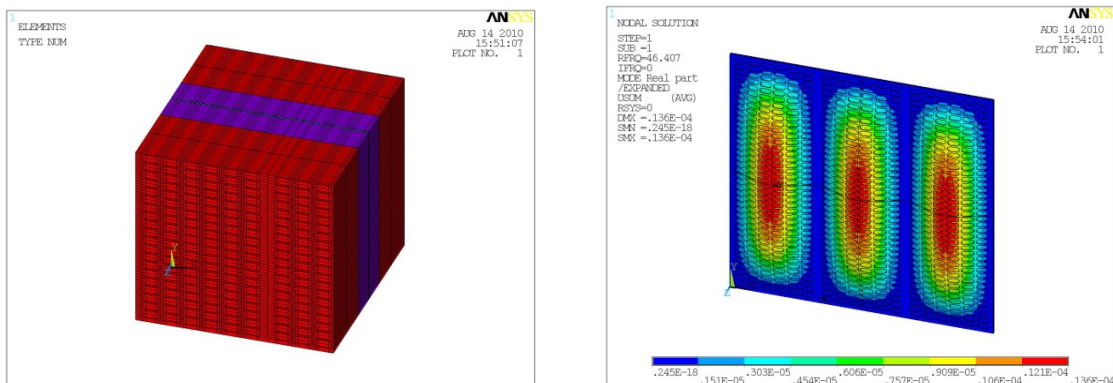


Fig. 6.9: (a)

(b)

Fig. 6.9: (a) FE model of water backed PPL with SHELL63 element for BC1, (b) Mode shape for $m=1$ and $n=1$ of PPL for BC1.

The mode shape with modal index $m = 1$ and $n = 1$ is shown in Fig. 6.9(b). The frequencies for different modal indices for PPL are shown in Table 6.4. The natural frequency of PPL for SHELL63 is plotted against modal index ‘ n ’ ‘in vacuum’ and water backed condition independently and shown in Fig. 6.10(a) and Fig. 6.10(b). In case of PPL, the variation in natural frequency is negligible for modal indices $m = 1$ to 3.

Similar variation is observed for PPL with water backed system. The natural frequency with reference to modal index 'n' is plotted in Fig. 6.10(b). However as modal index 'n' increases for each 'm' value, the variation in natural frequency reduces.

Table 6.4: Natural frequencies of PPL 'in vacuum' and in water backed condition for SHELL63 element for BC1.

Modal index		Stadium - SHELL63 – for BC1	
		Natural frequency (Hz)	
m	n	In vacuum	Water backed
1	1	430	46.4
	2	464.8	54.9
	3	531.3	153.0
	4	633.2	201.2
	5	769.6	277.0
	6	935.7	348.4
	7	1123	451.6
	8	1317.6	524.4
	9	1498.6	645.9
2	1	354.3	48.5
	2	398.5	58.7
	3	477.1	144.9
	4	590.8	197.9
	5	737.1	272.1
	6	911.2	356.3
	7	1104.8	448.5
	8	-	-
	9	1490.5	660.4
3	1	247.5	67.4
	2	305	91.7
	3	399.7	130.1
	4	528.4	192.7
	5	687.4	257.9
	6	871.9	-
	7	1076.2	442.4
	8	1282.8	544.2
	9	1476	-

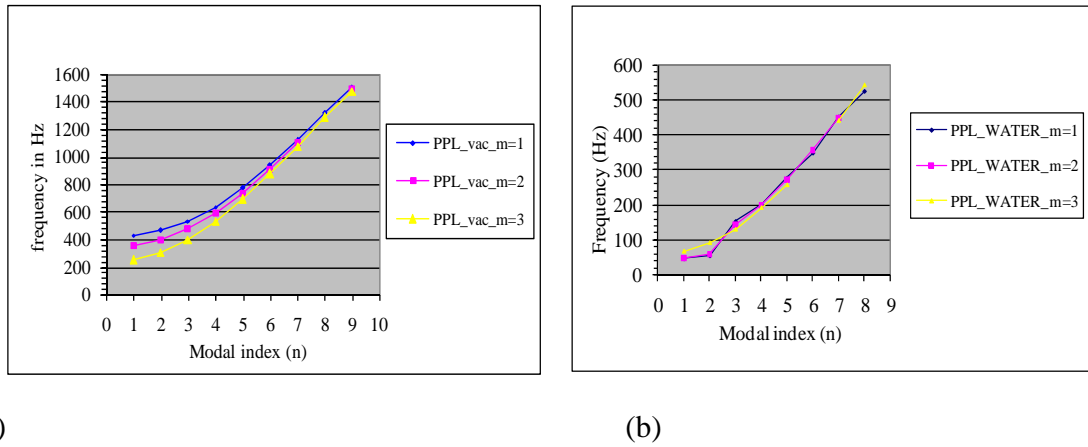


Fig. 6.10: (a) Natural frequency of PPL 'in vacuum' for modal index $m=1$ to $m=3$, and (b) Natural frequency of PPL in water backed condition for modal index $m=1$ to $m=3$.

6.5.1 Effect of water medium on natural frequency

In order to evaluate the change in natural frequency due to the presence of water medium, the variation in natural frequency of the PPL is calculated and expressed as percentage. The percentage variation is plotted against the modal index 'n' and shown in Fig. 6.11. It is observed that the variation in natural frequency due to the presence of water medium is about 90%. It reduces to about 50% when the modal index 'n' increases from 1 to 9.

The influence of the water medium to reduce the natural frequency of the submerged plate system, is strongly felt and has to be effectively considered in the prediction of dynamics of such structural system.

6.5.2 Effect of lining plate on natural frequency

To study the effect of lining plate on natural frequency, the variation in natural frequency is arrived with the ratio of the difference in natural frequency of PP and PPL to that of PP and is expressed as percentage. In vacuum, at lower value of 'n' (1 and 2) the natural frequency of PP is less than that of PPL as 'n' increases. This trend is reversed as shown in Fig.6.12. When the water medium is introduced, the natural frequency of the PP is always higher than that of PPL for all the modal indices. However the variation in natural frequency decreases as the modal indices increases as evident from Fig. 6.13.

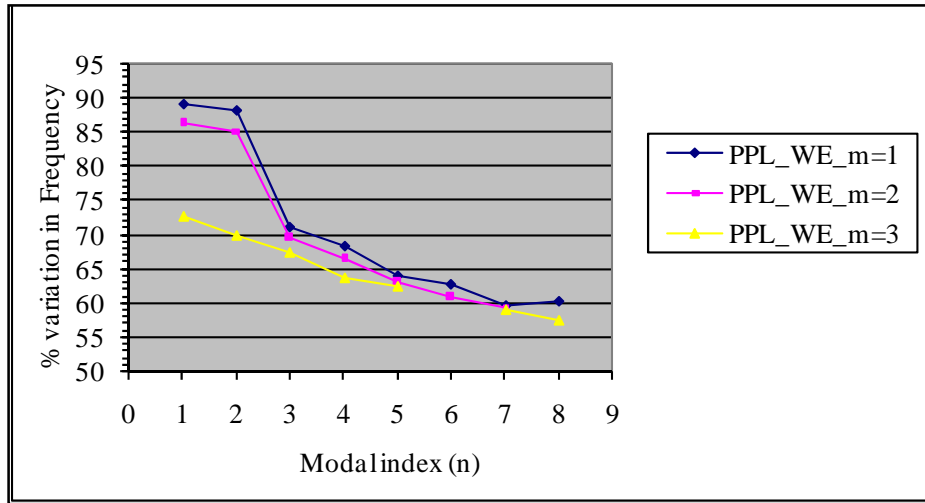


Fig. 6.11: Effect of water medium on natural frequency of PPL for modal index $m=1$ to $m=3$.

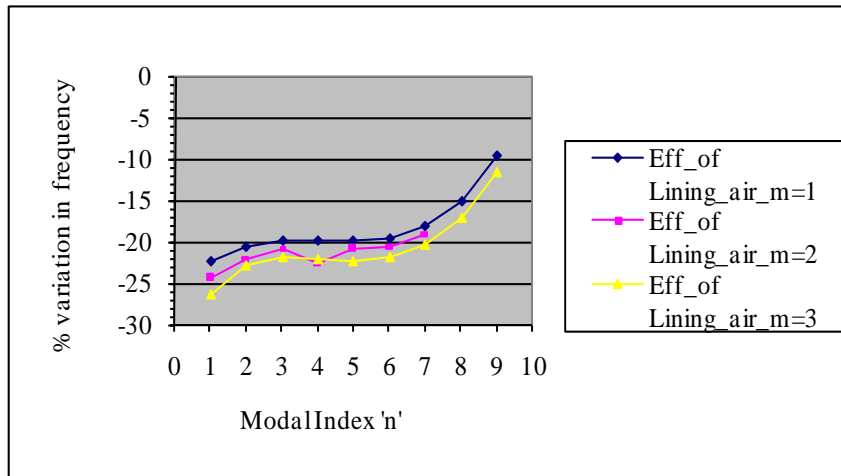


Fig. 6.12: Effect of lining plate 'in vacuum' on natural frequency for modal index $m=1$ to $m=3$.

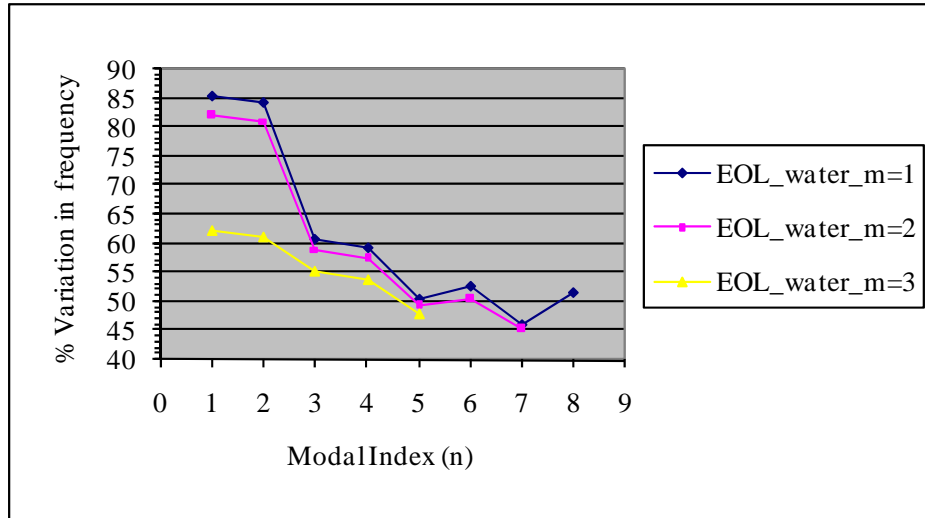


Fig. 6.13: Effect of lining plate for water backed condition on natural frequency for modal index $m=1$ to $m=3$.

6.6 SHOCK ANALYSIS

Shock analysis of the PPL on full model for the BC1 has been carried out using ANSYS LS-DYNA.

6.6.1 Description of finite element analysis

The structure is modeled using ANSYS with the geometry details, boundary condition and part details. For the analysis using ANSYS LS-DYNA, the explosive, structure and fluid are defined based on the EOS and material properties. The options mentioned in sections 5.9.2 to 5.9.5 are considered in this investigation also. The various parameters for EOS and Materials given in Tables 5.6 to 5.8 have been adopted here. Using ANSYS LS-DYNA solver module, 'k' file is generated.

Analysis has been conducted for three explosives viz., PEK, TNT and C4. The dimensions of the model for the explosive have been arrived from the density and volume of explosive. PPL is placed at a stand off distance of 1 m in such a way that the lining plate is facing the explosive. SHELL163 element is used for modeling the plate and SOLID164 is used for explosive and fluid. PPL has been defined as two parts (perforated

plate and lining plate) and these two parts are included under a ‘BOX’ definition using ANSYS LS-DYNA. The finite element model for PPL is shown in Fig. 6.14(a). The input for the shock analysis is same for PPL as given in section 5.9.8. In each analysis, the pressure is measured at a distance of 1 m from the detonation point in the fluid medium. The deflection and principal stress on the lining plate are also recorded.

6.6.2 Results and Discussion

The free field pressure as time history plot at a distance of 1 m from the explosive is given in the Figs. 6.14(b), 6.15(a) and 6.16(a) for explosives PEK, TNT and C4 respectively. However, the deflection and principal stress are evaluated at centroid of the plate. The deflection and principal stress are plotted for both, on lining (curve marked with ‘A’) and on perforated plate (curve marked with ‘B’). The time history curve for the deflection is shown in Figs. 6.14(c), 6.15(b) and 6.16(b) for explosives PEK, TNT and C4 respectively. The time history curve for the principal stress is shown in Figs. 6.14(d), 6.15(c) and 6.16(c) for explosives PEK, TNT and C4 respectively.

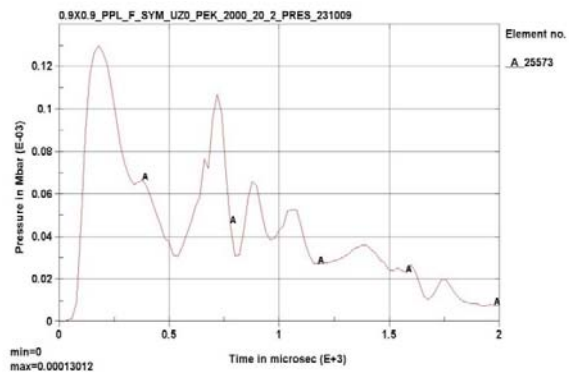
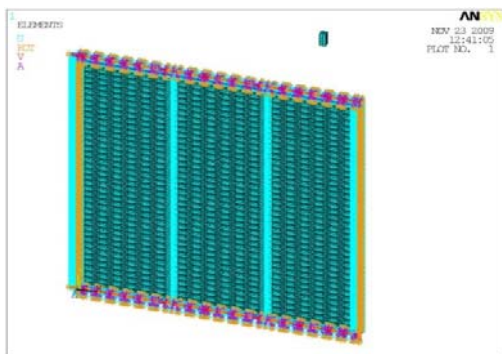


Fig. 6.14: (a)

(b)

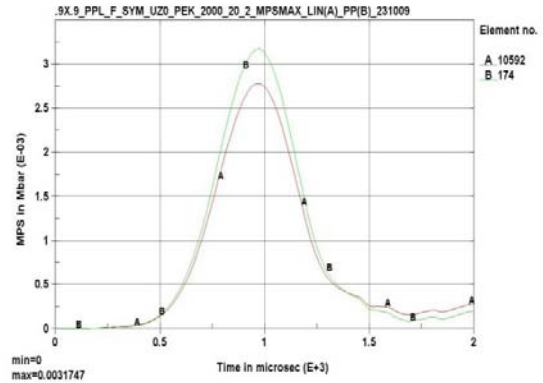
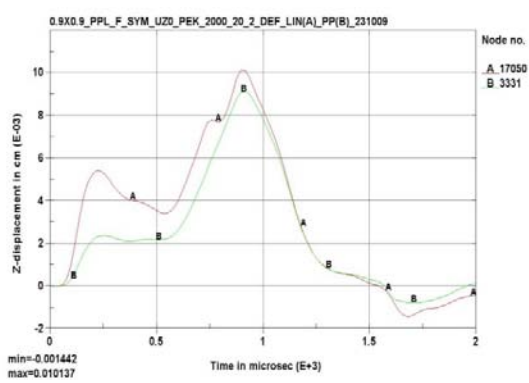


Fig. 6.14: (contd.) (c)

(d)

Fig. 6.14: (a) Finite Element model of PPL with SHELL163 element for geometry and SOLID164 element for PEK explosive and fluid for BC1, (b) Free field pressure history plot in front of Lining Plate for PPL due to explosion of PEK, (c) Deflection history plot for PPL due to explosion of PEK, and (d) Principal Stress history plot for PPL due to explosion of PEK.

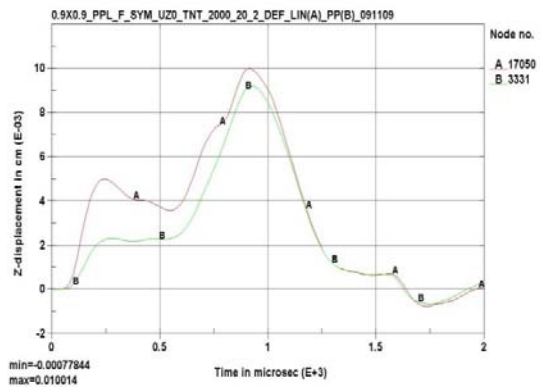
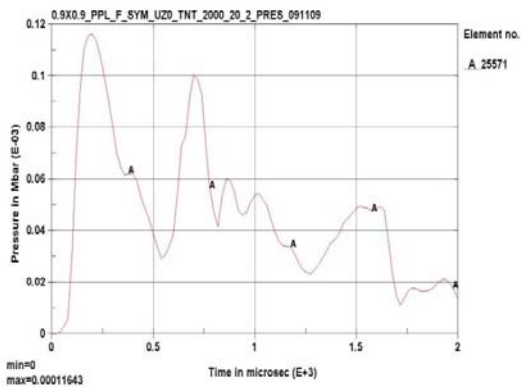


Fig. 6.15: (a)

(b)

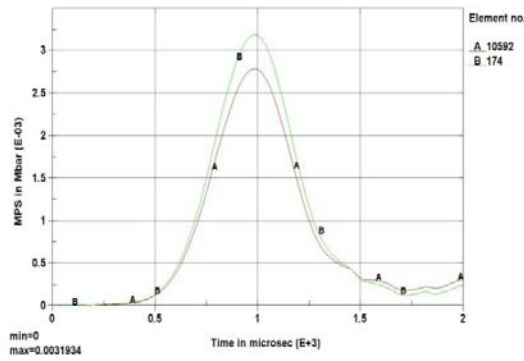


Fig. 6.15: (contd.) (c)

Fig. 6.15: (a) Free field pressure history plot in front of Lining Plate of PPL due to explosion of TNT for BC1, (b) Deflection history plot for PPL due to explosion of TNT, and (c) Principal Stress history plot for PPL due to explosion of TNT.

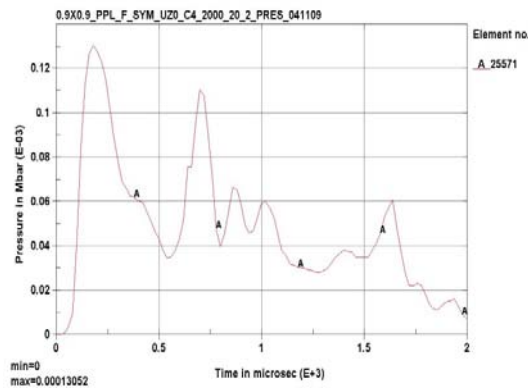


Fig. 6.16: (a)

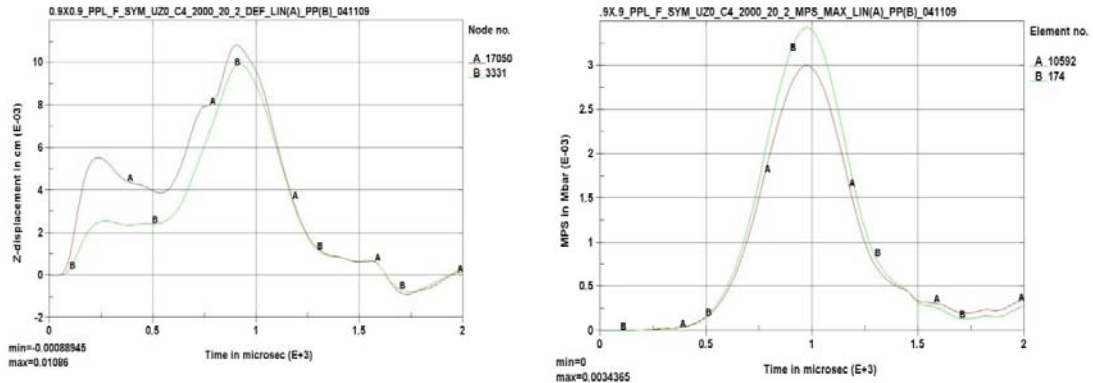


Fig. 6.16: (contd.) (b)

(c)

Fig. 6.16: (a) Free field pressure history plot in front of Lining Plate of PPL due to explosion of C4 for BC1, (b) Deflection history plot for PPL due to explosion of C4, and (c) Principal Stress history plot for PPL due to explosion of C4.

It is observed that the free field pressure history plot for all the three explosives is in same pattern but with different magnitude at the peak pressure. The free field pressure history plot for PPL has one additional peak with less magnitude at 1500 microsec compared to that of PP.

It is noticed that initially deflection on lining plate has marginally high value compared on the perforated plate side. The peak value of principal stress in the lining plate is lower than that in the perforated plate.

The free field pressure nearer to the lining side of PPL along with the maximum value, and the centroidal deflection and MPS on the PPL are estimated and given in Table 6.5. The variations in above parameters are evaluated from Table 5.9 and 6.5 and shown in Table 6.6. Though the free field pressure has to be same at a point in the fluid column theoretically, a difference of 3% has been observed between PP and PPL at a stand off distance of 1m. The maximum deflection occurred at the centroid of the plate and the change in deflection due to the addition of lining plate is negligible. Whereas the MPS at the PPL is around 14% more than that in PP, but at centroid of PPL by 24%.

Table 6.5: Free field pressure and structural responses of PPL due to 30 gm weight and 1m stand off distance for explosions of PEK, TNT and C4 for BC1.

Configuration (Stand off Distance R = 1m; charge weight w = 30 gms; Boundary condition = BC1)	Towards Explosion side				
	Free field pressure (MPa)	Deflection (mm) of plate		Principal stress (MPa) of plate	
		Close to Centre of plate	Maximum	at Centroid	Maximum
PPL Explosive: PEK	13.01	0.10	0.10	278	98
Explosive: TNT	11.64	0.10	0.10	279	91
Explosive: C4	13.05	0.11	0.11	300	101

Table 6.6: Variation of Deflection and Principal Stress in percentage due to the lining plate for PEK, TNT and C4 explosives

Effect of lining over perforated plate in percentage due to explosive load (PP & PPL)				
Explosive	Deflection		Principal stress	
	Maximum	at Centroid	Maximum	at Centroid
PEK	-4.2	-4.2	13.3	-24.2
TNT	0	0	13.9	-24.6
C4	0	0	14	-24.7

CHAPTER 7

EXPERIMENTAL INVESTIGATIONS ON PERFORATED PLATE WITH LINING

7.1 INTRODUCTION

Two separate experimental investigations on PPL are envisaged in the present study to determine the static deflection of the plate and to access the free field pressure in the fluid domain from an underwater explosion experiment conducted in a shock tank.

7.2 EXPERIMENTAL INVESTIGATIONS FOR STATIC DEFLECTION

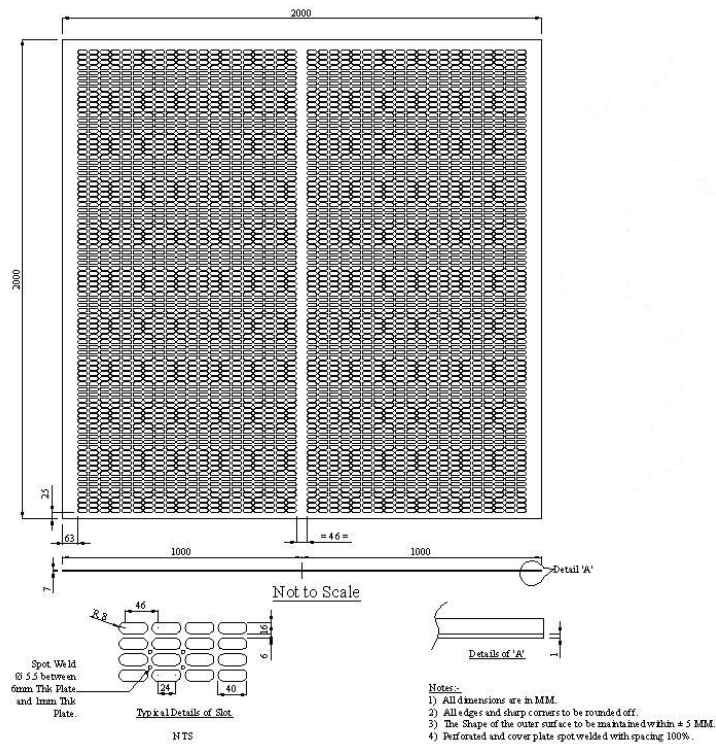


Fig. 7.1: Geometry of PPL as specimen for experimental investigations

7.2.1 Experimental setup

The PPL specimen is 2 m x 2 m with 0.006 m thick perforated plate and 0.001 m thick lining as shown in Fig. 7.1. The pressure testing chamber is used to carry out the experiment. The overall dimension of pressure testing chamber with inlet and outlet pipe is shown in Fig. 7.2. The height of the pressure testing chamber is 120 mm from the base and water inlet provision is given at 70 mm from the base. A pressure testing chamber is fabricated using mild steel and water is used as fluid medium to apply uniform pressure on the lining side of the plate. The assembly of the plate and pressure testing chamber is ensured for pressure tightness with proper neoprene rubber gasket. Over and above, all the joints are sealed with M-seal. Provision is made for filling up the water using hand pump and for air escape while filling the pressure testing chamber. In order to measure the pressure in term of kPa, a digital based pressure gauge with resolution of 100 Pa with measuring range of pressure from -100 kPa to maximum pressure of 100 kPa is used. The digital pressure gauge is manufactured by M/s. SMC Corporation, India and it has part no: 1 – ZSE 50F – 02 – 62L – A. All the four edges of the plate and pressure testing chamber is assembled with fasteners. In addition to that, two C – clamps are also used at the two sides of the edges where two half of the plates are welded together, since drilling of holes at the welded joint is not possible. Vernier caliper is used to measure deflection at the center of the plate on the perforated plate. The fixed jaw of the vernier caliper is rested over the perforated plate. Considering the maximum expected deflection, the moving jaw of the vernier caliper is adjusted and placed in position with the support of the L-angle which is again rested over two wooden blocks placed outside the pressure testing chamber. The photographs of the experimental setup is shown in Figs. 7.3(a) and 7.3(b). Fig. 7.3(c) shows the close up view of the pressure gauge and Fig. 7.3(d) is that of the vernier caliper.

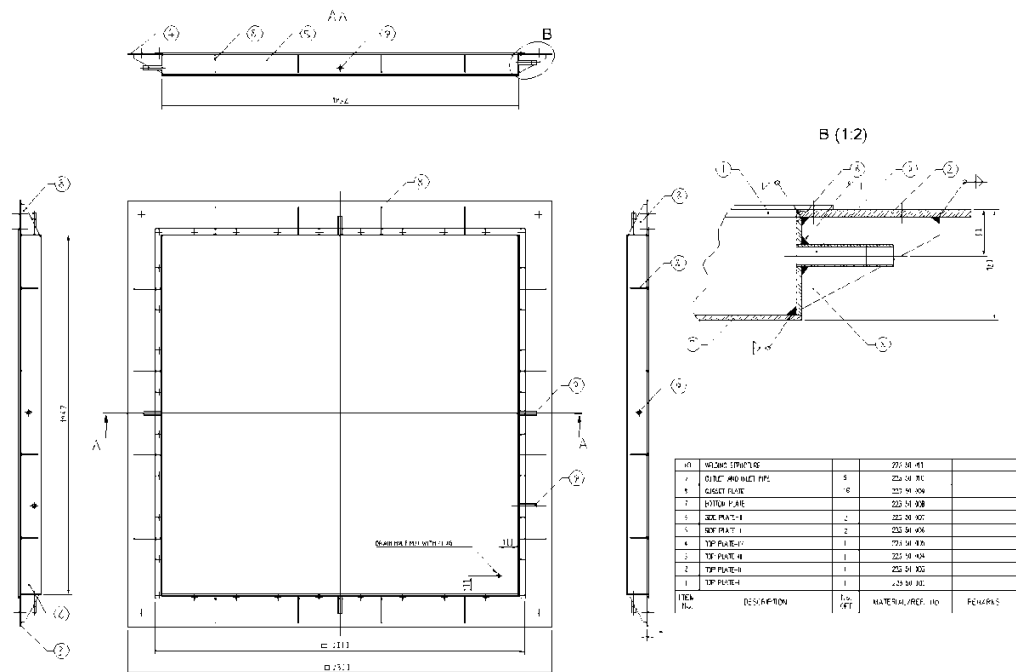


Fig. 7.2: Dimensioned sketch of Pressure Testing Chamber designed to provide pressure loading on PPL

7.2.2 Experimental procedure

Initially pressure testing chamber is filled with water. The perforated plate with lining is placed over the flange of the pressure testing chamber with lining plate facing the water. A hand pump is attached with the inlet of the pressure testing chamber. With a 'T' connection, provision is given to attach the digital micro pressure gauge. Uniform water pressure is applied over the lining plate area. Considering the pressure testing chamber height, the experiment is started with an initial pressure of 3 kPa. Using hand pump, pressure is increased at regular increment of 0.5 kPa and the corresponding deflection has been noted. At each increment, pressure is allowed to stabilize before recording the deflection. This procedure is repeated for the pressure upto 15 kPa. Two sets of reading are recorded by repeating the experiment twice with a time interval of 24 hours. Thus two sets of load deflection data are obtained and shown in Table 7.1. The average of two sets of deflection, for each pressure is given in Table 7.2.



Fig. 7.3: (a)



(b)



Fig. 7.3: (contd.) (c)

(d)

Fig. 7.3: (a) Experimental setup for load – deflection investigation of the perforated plate with lining, (b) Side view of the experimental setup indicating the pressure testing chamber and PPL, (c) View of digital based micro pressure gauge to measure the applied pressure on the lining side of the PPL, and (d) View of the vernier caliper to measure the deflection of the plate at the perforated plate side of PPL.

7.3 VALIDATION USING FINITE ELEMENT ANALYSIS

Geometric nonlinear analysis of the above mentioned PPL has been carried out using ANSYS software and the details are given under subsequent sub headings.

7.3.1 Description of the finite element model

SHELL63 element is used for the modeling and is shown in Fig. 7.4. The finite element model has 141506 nodes and 126136 elements. Geometrically nonlinear analysis of PPL has been carried out with the maximum load at 15 kPa, as in the case of experiment.

Table 7.1: Experimental measurement of load - deflection of PPL for BC3.

Sl. No.	PPL of 2m x 2m with BC3 boundary condition (EXPERIMENT)		
	Pressure (kPa)	Deflection (mm)	
		Set 1	Set 2
1	0	0	0
2	3	8	8.7
3	3.5	9	9.6
4	4	11.5	11.9
5	4.5	13	13.5
6	5	15.4	15.8
7	5.5	17	17.2
8	6	19.2	19.6
9	6.5	19.8	20.2
10	7	20.3	20.7
11	7.5	20.8	21.2
12	8	21.5	21.8
13	8.5	22	22.4
14	9	22.5	23
15	9.5	22.9	23.4
16	10	23.2	23.8
17	10.5	23.5	24.1
18	11	23.9	24.5
19	11.5	24.3	25.1
20	12	24.6	25.7
21	12.5	24.9	26.2
22	13	25.3	26.5
23	13.5	25.6	26.8
24	14	25.9	27.1
25	14.5	26.2	27.3
26	15	26.5	27.5

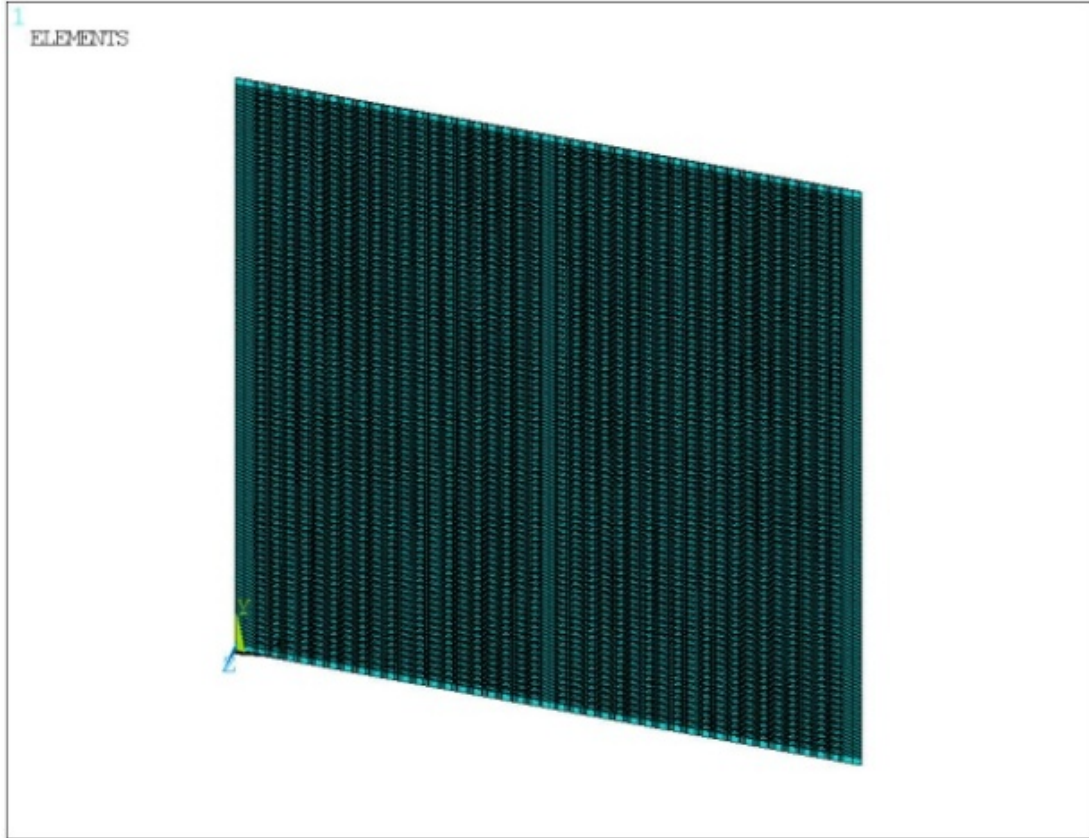


Fig. 7.4: Finite element model of PPL with SHELL63 element for BC3.

7.3.2 Results and Discussion

The analytical and experimental values of the deflection of PPL are given in Table 7.2 and the graphical representation is shown in Fig. 7.5. It is observed that in the initial stage of loading, the experiment values of deflection is found to be higher than the values from the finite element analysis, and later on, the deflections obtained from the experiment are lower than the values from the finite element analysis. The percentage difference of the experimental and numerical method values of deflection is around 8.0%

Table 7.2: Comparison of deflection measured from experiment and estimated deflection through finite element method.

Load (kPa)	Experiment – Deflection (mm)	Analysis – Deflection (mm)	Percentage difference
	(average of I & II)	SHELL63	
0	0	0	0
3	8.35	13.5	61.7
4.5	13.25	15.9	20
6	19.4	17.8	-8.2
7.5	21	19.4	-7.6
9	22.75	20.8	-8.6
10.5	23.8	22	-7.6
12	25.15	23.1	-8.1
13.5	26.2	24.1	-8.0
15	27	25	-7.4

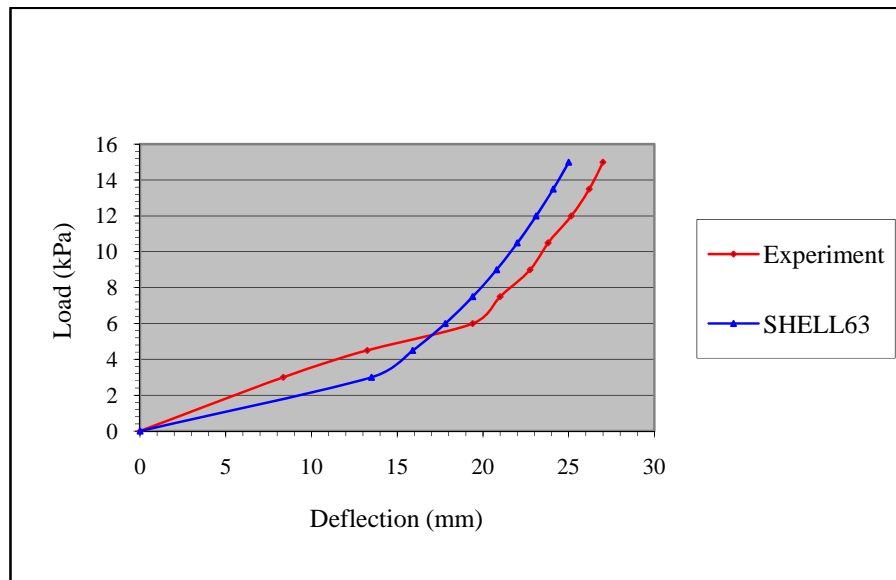


Fig. 7.5: Load – Deflection plots of PPL obtained from experiment and from finite element method.

7.4 EXPERIMENTAL INVESTIGATIONS FOR FREE FIELD PRESSURE

The shock tank facility available at Visakhapatnam, India is used for the experimentation. Noncontact underwater explosions are made using the explosive PEK and pressure blast gauge measurements are made for the free field before and after the PPL which is kept at a stand off distance 1m from the explosive. The details of the experiments are given in the subsequent paragraphs.

7.4.1 Experimental set up

The approximate dimension of the shock tank is 15 m x 12 m x 10 m (L x W x D). PPL with stadium geometry perforation as shown in Fig. 7.1 is used for the experiment. The edges of PPL are arrested to simulate BC3 boundary condition. In order to avoid the reflection of pressure wave from shock tank side walls, acoustic barriers are used. Acoustic barrier is made of plywood sheets and stiffened with flats and these are fixed with PPL. The acoustic barrier is extended by 1m from all the sides except in the rear side. Eight underwater pressure blast gauges are positioned in line with center of PPL at known distances from the explosive charge. PPL with acoustic barrier is suspended using overhead crane and immersed to 2.0 m water depth. The cables from pressure blast gauges are connected to Data Acquisition System. Schematic sketch of the plan view of the experimental setup along with the location of the pressure blast gauges (G_1 to G_8) are shown in Fig. 7.6. Fig. 7.7(a) to Fig. 7.7(d) shows the photographs of PPL with acoustic barrier and blast gauges.

7.4.2 Instrumentation

The instrumentation mainly consists of pressure blast gauges, 8 channel data acquisition system with its software. The underwater pressure blast gauges have capacity to measure peak pressure of 5000 psi and to withstand peak mechanical shock of 20000 g. The data acquisition system consists of a personal computer based Computer Aided Test (CAT) system operating on Windows XL and transient analog to digital converter cards. Necessary software with CAT system is used during the experiment.

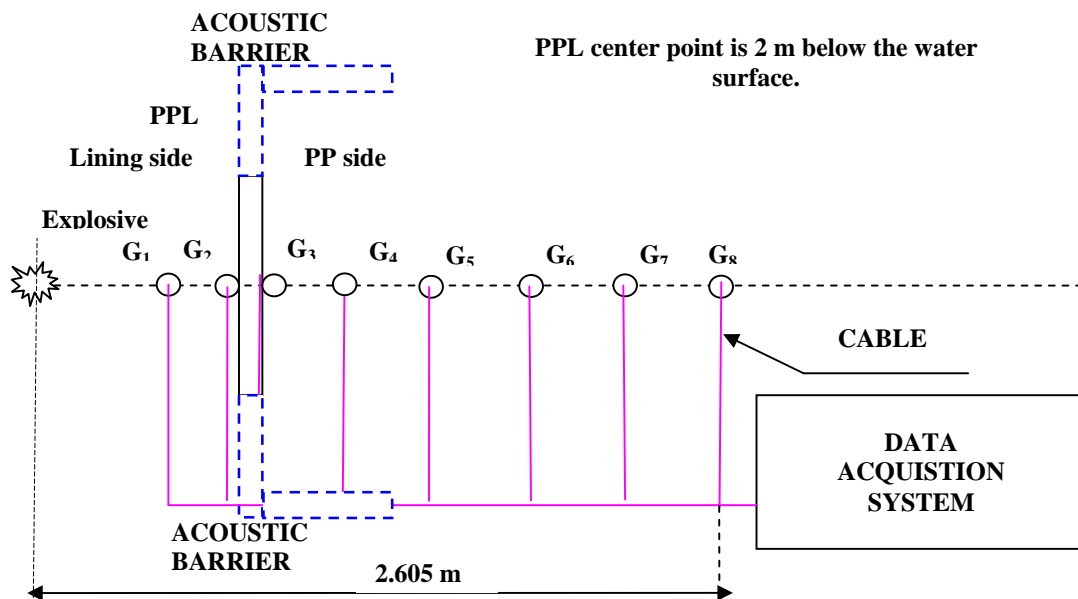


Fig. 7.6: Schematic sketch of plan view of experimental set up indicating PPL with acoustic barrier, explosion location, 8 numbers of pressure blast gauge positions and data acquisition system.

7.4.3 Experimental procedure

The acoustic barrier is fabricated with the provision of fixing PPL at the center. PPL is assembled over the acoustic barrier frames using fasteners. The assembly is erected to vertical position using overhead crane. In order to place the underwater blast gauges at the specified distances, two flats are placed each at top and bottom of PPL. The underwater blast gauges are positioned in its location with kevlar threads. The arrangement can be seen in Fig. 7.7(c) and 7.7(d). The complete arrangement is lowered in the shock tank and supported using overhead crane. The PEK explosive has been weighed and inserted into a plastic container and positioned at 1 m stand off from PPL such that its center coincided with the center of the plate. A firing cable has been laid from the detonator to the firing circuit situated in a control room. The whole set up has been submerged in an underwater shock tank during the experiment at a depth of 2 m from the top horizontal plane of the acoustic barrier frame. Charges of 30 gm of PEK have been exploded and pressures are measured using 8 blast gauges positioned at

different distances. To ensure consistency in the experiment, 6 trials are conducted. On completion of each trial, PPL with underwater blast gauges are lifted from the tank and visual inspection on PPL and underwater blast gauges have been carried out. Fig. 7.7(e) shows the plume generated during one of the shock trial.

7.4.4 Results and Discussion

The weight of explosive, pressure blast gauge distances with reference to explosive location and free field pressure are tabulated in Table 7.3. Pressure history for all the 8 gauges (channels) is shown in Fig. 7.7(f) and the same for channel 2 and channel 3 are given in Fig. 7.7(g) and Fig. 7.7(i) respectively. Fig. 7.7(h) shows pressure history plot of channel 2 for 400 microseconds. These time history plots are taken from trial 2. The peak pressures recorded in one of the trial with reference to locations of blast gauge are shown in Fig. 7.8. The position of the PPL is superimposed in this figure.

The free field pressure measured at channel 2 is taken as the reference and for the given PPL and boundary condition. In case of TNT explosive, the free field pressure is estimated using Cole's empirical formula. From the Table 7.3, it is observed that the free field pressure at channel 1 is higher in three trails compared to that of at channel 2. This should have been the case in all the six trials. However the free field pressure is in descending order, as expected for the remaining seven channels in all the six trials.

From the Table 7.3, the pressure measured at channel 2 and channel 3 is used to estimate resistance offered by the PPL to the shock pressure. The resistance is calculated as the ratio of the difference in pressure between channel 2 and channel 3 to that of the pressure in channel 2 and expressed as percentage. This resistance can be considered as a part of the design load for the PPL during structural analysis.



Fig. 7.7: (a)

(b)

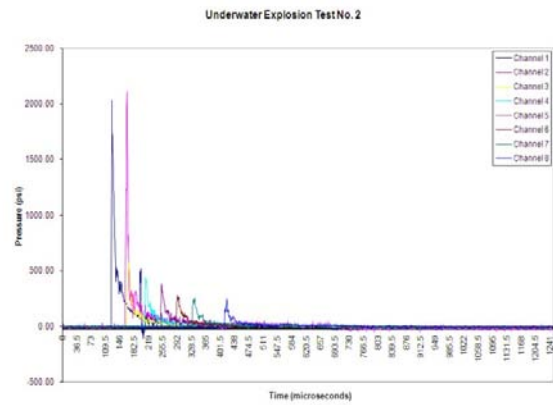


(c)

(d)



(e)



(f)

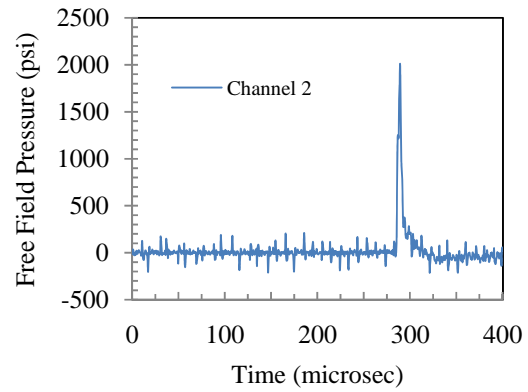
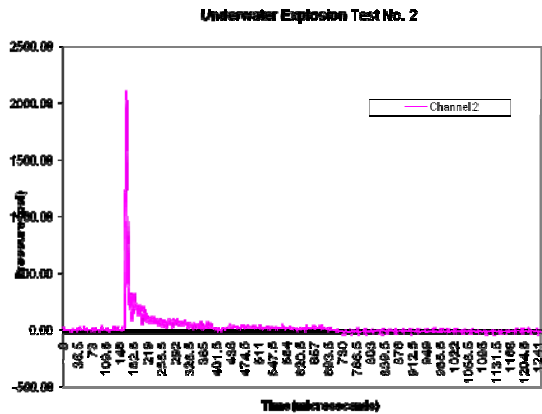
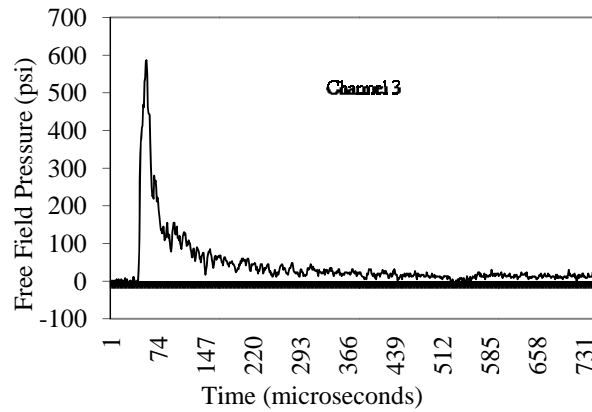


Fig. 7.7: (contd.) (g)

(h)



(i)

Fig. 7.7: (a) View of lining plate along with the acoustic barrier made of plywood assembled with the PPL, (b) View of perforated plate along with the acoustic barrier made of plywood assembled with the PPL, (c) Two numbers of blast gauge placed in front of the lining plate, (d) Six numbers of blast gauge placed at the rear side of lining plate and at the perforated plate side, (e) Plume emanating from water surface after explosion of 30 gm of PEK explosive placed at a stand off distance of 1m, (f) Time history plot of free field pressure recorded by 8 numbers of pressure blast gauges using data acquisition system, (g) Time history plot of free field pressure recorded by pressure blast gauge positioned in front of lining plate through channel 2, (h) Time history plot of free field pressure recorded through channel 2 for 400 microseconds, and (i) Time history plot of free field pressure recorded by pressure blast gauge positioned at the rear side of lining plate through channel 3.

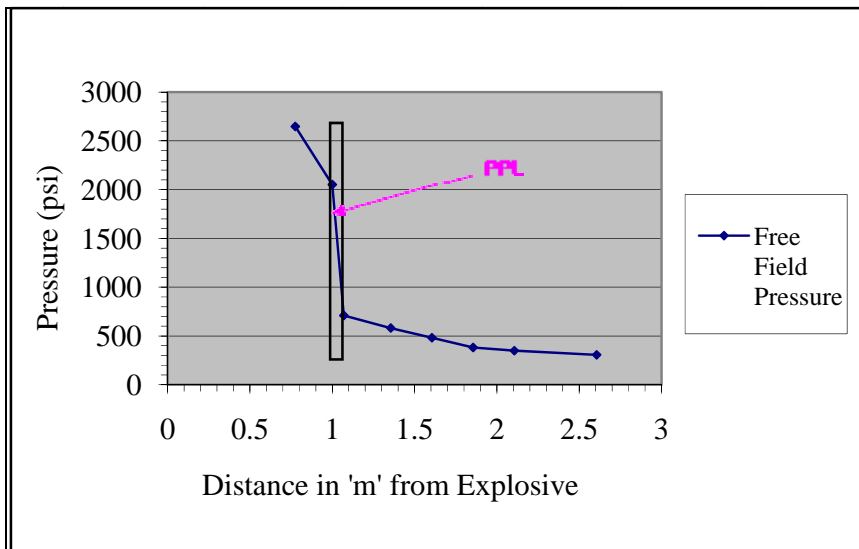


Fig. 7.8: Maximum pressure at various distances as measured using pressure blast gauges superimposed with the PPL.

Table 7.3: Free field pressure measured by pressure blast gauges from noncontact underwater shock explosion experiments for 30gm of PEK explosive placed at a stand off distance of 1m from PPL.

Trial No.	Distance from Charge (m)	Pressure in psi								Resistance of Shock pressure by PPL (%)
		0.775	1	1.07	1.355	1.605	1.855	2.105	2.605	
	Channel Number	1	2	3	4	5	6	7	8	
1		2646	2051	709	581	481	381	349	306	65
2		2035	2115	586	443	384	280	255	251	72
3		2400	2011	661	571	473	415	352	268	67
4		2486	2170	716	625	511	421	391	298	67
5		2156	2313	605	463	379	302	282	237	74
6		2230	2358	628	424	345	289	288	217	74

7.5 NUMERICAL INVESTIGATIONS

Shock Analysis of PPL used for experiment on the noncontact underwater explosion has been carried out using ANSYS LS-DYNA. The geometry and boundary conditions of PPL are adopted as it has been considered for experiment. The free field pressure due to explosion at a distance of 1 m from the explosive is also estimated so as to compare with the pressure obtained through channel 2 during experiment. This analysis is carried out for PEK, TNT and C4 explosives.

7.5.1 Finite element analysis

The finite element model for PPL is shown in Fig. 7.9(a) which has been explained in section 6.6.1. The input for the shock analysis is same for PPL. To establish the convergence of free field pressure, the mesh density of the explosive and fluid column has been varied as suggested by Kim and Shin (2008). In case of fluid, gradient mesh density is applied. The mesh near the plate is fine and away from the plate is coarse. The mesh density of the fluid domain at explosive area is same as that of the explosive which is also a fine mesh, for the assured nodal connectivity between the explosive and fluid. In each analysis, the free field pressure is estimated at a distance of 1m from the explosive. The deflection and principal stress at the centroid of PPL are also estimated.

7.5.2 Results and Discussion

The free field pressure as time history plots are given in the Figs. 7.9(b) and 7.9(c). The deflection and principal stress as time history plots are given in the Figs. 7.9(d) and 7.9(e) respectively for explosions of PEK. The maximum value and values of deflection and principal stress at centroid of PPL have been obtained in each case and are shown in Table 7.4. The free field pressure obtained from experiment and finite element analysis along with percentage variations are shown in Table 7.5. The variation has been found around 6.8%.

Table 7.4: Estimation of free field pressure and structural responses of PPL due to shock analysis.

Configuration (Stand off Distance R = 1m; charge weight w = 30 gm; BC3 boundary condition)	Towards explosion side				
	Free field pressure (MPa)	Deflection (mm)		MPS (MPa)	
		Close to Centre of plate	Max	Cen	Max
<u>PPL (Specimen)</u> Explosive: PEK	13.7	0.55	0.55	948	88
Explosive: TNT	12.6	0.50	0.50	935	92
Explosive: C4	13.87	0.54	0.54	936	95

Table 7.5: Comparison of free field pressure obtained from experiment and finite element method due to noncontact underwater explosion using PEK on PPL for BC3

Experiment - average value	FE Method	% variation
2132 psi (14.7MPa)	1987 psi (13.7MPa)	-6.8%

Similarly the pressure obtained at a stand off of 1m, due to TNT explosion is also compared with Cole's empirical formulae. The pressure obtained is compared with finite element method and shown in Table 7.6. The observed variation is 9.8%.

Table 7.6: Comparison of free field pressure obtained from Cole's method and finite element method due to noncontact underwater explosion using TNT on PPL.

Cole's formula	FE method	% variation
2028 psi (13.98MPa)	1828 psi (12.6MPa)	9.8%

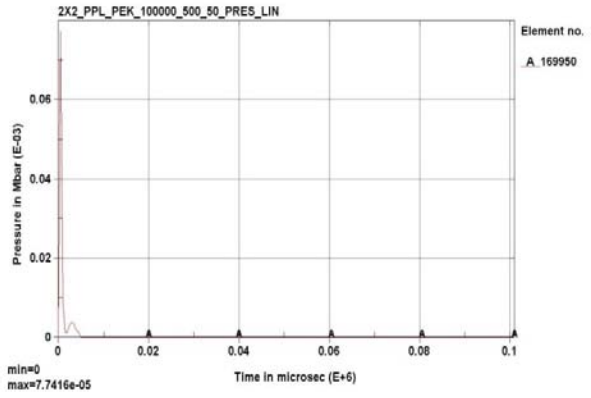
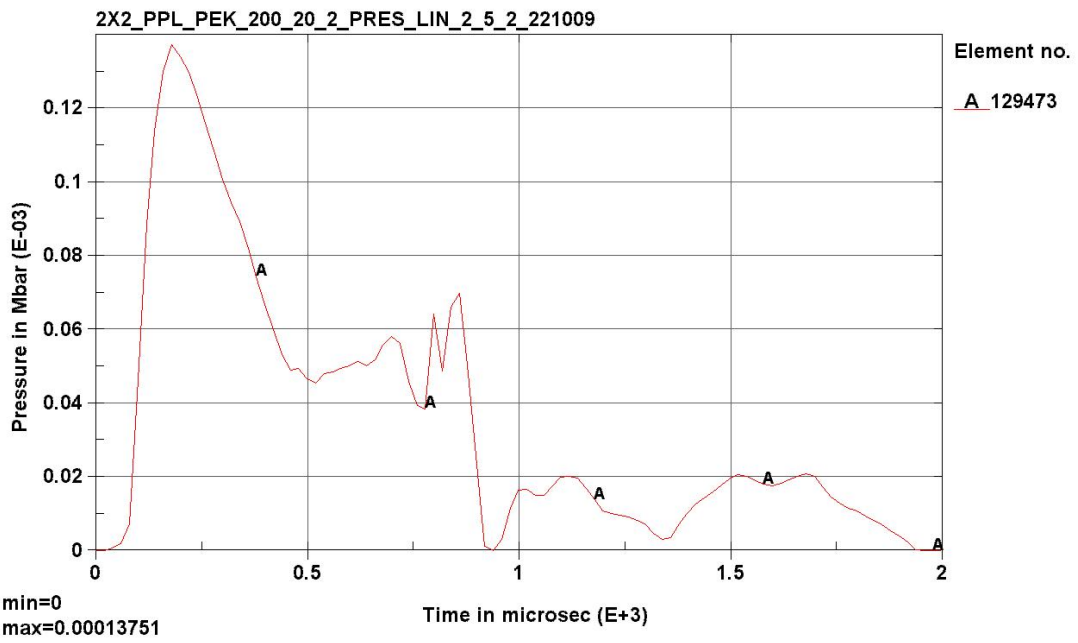


Fig. 7.9: (a)

(b)



(c)

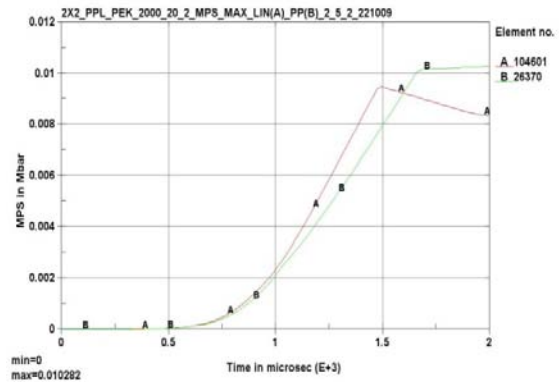
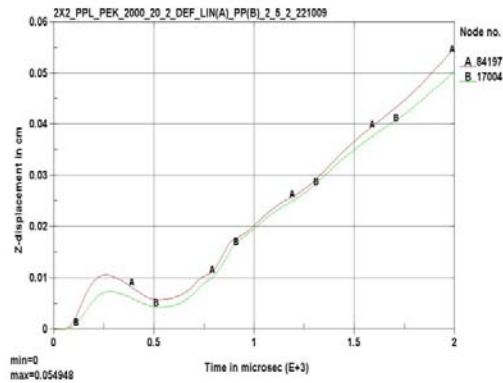


Fig. 7.9 (contd.) (d)

(e)

Fig. 7.9: (a) Finite Element model of PPL with SHELL163 element for geometry and SOLID164 element for PEK explosive and fluid for BC3, (b) Free field pressure history plot in front of Lining Plate for PPL due to explosion of PEK, (c) Free field pressure history plot in front of Lining Plate for PPL due to explosion of PEK for 2000 microseconds, (d) Deflection history plot at centroid of lining plate of PPL due to explosion of PEK, and (e) Principal Stress history plot at centroid of lining plate of PPL due to explosion of PEK.

It is also observed that the free field pressure time history plot obtained from the experiment and numerical analysis are compared for the peak pressures at the same location as that of channel 2 placed during the experiment. The plot taken from the numerical analysis as shown in Fig. 7.9(b), also exhibits similar trend as that of experiment. From Fig. 7.9(c), it is observed that a slight disturbance next to the pulse may be attributed due to the reflection of the pressure pulse from the PPL.

Pressure evaluated from the experiment and numerical analysis has been compared. The pressure time history at channel 1 of the experiment is compared with that at the point closer to that location. Considering the coarse element mesh of the model in the region of fluid, the element nearest to the channel 1 location is referred for comparison (at a distance of 0.6622 m). The pressure blast gauge at channel 1 is placed at a distance of 0.775 m from the explosion. The maximum pressure estimated using numerical method

gives 6.2% higher than that obtained using Cole's formula. It is also observed that pressure time history plot has one pulse in both the experiment and numerical method.

Since the pressure estimated from numerical analysis is in agreement with that measured from the experiment for PEK and from Cole's formula for TNT, the deflection and stress estimated using numerical analysis can be used for the structural design.

The free field peak pressure and duration of pressure pulse depend on the explosive charge weight, stand off distance, EOS, material properties and finite element mesh size. In this investigation, finite element mesh size is varied and the effect is studied. However due to the available hardware configuration, very fine mesh could not be solved. By refining the mesh, the duration of the pressure pulse may be controlled.

CHAPTER 8

SUMMARY AND CONCLUSIONS

The summary of the investigations carried out in the present study and the conclusions derived out of it have been grouped under various sub headings and presented below.

8.1 SUMMARY

Perforated plate carries geometric imperfections in the form of cutouts and subsequently their finite element models are to be comprised of many nodes and elements. The parametric investigations like those envisaged in the present study will become voluminous and cumbersome, if those are performed on the plates of original dimension. A unit cell of PP, which is a geometric miniature of the original plate, is carved out from it, where the dimension of the perforation, ligament width and thickness are preserved but the number of perforations has been restricted to 16. The numerical investigations carried out in the present study extensively make use of ANSYS for static and dynamic analysis, and ANSYS LS-DYNA for shock analysis. Convergence studies are performed for the four finite elements available with the ANSYS, viz., SHELL63, SHELL93, SOLID45 and SOLSH190 on NPP and PP, for various geometry and orientations of the perforation, as well as for various boundary conditions. Deflection, von Mises stress and maximum principal stress are the desired output from finite element analysis. Results obtained for the linear elastic analysis of unit cell are processed to obtain the SCF and DF at neighboring locations along the periphery of the perforation. Based on these values recommendations have been made regarding the selection of geometry and orientation of the perforation.

Structural analysis of PP has been carried out using software packages based on finite element method. A perforated plate with 0.9m x 0.9m x 0.006m with stadium horizontal perforations has been considered as the structure for analysis and linear elastic analysis has been carried out for a unit normal pressure. The effect of rotation restraint at the boundary nodes on the structural responses has been investigated. Linear and nonlinear

static, free vibration and shock analysis have been carried out and the results are reported. In case of free vibration analysis of water backed structure, FLUID30 element has been used to model water.

The influence of lining plate in the response of the PP has been studied by adding 0.001m thick lining plate over the perforated plate. This PPL has been considered for the analysis, and linear elastic analysis has been carried out for a unit normal pressure. Three structural models viz., plate, solid and grillage models of PPL have been studied and the structural responses are compared.

Shock analysis of PP and PPL of above dimension has been carried out using ANSYS LS-DYNA. In the shock analysis, three explosives viz., PEK, TNT and C4 are placed at a distance of 1m from the structure. In each analysis, 30gm of explosive is used. SHELL163 of ANSYS LS-DYNA is used to model structure and SOLID164 element of ANSYS LS-DYNA is used to model fluid and explosive.

Experimental investigations are carried out on PPL to plot the load deflection curve and have been compared with analytical results.

Underwater explosion experiments are conducted in shock tank for PPL using PEK explosive. The free field pressure is measured at different locations using underwater pressure blast gauges. Results are corroborated with that of numerical investigations using ANSYS LS-DYNA.

8.2 CONCLUSIONS AND RECOMMENDATIONS

The present thesis contributes to the understanding of the behavior of perforated plate and perforated plate with lining 'in vacuum' as well as in the water backed condition based on the numerical investigation. Similarly the experiments carried out on PPL and underwater explosion experiments yielded significant knowledge on the behavior of perforated plate with lining. The conclusions drawn from this research study are listed below.

- Considering the geometric parameter of the perforated plate under investigation, a unit cell configuration with 8 rows and 2 columns of perforation is established.
- The performance of four finite elements viz., SHELL63, SHELL93, SOLID45 and SOLSH190 available in the ANSYS library has been studied. The superiority of SHELL63 over other elements has been established based on the convergence studies conducted on the unit cells of perforated plate and perforated plate with lining.
- The deflection and stresses have shown a variation of 300 to 500% and 110 to 160% on release of rotation restraint on the boundary nodes. This has to serve as the precaution to ensure perfect fixity of kinematics along the boundary edges.
- The superiority of SHP has been established based on the investigations on unit cell and subsequent evaluation and comparison of SCF and DF. This orientation and geometry has been recommended for water backed subsea applications.
- The results and conclusions based on the various types of linear elastic analysis conducted on PP, guide the designer to select proper finite element and mesh size. At the same time he is relieved of the anxiety about the effect of rotation restraint on the boundary nodes.
- The investigation on the effect of perforation and lining indicates that the finite element modeling is to be carried out without approximating the perforation geometry.
- The load deflection behavior of PP, PPL have been estimated using geometric nonlinear analysis and are graphically presented. The load at which the linear behavior gets missing has been identified.

- The vibration characteristics of NPP, PP and PPL have been studied by incorporating the 'water backed condition' as well as 'in vacuum' condition. It is observed that the natural frequency of the NPP and PPL decreases to 90% and 20% respectively. Hence it is strongly recommended to introduce the effect of water medium in the analysis of water backed underwater structures.
- The deflection at center of PPL is compared with the experimental results and thereby the method of numerical analysis is proved in the investigation.
- The peak free field pressure estimated from the analysis has been validated through the experiment and good agreement has been found. The deflection and stress estimated are also within the acceptable level.
- The duration of pressure pulse obtained through numerical analysis has been found to be more than that of experimental one. The pressure pulse is dependent on the explosive & fluid material property, equation of state of explosive & fluid, and element mesh size. Among these three factors, the first two are standardized and the third one i.e., regarding the mesh grading is dependent on the capability on the computing environment. A better prediction of the numerical analysis using a finer mesh in an advanced computing environment could have brought down the parity observed above. The criticality of mesh size and its effect on free field pressure and the shape of the pressure pulse have been brought out by this.
- The experimental investigation on PPL dealing with the free field pressure measurements can be used for estimating the differential pressure due to underwater explosion. This differential pressure can be treated as the resistance to be considered as a part of the design load for the PPL during structural analysis and can be helpful in optimizing the structural design.

8.3 SIGNIFICANT CONTRIBUTIONS

- The effect of water backed condition on natural frequency of the plate is established through numerical study.
- Experimental investigations on PPL for water backed condition of underwater explosion has been carried out for first time and validated with numerical method.
- The geometric nonlinearity of PPL has been investigated using numerical and experimental procedures and presented through graphical output.

8.4 RECOMMENDATIONS FOR THE FUTURE WORK

- Parametric studies can be carried out on the unit cell of PP and based on regression and correlation analysis, equation can be generated for maximum SCF and variation of SCF along the perforation profile.
- Using Coupled Eulerian – Lagrangian approach available in UNDEX software, the free field pressure can be estimated with water backed structure.
- Similar investigations can be carried out on Curved Plates for Underwater explosion and the effect of curvature of plate in resisting shock loads can be quantified.
- Structural responses and natural frequencies due to water medium for the non metallic structures can be investigated.

REFERENCES

1. **Adamik V., V. Jiri, V. Pavel and A.T. Waldemar** (2004) Effect of TNT charges orientation on generated air blast waves – Numerical simulation using LS-DYNA, 12th *ANSYS User's Meeting*, 30.
2. **ANSYS Inc.** *Acoustics & Fluid – Structure Interaction*. A revision 5.0. Tutorial, 1992.
3. **ANSYS Inc.** *Explicit Dynamics with ANSYS LS-DYNA*, Release 7.1, Training Manual, 2003.
4. **ANSYS Inc.** *Release 9.0 Documentation* for ANSYS software, 2004.
5. **Batra R.C. and N.M. Hassan** (2007) Response of fiber reinforced composites to underwater explosive loads, *Composites: Part B* **38**, 448 – 468.
6. **Blevins R.D.** *Formulas for Natural Frequency and Mode shapes*, McGraw-Hill Book company, 1978.
7. **Cantemir D., L. Bertini and M. Beghini** (2004) Finite element modeling and simulation of multipass welding for the perforated plates case, Paper presented at the *First International Conference on Computational Mechanics*, 15-17 November, Belgrade.
8. **Cantemir D., L. Bertini, M. Beghini, L. Barbieri and F. Spadaccini** (2007) A finite element procedure for prediction of tube hole distortion due to welding of large perforated plates, *Int. Jr. of Pressure Vessels and Piping*, **84**, 460-468.
9. **Chen C.J, W. Liu and S.M.Chern** (1994) Vibration Analysis of Stiffened Plates, *Computers & Structures*, **50**, No.4, 471 – 480.
10. **Cole R.H.** *Underwater Explosions*, Dover Publications Inc, Newyork, USA, 1948.
11. **David A. P. and H.P.Hoshi** (1983) Elastoplastic analysis of thick perforated plates with application to prestressing anchor heads, *Computers & Structures*, Vol **17**, No.4, 539 – 553.
12. **D'Souza K., S. Sett, W. Jung, K.Shin and Y. Lee** (2006) Modeling the Structural and Acoustic Behaviour of a Sonar Dome with ABAQUS, *ABAQUS Users' Conference*.
13. **Everstine G.C.** (1981) A Symmetric Potential Formulation for Fluid – Structure Interaction, *Journal of Sound and Vibration*, **79** (1), 157 – 160.
14. **Geers T. L.** (1978) Doubly Asymptotic Approximation for transient motions of submerged structures, *Journal of Acoustic Society of America*, **64**, 1500 – 1508.

15. **Geers T. L.** and **C. Felippa** (1983) A, Doubly asymptotic approximations for vibration analysis of submerged structures, *Journal of Acoustic Society of America*, Vol.73, No.4, 1152-1159.
16. **Geers T. L.** and **P. Zhang** (1994a) Doubly asymptotic approximations for Submerged Structures with Internal Fluid Volumes: Formulation, *Journal of Applied Mechanics*, Vol.61, 893 – 899.
17. **Geers T. L.** and **P. Zhang** (1994b) Doubly asymptotic approximations for Submerged Structures With Internal Fluid Volumes: Evaluation, *Journal of Applied Mechanics*, Vol. 61, 900 – 906.
18. **George C.** (1970) Transient flexural vibrations of a ship like structures exposed to underwater explosion, *Journal of Acoustic Society of America*, **48**, 170-180.
19. **Guo J., G. Shi, Y. Wang** and **C. Lu** (2003) Efficient modeling of panel – like structures in perforation simulations, *Computers & Structures*, **81**, 1-8.
20. **Hagedorn P.** (1994) A note on the Vibrations of Infinite Elastic Plates in Contact with Water, *Journal of Sound and Vibration*, **175** (2), 233 – 240.
21. **Harnau M.** and **K. Schweizerhof** (2002) About linear and quadratic “Solid-Shell” elements at large deformations, *Computers & Structures*, Vol. **80**, No.9-10, 805-817.
22. **Hauptmann R, S. Doll, M. Harnau** and **K. Schweizerhof** (2001) ‘Solid-Shell’ elements with linear and quadratic shape functions at large deformations with nearly incompressible materials, *Computers & Structures*, **79**, 1671-1685.
23. **Hung C.F., B.J. Lin, J.J. Hwang-Fuu** and **P.Y. Hsu** (2009) Dynamic response of cylindrical shell structures subjected to underwater explosion, *Ocean Engineering*, **36**, 564 – 577.
24. **Imaizumi M, H. Kobayashi, Y. Koyama, H. Nuno, S. Kuga** and **Y. Matsushima** Effective elastic method for perforated plate with irregular penetration patterns, SMiRT – 12 / Kussmaul K (Editor), 49 – 55, F04 / 1, Elsevier Science Publishers B.V, 1993.
25. **Jo J.M.,** and **J.C. Jo** (2006a) Equivalent material properties of perforated plate with triangular or square penetration pattern for dynamic analysis, *Nuclear Engineering and Technology*, Vol. **38**, No.7, 689 - 695.
26. **Jo J.M.,** and **J.C. Jo** (2006b) Free vibration Analysis of Perforated Plate Submerged in Fluid, *Journal of Mechanical Science and Technology*, Vol **20**, No.9, 1323 – 1338.
27. **Jones D.P, J.L. Gordon, D.N. Hutula, D. Banas** and **J.B. Newman** (1999) *An elastic-perfectly plastic flow model for Finite element Analysis of perforated materials*, Report DE-AC11-98PN38206.

28. **Kaap D.L, M.A. Sprague and R.L. Engelstad** (1997) *A finite element benchmark for the Dynamic Analysis of Perforated Plates with a Square Penetration Pattern*, Report no. UWFD-1034.
29. **Keith G.W.** (2007) *Investigation of Close Proximity Underwater Explosion Effects on a Ship-Like Structure Using the Multi-Material Arbitrary Lagrangian Eulerian Finite Element Method*, MS Thesis report, Virginia Polytechnic Institute and State University, January 2007.
30. **Kim J.H. and H.C. Shin** (2008) Application of the ALE technique for underwater explosion analysis of a submarine liquefied oxygen tank, *Ocean Engineering*, **35**, 812 – 822.
31. **Lai W.H.** (2007) Transient dynamic response of submerged sphere shell with an opening subjected to underwater explosion, *Ocean Engineering*, **34**, 653 - 664.
32. **Lal H. and Rajesh Kumari** (2004) Estimation of Primary Shock Effects of Underwater Explosions from Blast data of Free Air Explosion, Internal Report, TBRL, Chandigarh.
33. **Liang C.C. and Y.S. Tai** (2006) Shock responses of a surface ship subjected to noncontact underwater explosions, *Ocean Engineering*, **33**, 748 – 772.
34. **LS-DYNA** *Keyword User's Manual Vol. I and Vol. II*, Version 971, 2007.
35. **Ma Q.W and K.J. Andrews** (2001) *On Techniques for Simulating effects of Cavitation Associated with the Interaction Between Structures and Underwater Explosions using LS-DYNA*, 3rd European LS-Dyna Conference.
36. **Maiorana E., P. Carlo and M. Claudio** (2009) Non-linear analysis of perforated steel plates subjected to localized symmetrical load, *Journal of Constructional Steel Research*, **65**, 959 – 964.
37. **Mair H.U.** (1999a) Review: “Hydrocodes for structural response to underwater explosions, *Shock and Vibration*, **6**, 81 - 96.
38. **Mair H.U.** (1999b) Benchmarks for submerged structure response to underwater explosions, *Shock and Vibration*, **6**, 169 – 191.
39. **MIL-E-16400 G (Navy)** *Shock Isolation*, 24 December, 1974.
40. **Nagesh Lt.Cdr.** (2005) Transient dynamic finite element analysis of plate panels under air blast loading, *Journal of Ship Technology*, Vol.1, 32 - 49.
41. **Nakamura K, M. Takenaka and T. Muto** (2003) *Inelastic Behavior of Perforated Plates Subjected to Bending*, Report L15 / 3.

42. **Namkoong K, H.G. Choi and J.Y. Yoo** (2005) Computation of dynamic fluid – structure interaction in two dimensional laminar flows using combined formulation, *Journal of Fluids and Structures*, **20**, 51 – 69.
43. **Nedwell J.R and F.J. Fahy** (1989) Technique for the Experimental Determination of the Acoustic Transmission and Reflection Characteristics of Submerged Plates, *Journal of Sound and Vibration*, **133**(1), 29 – 54.
44. **Paik J. K.** (2007) Ultimate strength of perforated steel plates under shear loading, *Thin-Walled Structures*, **45**, 301 – 306.
45. **Peiran D. and B. Arjaan** (2006) *Simulation of Under Water Explosion using MSC Dytran*, Internal Report, MSC Software Corporation, MI 48105.
46. **Peter A.** (2001) Experimental Modal Analysis, *Sound and Vibration*.
47. **Prabu B.S., L. Karunamoorthy and G.S. Kandasami** (2004) A finite element analysis study of micromechanical interfacial characteristics of metal matrix composites, *Journal of Materials Processing Technology*, 153 – 154, 992 – 997.
48. **Prusty B.G. and S.K. Satsangi** (2001) Analysis of stiffened shell for ships and ocean structures by finite element method, *Ocean Engineering*, **28**, 621 – 638.
49. **Qiu X, V.S. Deshpande and N.A. Fleck** (2003) Finite element analysis of the dynamic response of clamped sandwich beams subject to shock loading, *European Journal of mechanics A/Solids*, **22**, 801 – 814.
50. **Rajendran R.** (2008) Reloading effects on plane plates subjected to non-contact underwater explosion, *Journal of Materials Processing Technology*, **206**, 275 – 281.
51. **Rajendran R.** (2009a) Effective shock factors for the inelastic damage prediction of clamped plane plates subjected to non-contact underwater explosion, *Journal of Strain Analysis*, Vol.**44**, 211 – 220.
52. **Rajendran R.** (2009b) Numerical simulation of underwater explosion bulge test, *Materials and Design*, **30**, 4335 – 4341.
53. **Rajendran R. and J.M. Lee** (2008) A Comparative damage study of Air- and Water-Backed plates subjected to Non-Contact underwater explosion, *International Journal of Modern Physics*, Vol.**22**, Nos.9, 10 and 11, 1311 – 1318.
54. **Rajendran R. and J.M. Lee** (2009) Blast loaded plates, *Marine Structures*, **22**, 99 – 127.

55. **Rajendran** and **Narasimhan** (2006) A shock factor based approach for the damage assessment of plane plates subjected to underwater explosion, *Journal of Strain Analysis*, Vol. **41**, Issue 6, 417 – 425.
56. **Ramajeyathilagam.K.** (2000) *Experimental and Numerical Investigations on the Response of Structural elements to Underwater Explosion*, Ph.D. Thesis report, Indian Institute of Technology, Madras, December.
57. **Shin Y.S.** and **L.D. Santiago** (2002) Surface ship shock modeling and simulation: two-dimensional analysis, *Shock and Vibration*, **5**, 2002, 129 – 137.
58. **Singh R.K.** and **H.A. Smith** (1994) Comparison of Computational Effectiveness of the Finite Element Formulations in Free Vibration Analyses, *Computers & Structures*, Vol. **51**, No.4, 381 – 391.
59. **Singh V.P.** (1982) On Under Water Explosions – A Comparative Study, *Defence Science Journal*, Vol.**32**, No.4, 327 – 332.
60. **Sinha J.K, S. Singh** and **R.A. Rao** (2003). Added mass and damping of submerged perforated plates, *Journal of Sound and Vibration*, **260**, 549 – 564.
61. **Sourne H.L., N. Couty, F. Besnier, C. Kammerer, H. Legavre, Marine Principa** and **Nantes** (2003) LS-DYNA Applications in Shipbuilding, *4th European LS-DYNA Users Conference*.
62. **Suneel K.M., P. Alagusundaramorrthy** and **R. Sundaravadivelu** (2007) Ultimate Strength of square plate with rectangular opening under axial compression, *Journal of Naval Architecture and Marine Engineering*, **4**, 15 – 26.
63. **Timoshenko S.P.** *Theory of Plate and Shell*, Second edition. McGraw-Hill Book Company, 1959.
64. **Urtiew P.A, K.S. Vandersall, C.M. Tarver, F. Garcia** and **J.W. Forbes** (2008) Shock Initiation of Composition B and C4 Explosives: Experiments and Modeling, *Russian Journal of Physical Chemistry B*, 162 – 171.
65. **Vulitsky M.Z.** and **Z.H. Karni** (2009) Ship Structures Subject to High Explosive Detonation, *07th International LS-DYNA Users Conference*.
66. **Webb D.C, K. Kormi** and **S.T.S. Al-Hassani** (1995) Use of FEM in performance assessment of perforated plates subject to general loading conditions, *Int. Journal of Pressure Vessel & Piping*, **64**, 137 – 152.
67. **Young Warren C.** (Ed. 6) *ROARK'S Formulas for Stress and Strain*, McGraw-Hill Book Company, 1989.

PUBLICATIONS BASED ON THIS THESIS

1. **Nandagopan O.R., CG.Nandakumar and S.Ranjith Kumar** Free vibration analysis of Plain & Perforated plate submerged in Fluid, (Communicated to *Computers & Structures*).
2. **Nandagopan O.R., CG.Nandakumar and S.Ranjith Kumar** Structural Response of Perforated Plate with Lining due to underwater explosion, (Communicated to *Journal of Ship Research*).
3. **Nandagopan O.R., CG.Nandakumar, Sameer Abdul Azeez and K.Ajithkumar** Measurement of underwater explosion pressure for a water backed structure, (Communicated to *Ocean Engineering*).
4. **Nandagopan O.R., CG.Nandakumar, Rajesh and K.Manoharan** Experimental Investigation on Perforated Plate with Lining, (Communicated to *Defence Science Journal*).

CURRICULUM VITAE

1. Name : O.R.NANDAGOPAN

2. Date of Birth : 15 May 1961

3. Education Qualifications :

1983 Bachelor of Engineering (B.E.)

Institution : Madurai Kamaraj University, Madurai
Specialization : Mechanical Engineering

1985 Master of Engineering (M.E.,)

Institution : Anna University, Chennai
Specialization : Production Engineering

Doctor of Philosophy (Ph.D.)

Institution : Cochin University of Science & Technology,
Kochi

Registration Date : 18 – 08 – 2006

4. Employment Details

Sl.No.	Employer Name	Designation	From	To
1	Hindustan Aeronautics Ltd., Nasik	Assistant Engineer	Mar. 1985	Oct. 1986
2	L&T, ACW, Chandrapur	Assistant Material Control Engineer	Oct. 1986	Dec. 1986
3	NPOL, DRDO, Ministry of Defence, Govt. of India	Scientist B	Dec. 1986	June 1991
		Scientist C	July 1991	June 1996
		Scientist D	July 1996	June 2001
		Scientist E	July 2001	June 2006
		Scientist F	July 2006	----